Using Sea Turtle Biomimetics for Increasing Swimming Efficiency in Humans

University of the South Pacific

University of Twente. Internship

Author:
Thomas Schot *s0199958*

Supervisor:
Dr. David Aitchison

June 24, 2015

Contents

1 Preface

The field of engineering of this project lies within Computational Fluid Dynamics, Finite Element Analysis and mechanisms. As my field of engineering lies in the Solid Mechanics, this project is outside my ”comfort zone”. Instead of using my existing knowledge in this project, I will explore new fields of engineering. My personal goal for this project is to become familiar with the designing, CFD and FEA in SolidWorks, as this will help me in my future career in the industry.

2 Introduction

Humans are inefficient when it comes to swimming. An average human is able to convert about 3% of its energy in propulsion; this can be enhanced by the use of flippers which increases the efficiency up to 10%. When however a closer look is taken at sea turtles, it is to be observed that they are able to convert up to 48% of their energy into propulsion. [1][2][3][4]

The scope of this project is to make use of biomimicry of the swimming behavior of sea turtles in order to design a mechanical device which allows humans to increase their locomotion efficiency in water. To do so several concepts are proposed which then will be analyzed both statically and dynamically using Finite Element Analysis and Computational Fluid Dynamics in Solid Works. In the end a final design of the most feasible concept will be proposed as a possible solution to increase locomotion efficiency in humans.

3 Problem Specification

3.1 Swimming Behavior

When swimming most of the different species of sea turtles use two different types of motion with their front flippers: flapping (vertical up-and-down movement) and rowing (horizontal back-and-forth movement). Flapping motion occurs during routine swimming (see figure 1(a)), whereas a combination of flapping and rowing occurs during vigorous swimming, resulting in a lemniscate-shaped motion (see figure 1(b)). During the routine swimming the sea turtle relies on lift-based locomotion while during vigorous swimming the sea turtle relies on thrust-based locomotion. [5][6][7][8][9][10]

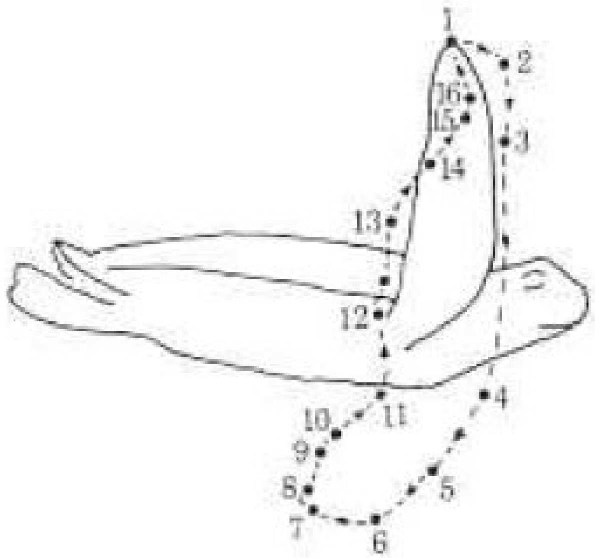

(a) Flapping motion of a sea-turtle during routine swimming [5]

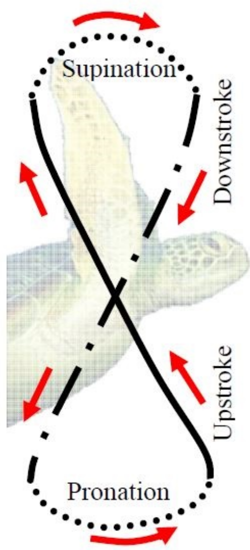

(b) Lemniscate-shaped motion of a sea-turtle during vigorous swimming [6]

Figure 1: Two different types of kinetics in the swimming behavior of sea turtles

Even though flapping motion requires less energy than lemniscate-shaped motion, the energy efficiency increases when swimming speed increases, reaching a maximum efficiency at 75% of the maximum swimming speed. Hence lemniscate-motion is applied by the sea turtle at higher swimming speeds. [11] Furthermore the flipper shows a feathered motion at the end of the power stroke; this is to reduce the drag and control rearward tilt when the power stroke movement comes to a halt, as well as positioning the flipper such that the drag is as low as possible during the return stroke. [12][13]

During the power stroke the flipper is tilted such that the angle of attack creates a thrust coefficient C_T which is as high as possible, whereas during the return stroke the flipper is tilted in such a way that the angle of attack is 0° with respect to the flow direction to decrease the drag coefficient C_D as much possible. [14] Between the power stroke and return stroke the flipper shows supination to adjust the angle of attack such that the drag coefficient is minimized; between the return stroke and the down stroke the flipper shows pronation in order to adjust the angle of attack to maximize the thrust coefficient.

3.2 Translation to Mechanical Model

In this report a distinction is made between the lemniscate motion and the flapping motion and hence the mechanical models to be created. Reasoning behind this is that sea turtles show both types of motion during swimming, each with its own advantages and disadvantages.

Furthermore the flippers are able to pronate and supinate to adjust the angle of attack during power- and return stroke; this motion is to be included in the designs as well and in such a way that this motion is passively achieved.

3.3 Requirements

To create a mechancial device able of enhancing efficiency a set of requirements to be met are thought of:

- The mechanical model must increase locomotion efficiency in water for low-frequency motion
- The artificial flippers must mimic the sea turtles' flippers morphology as close as possible
- The artificial flippers must mimic the sea turtles' flippers physical properties as close as possible
- The motion of the mechanical model must resemble either of the swimming motions of the sea turtle
- The flipper must be able to pronate and supinate
  - This action must be passive
- The flippers' angle of attack during the power stroke must be such that maximum thrust or lift is generated
- The flippers' angle of attack during the return stroke must be such that minimal drag is generated
- It must be possible to produce the mechanical device on Fiji without use of exotic or expensive materials
- The mechanical device must be as light-weight as possible
  - The mechanical device must be able to resist the internal stresses as a result of the forces acting upon it
  - The mechanical device must be as stiff as possible to prevent energy loss due to deformation
    - The maximum deflection is set to be 10 mm
- The material must be seawater resistant
- The mechanical device must be safe to use (i.e. prevent injuries due to sharp edges, clamping)

4 Concept Development

Before creating the concepts, a distinction has been made between the flapping motion and lemniscate motion of the sea turtle. This distinction is to be found between concept 1 and concept 2 and 3. Note that flapping motion relies on lift-based propulsion whereas lemniscate motion relies on thrust-based propulsion. [8]

4.1 Concept 1

Concept 1 consists of a lift-based propulsion which can be achieved as shown in figure 2.

Motion Resemblance The concept in figure 2(a) is to be attached to the lower legs of the swimmer; during swimming the lift force generated comes mostly from the muscles around the hip joint and just a little from the knee joint, as the legs remain flexed during swimming motion. The deflection during swimming motion is small and the radius of the motion is large, hence this motion can be considered as a parallel motion, see figure 2(b). Whereas turtles make use of symmetric flipper motion, this concept makes use of asymmetric flipper motion. [8][15]

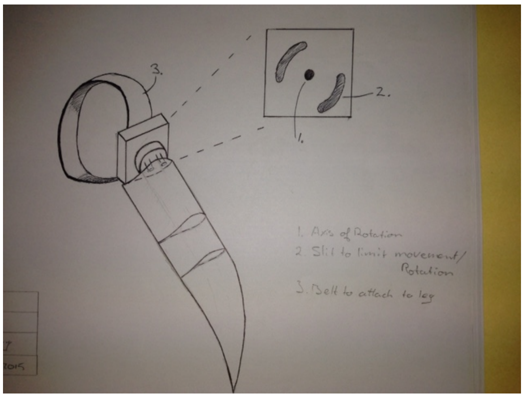

(a) Concept 1 - Swimming enhancement device to be attached to the lower legs

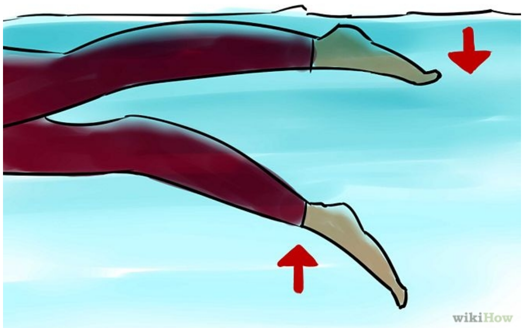

(b) Swimming motion of the legs during swimming [16]

Figure 2: Concept 1 and the swimming motion of a human

Translation to Mechanical Model The concept can be attached to the lower legs to enhance swimming efficiency. It is to be expected that this concept generates a torque upon the legs of the swimmer; the amount of torque shall be calculated in section 5.1.2.1. The length of the flipper is empirically chosen to be similar to the length of the commonly used scuba swimfins to provide enough thrust without becoming too big to handle.

An additional requirement following from this concept is as follows:

- The mechanical device shouldn't generate an uncomfortable amount of torquue upon the legs of the swimmer

4.2 Concept 2

Concept 2 consists of a thrust-based propulsion which can be achieved as shown in figure 3.

Motion Resemblance The concept is based on lateral motion and makes use of a set of leverages and hinges to provide an oscillating rotational motion at the endpoint. The concept can be thought of to be attached to a body board in which the user pushes and pulls the levers (1) back and forth, which rotates about point (2). Energy during the return stroke can be stored in a spring (3) to provide for a larger powerstroke. Note that in figure 3 point (4) is where the cylinder is to be attached and that the part of the bar between points (4) and (5) resembles the flipper. The model was validated using Blocks in SolidWorks.

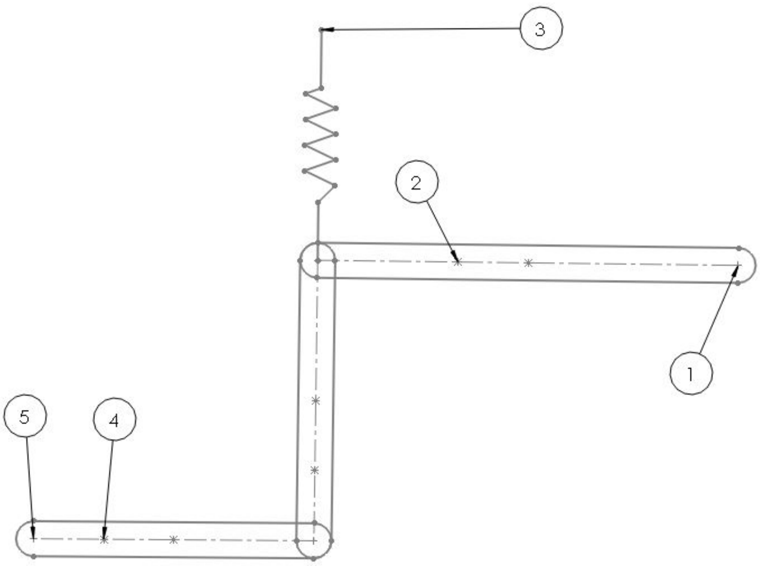

Figure 3: Concept 2 - Top view of the mechanism which translates a lateral motion into a rotational motion

Translation to Mechanical Model The motion can be provided by pushing and pulling the lever (1) downwards as shown in figure 3. The hinge point of the lever is located at (2). The vertical bar then transfers the vertical motion to the bar with point of rotation (4), to which a cylinder is to be attached with a flipper, here displayed as the part between point (4) and (5). Note that during the pulling part the power stroke is simulated and hence more energy is needed than during the pushing part. However, humans are capable of delivering force in both directions; (3) is an added spring to store energy during the pushing part and release it during the pulling part to increase the torque available at (4).

4.3 Concept 3

Concept 3 consists of a thrust-based propulsion which can be achieved as shown in figure 4.

Motion Resemblance This concept is called a Whitworth mechanism and is based on a rotational movement. The mechanism makes use of a set of different leverages and hinges to provide an oscillating motion at the point of rotation. The model is thought to be implemented in a pedalo-like manner. The model was validated using Blocks in SolidWorks; figure 4 shows the mechanism. The motion is slow during the power stroke, but has a quick retracting motion during the return stroke.

Translation to Mechanical Model The motion can be provided by rotating wheel (1) around axis (2). A pin attached to the wheel is able to slide through the slit (3). The crank then rotates in an oscillating motion about axis (4). Note that this motion is highly nonlinear and can be influenced by adjusting the distance between the path (3) follows and point of rotation (4). The nonlinear behavior can be advantageous since the force needed during the power stroke of the flipper is much bigger than the force needed during the return stroke.

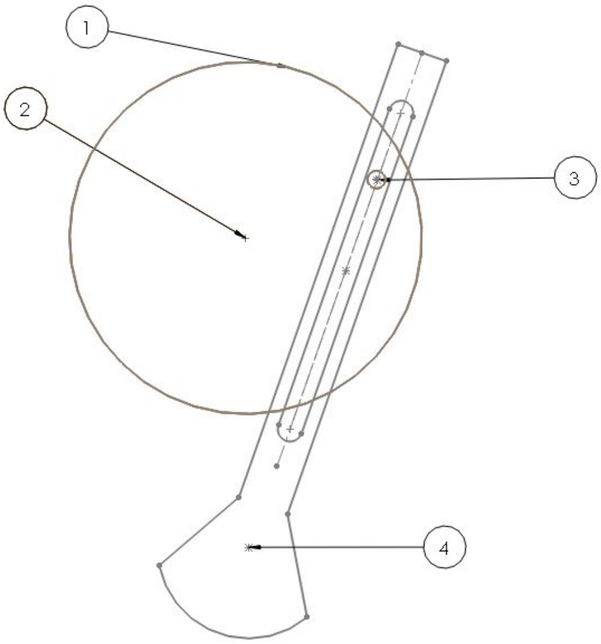

Figure 4: Concept 3 - Mechanism which uses rotational motion to provide a rotational oscillating motion at the point of rotation (4)

An additional requirement following from this concept is as follows:

- The force distribution during rotational movement must be smooth such that it is comfortable for the user

4.4 Feathering motion

4.4.1 Concept 1

During the power stroke the angle of attack of the flipper must be such that the lift is maximal while retaining a low drag coefficient. During the upstroke the angle of attack must be such that the drag is as low as possible and preferably no lift is generated either. The magnitude of the angular deflection of the flipper shall be calculated and discussed in section 5. The feathering motion can be provided with a mechanism as shown in figure 6.

4.4.2 Concept 2 and 3

Power Stroke Both thrust-based concepts consist of an oscillating point of rotation. This point then can be used to attach to a mechanism which resembles the feathered swimming motion of a sea turtle. Figure 5 shows a cylinder with two discs (1) which rotate around axis (3). An axis (2) is mounted between the two discs and provides a point of attachment for the flipper. It is chosen to have a vertical axis of rotation in order to provide a full thrust-based motion.

Return stroke During the return stroke the angle of attack of the flipper must be such that the drag is as low as possible. It is chosen to have a passive mechanism in which the fin is able to find its own way of the least resistance. A mechanism as such is proposed in figure 6.

The mechanism consists of an axis of rotation (1) to which the flipper is to be attached. Then two slits (2) can provide room for two pins to slide through. Those pins have to be attached to the fins as well. The inclination of the slits depends on the angle of attack during power stroke and return stroke and are yet to be determined in section 5.

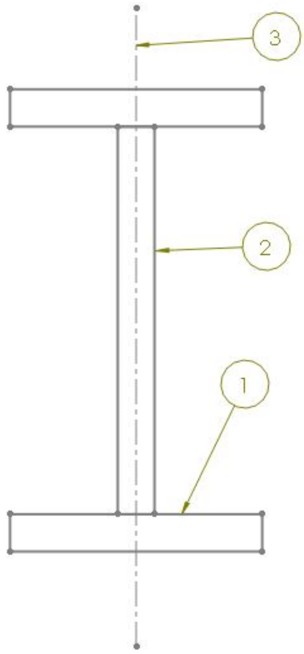

Figure 5: Mechanical configuration to translate the oscillating rotational motion into flapping motion.

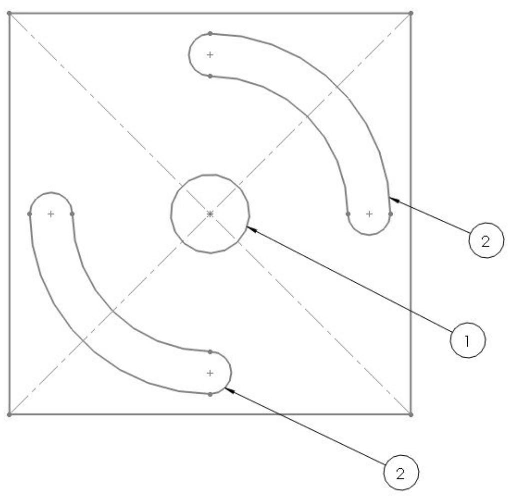

Figure 6: Mechanism enabling a passive rotational motion during return stroke, while returning to its original position during power stroke

5 Preliminary Design

All three concepts are considered achievable; this section covers some analytical calculations to give an estimation of the dimensions of the mechanisms and the forces involved.

5.1 Analytical Calculations

In order to provide a decent detailed design, some analytical calculations have to be made to give an estimation about the forces needed to propel the mechanical devices. These calculations consist of the generated lift in flapping motion and generated thrust in paddling motion, as well as the torque generated on the legs by concept 1.

5.1.1 Lift Coefficient, Drag Coefficient and Thrust Coefficient

Lift Coefficient The lift coefficient of the sea turtle's flipper can be found either by using the Kutta-Joukowski Theorem or by experimental measurements. Kutta-Joukowski states that the lift per unit width (denoted L') can be calculated as follows: [17]

$$L' = -\rho_\infty V_\infty \Gamma \tag{5.1}$$

$$\Gamma = \oint_C V \cos\theta \; ds \tag{5.2}$$

Variable	Symbol	Unit
Lift per unit length	L'	N/m
Fluid Density at ∞	ρ_∞	kg/m^3
Fluid Velocity at ∞	V_∞	m/s
Circulation	Γ	m/s
Fluid Velocity at C	V	m/s
Tangent contour	θ	$^\circ$
Infinitesimal length on curve C	ds	m

Combining and working out the contour integral gives the lift coefficient C_L: [18]

$$C_L = \frac{2L}{\rho V^2 \bar{A}} \tag{5.3}$$

Variable	Symbol	Unit
Lift coefficient	C_L	-
Lift	L	N
Fluid Density	ρ	kg/m^3
Fluid Velocity	V	m/s
Projected Area	A	m^2

Since for the flipper both Γ and V are a function of x, y and z and are not prescribed, finding an analytical solution for the lift coefficient C_L is difficult and considered outside the scope of this project.

Drag Coefficient Similar to the lift coefficient, the drag coefficient can be calculated using: [19]

$$C_D = \frac{2D}{\rho V^2 \bar{A}} \tag{5.4}$$

Variable	Symbol	Unit
Drag coefficient	C_D	-
Drag	D	N
Fluid Density	ρ	kg/m^3
Fluid Velocity	V	m/s
Projected Area	A	m^2

Similar to the lift coefficient C_L, the drag coefficient C_D and thus the drag D are a function of x, y and z and are not prescribed. However, Sun, X. et al. have used figure 7 for their design of a prosthetic front flipper for a sea turtle; their results shall be used in further calculations. [20]

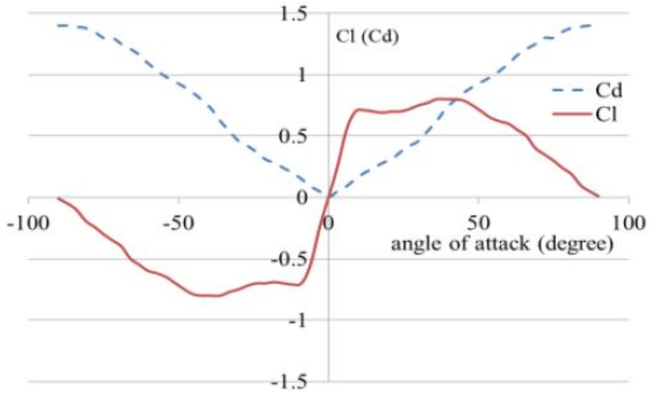

Figure 7: C_L and C_D for different angles of attack [20]

As is to be observed both the lift coefficient and drag coefficient are 0 at a 0 angle of attack, indicating no washdown, vortex shedding or other energy losses are assumed by Sun, X. et al. [20] Both the lift- and drag coefficient show a symmetric graph, indicating a symmetrical foil was used. The lift coefficient has a maximum value of ~ 0.8 at an angle of attack of $\sim 40°$ and a slightly lower lift coefficient of ~ 0.7 at an angle of attack of $\sim 10°$. However the drag coefficient is significantly lower at $10°$ than at $40°$, having values of ~ 0.1 and ~ 0.8 respectively. Therefore an angle of attack of $10°$ is more desirable due to the lower drag coefficient. This value thus shall be used in the designing process.

Thrust Coefficient When the flipper is moving with respect to the water, the drag coefficient C_D can be considered as the thrust coefficient C_T. This means that during vigorous swimming, the flipper has a thrust coefficient of $C_D = 1$ when the flipper is is inclined at an angle of $-50°$. The drag coefficient as given in figure 7 therefore shall be used as the thrust coefficient in further calculations.

5.1.2 Concept 1

This section covers both the amount of torque generated as the amount of forward propulsion gained as a result of the lift and drag acting upon the flipper.

5.1.2.1 Torque The amount of torque generated depends on the force the hydrofoil experiences in the vertical direction. Since only an indication of the amount of torque is needed, the calculations shall be simplified by assuming a flipper with a uniform cross section. To calculate the amount of torque exerted on the lower legs the following formula can be used:

$$\begin{aligned} \tau &= rF \qquad (5.5) \\ &= \frac{1}{2}\omega r^2 \end{aligned}$$

Here τ is the torque, r is the length of the arm, F is the force exerted on the tip of the arm and ω the distributed load per unit width on the arm. To be able to determine ω the flippers dimension has to be determined. As stated in section , it is chosen to have a flipper with a length approximating the length of a scuba swimfin, which is roughly about 0.5 m. To simplify the calculations, a uniform hydrofoil is assumed with a chord length c equal to the average chord length $\bar{c}$ of a real sea turtle's front flipper, which is $1/4^{th}$ of the flipper's length. [20] The area of the flipper now becomes:

$$\begin{aligned} A_{flipper} &= l \cdot \bar{c} \qquad (5.6) \\ &= 0.5 \cdot 0.125 \qquad (5.7) \\ &= 6.25 \cdot 10^{-2}\ m^2 \end{aligned}$$

The upward force is based upon the lift generated trough paddling, which can be calculated using equation A.3. The velocity at which average scuba divers swim is up to 0.8 m/s. [21][22] Furthermore the legs move with a frequency of approximately 30 strokes per minute with an amplitude of approximately 0.5 m. [23] This leads to an average leg velocity in vertical direction of:

$$\bar{V} = 0.5\ m/s \tag{5.8}$$

Since the directions of the swimming- and paddling velocities are orthogonal, Pythagoras' law can be used to find the resulting velocity:

$$V_{res} = \sqrt{\frac{0.5^2}{0.8^2}} = 0.94\ m/s \tag{5.9}$$

Using trigonometric identities, it can be calculated that the vector V_{res} of the water approaches the hydrofoil at an angle of $\gamma = 32°$ with respect to the horizontal. Figure 8(a) shows the resultant velocity vector together with the resultant force acting upon the hydrofoil when under an angle of attack of $\alpha = 10°$, as the lift coefficient is optimal at this angle of attack. The vectors are scaled; the lift and drag are a function of the projected area A and are computed using equations A.3 and 5.4. The lift and the drag vector act upon 1/4 cord length, as this is the center of pressure and hydrodynamic center. [24]

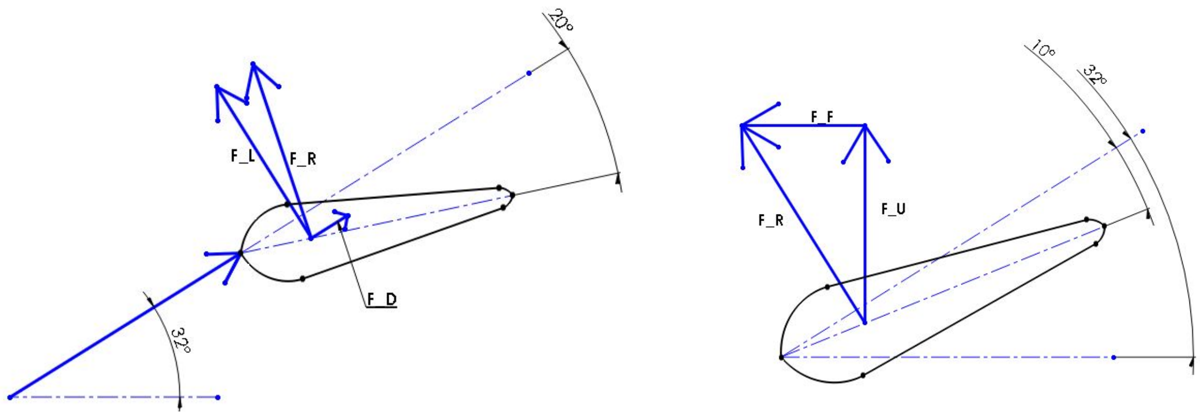

(a) Resultant force on the hydrofoil as a result of the flow direction, lift and drag. F_L is the lift force vector, F_D is the drag force vector and F_R is the resultant force vector.

(b) Resultant forces on the hydrofoil with F_U the vertical force vector and F_F the horizontal force vector

Figure 8: Force vectors acting upon the hydrofoil

As is to be observed in figure 8(b) the resultant force has a large vertical component and a small horizontal component. Considering the lift- and drag vectors, both vectors consist of a horizontal and vertical component. By taking the vertical component of each vector the upward force can be calculated and by taking the horizontal component of each vector the forward force can be calculated:

$$F\_U = F\_L \cdot \cos\gamma + F\_D \cdot \sin\gamma \tag{5.10}$$
$$F\_F = F\_L \cdot \sin\gamma - F\_D \cdot \cos\gamma \tag{5.11}$$

Here γ is the angle at which the free stream velocity approaches the foil, in this case $\gamma = 32°$. The value of each vector is to be found in table 1. Note that the values yet have to be multiplied with the projected area $\bar{A}$.

Vector	Force [N]
F_L	$308.6 \cdot \bar{A}$
F_D	$88.0 \cdot \bar{A}$
F_R	$316.8 \cdot \bar{A}$
F_U	$269.2 \cdot \bar{A}$
F_F	$168.3 \cdot \bar{A}$

Table 1: Force vectors acting upon the hydrofoil

The projected area for thin airfoils can be written as the chord length c times the sine of the angle of attack $\alpha = 10°$ times the foil width l, see figure 9.

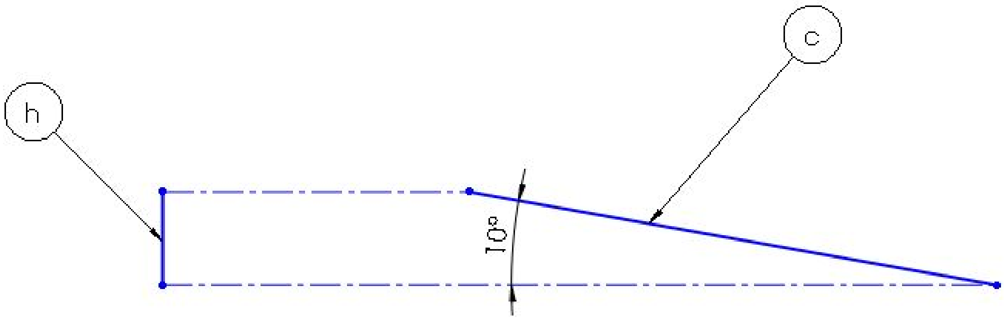

Figure 9: Projected height h of chord length c under an angle of attack of $\alpha = 10°$

To calculate the torque acting upon the leg, the upward force vector F_U is used. The torque becomes: [25]

$$\begin{aligned}\tau &= \frac{1}{2}\omega l^2 \\ &= \frac{1}{2} \cdot 269.2 \cdot \bar{A} \cdot 0.5^2 \\ &= \frac{1}{2} \cdot 269.2 \cdot A \sin\alpha \cdot 0.5^2 \\ &= 0.37\ Nm\end{aligned} \tag{5.12}$$

The amount of torque acting upon the leg appears to be small; the exact amount of torque shall be determined using SolidWorks in section 6. Since no adequate numbers are to be found either in papers or by the Biomedical Engineering dpt. of the University of Twente about the maximum allowable torque on a human leg, no conclusions can be made whether the found torque is tolerable.

5.1.2.2 Forward Propulsion

Power Stroke The forward propulsion is achieved during the power stroke. The results of table 1 in section 5.1.2.1 can be used to give the amount of forward propulsion gained during the power stroke of one leg:

$$\begin{aligned}F_{prop} &= F\_F \cdot \bar{A} \\ &= 168.3 \cdot A \sin\alpha \\ &= 29.22\ N\end{aligned} \tag{5.13}$$

The force needed for the power stroke of one leg can be calculated as follows:

$$\begin{aligned} F_{tot} &= F\_R \cdot \bar{A} \\ &= 320.6 \cdot A \sin\alpha \\ &= 55.01\ N \end{aligned} \tag{5.14}$$

Both the force needed for the power stroke as the forward propulsion seems to be small; as a comparison, the thrust produced by swimfins during a 20 second power stroke can be up to 192 N. [26] Determination of the exact amount of forward propulsion and optimization shall be done using SolidWorks in section 6.

Return Stroke During the return stroke the resultant velocity vector is the same size but inclined at $-32°$ with respect to the horizontal. The hydrofoil will have an angle of attack of $0°$ with respect to the velocity vector to have a lift- and drag coefficient equal to zero, leading to zero drag force. This however is an ideal situation; in section 6 the calculations shall be done for a real fin.

Feathering Motion The angle of the fin during the power stroke has been determined to be $32 - 10 = 22°$ with respect to the horizontal. The angle during the return stroke has been determined to be $-32°$. Therefore the fin is estimated to rotate over a range of $54°$. The mechanism ensuring this movement must be designed such that this motion is possible; this shall be done in section 6.

5.1.3 Concept 2

This section covers the optimization for the dimensions of the flipper based upon the hydrofoil's lift- and drag coefficient as found in section 5.1.

5.1.3.1 Leverage, Displacement and Dimensions

The output force of the device F_{output} compared to the input force F_{input} is based on leverage, which simply states that $F_{left} \cdot A_{left} = F_{right} \cdot A_{right}$. Since the leverage is based upon rotation, the small angle approximation is to be used, stating that $\sin\theta \approx \theta$ for small θ. [27] Angles up to $32°$ are allowable to retain a relative error of less than 5%. Using this approximation considerably decreases the complexity of the formulas while retaining sufficient accuracy. The ratio between the output torque τ and the input force F_{input} is as follows:

$$\tau = \frac{(a \cdot F_{input} + b \cdot k\Delta x)\, c}{b} \tag{5.15}$$

Using goniometric relations, the displacements and angles are as follows:

$$\left.\begin{aligned} \beta &= \sin^{-1}\left(\tfrac{\Delta 2}{c}\right) \\ \Delta 2 &= \sin(\alpha) \cdot b \\ \alpha &= \sin^{-1}\left(\tfrac{\Delta 1}{a}\right) \end{aligned}\right\} \beta = \sin^{-1}\left(\frac{\sin\left(\sin^{-1}\left(\frac{\Delta 1}{a}\right)\right) \cdot b}{c}\right) \tag{5.16}$$

The symbols are to be found in figure 10. Note that length d represents the flipper and yet has to be determined.

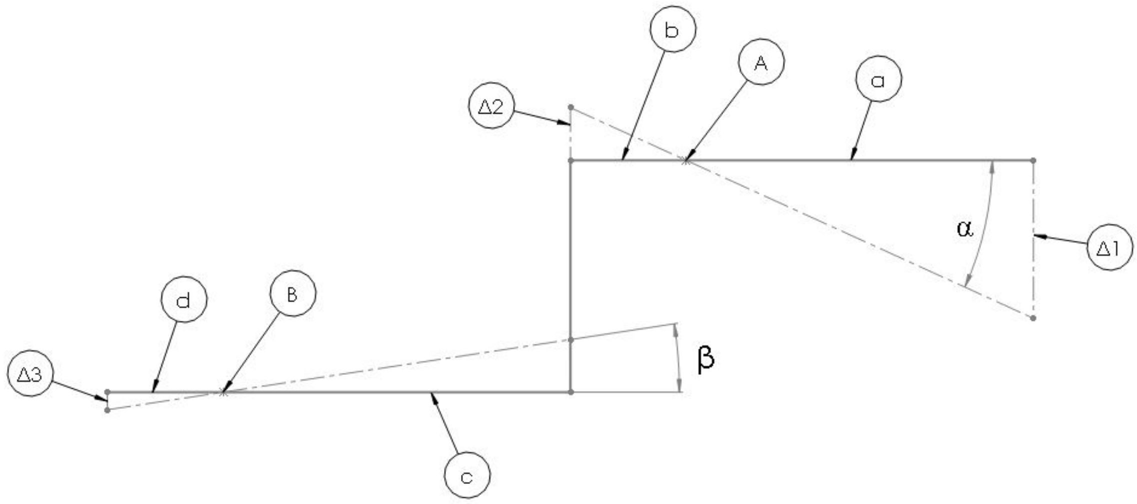

Figure 10: Mechanical linkage of Concept 2. The dashed line shows the displaced linkage. The arm lengths are defined for each lever: a and b are the lengths of the bar on which the applied force acts, with point of rotation A; c is the length of the bar providing the rotation at point B; Δ *1-3* are the vertical displacements of the end points of both horizontal bars; α is the angle as a result of the stroke exerted by the user and β is the angle of the flipper.

Since the average human arm length is about 57.4 cm, length $\Delta 1$ can be determined to be $\frac{1}{2} \cdot 57.4 = 28.7\ cm$. [28] Furthermore the force the flipper exerts on the water during power stroke is always normal to the flippers surface, meaning that the force vector of the forward propulsion decreases as β increases, as shown in figure 11.

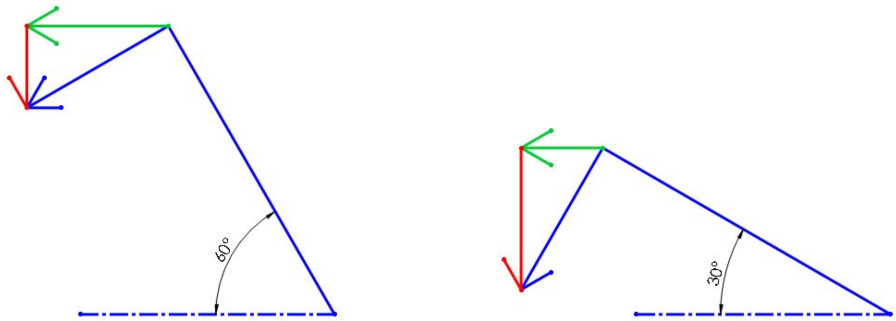

Figure 11: Graphical representation of the thrust vector (red) as a result of the force vector (blue) at big angle (left) and small angle (right). The green vector shows the sideway force vector.

It is chosen to have a maximum angle of $\beta = 30°$ in order to increase efficiency. Using the first equation in equation 5.16 length a can be determined. Using steps of 5 degrees, the results are listed in table 2.

Angle α [°]	**Length** a [m]
10	1.65
15	1.11
20	0.84
25	0.68
30	0.57

Table 2: Lengths for a calculated for different angles α

Taking equation 5.15 into consideration it is desirable for a to be as high as possible, generating a higher torque. However from a practical point of view it is desirable to have smaller dimensions. Therefore it is chosen to use $a = 0.57\ m$, leading to an acceptable size of the lever.

From equation 5.15 and figure 10 it can be determined that $\frac{\Delta 1}{a} = \frac{\Delta 2}{b}$. Since $\Delta 1$ and a are known, the ratio $\Delta 2/b$ can be determined:

$$\frac{\Delta 2}{b} = \frac{0.287}{0.57} = 0.50 \tag{5.17}$$

Furthermore it follows from equation 5.15 that $\sin\beta = \Delta 2/c$ with $\sin\beta = \sin 30 = 0.5$. Combining this with equation 5.17 gives the following result:

$$\frac{\Delta 2}{c} = \frac{\Delta 2}{b} \longrightarrow b = c \tag{5.18}$$

By setting $b = c$ in equation 5.15 it follows that the torque only increases if $b \cdot k\Delta x$ increases. However this variable can be adjusted by changing the spring stiffness k, therefore b and c can be chosen freely. From a design point of view it is desirable to decrease b and c as much as possible, therefore an arbitrary chosen length of 0.10 m is chosen as length.

By taking $\alpha = \beta = 30°$ an relative error under 5% is ensured. The dimensions as chosen are listed in table 3.

Variable	**Dimension [-]**
a	0.57 m
b	0.10 m
c	0.10 m
α	30°
β	30°

Table 3: Dimensions found for the design of concept 2

5.1.3.2 Forward Propulsion

Power Stroke To find the thrust during the power stroke, the maximum push-pull force of a human must be considered. For both males and females the one-handed pushing- and pulling force while lying down in prone position ranges between 285 − 330 N and 270 − 283 N, respectively. [29] To endure highly repetitive motions, the force applied reduces to 30% of the maximum force. [30][31] This means that during pulling motion a force of 81 N is to be expected and during pushing motion a force of 86 N is to be expected. Using this information, the flipper's dimensions can be determined.

Using the equations given in section 5.1.1 the forward propulsion during the power stroke can be determined. Since this concept is thrust-based, the thrust coefficient C_T as given in figure 7 is to be used in the calculations. The thrust coefficient shows to be maximal at an angle of attack of $\alpha = 90°$, having a value of $C_T = 1.4$, while having a lift coefficient $C_L = 0$ at this inclination. Figure 12 shows the drag vector relative to the flow direction.

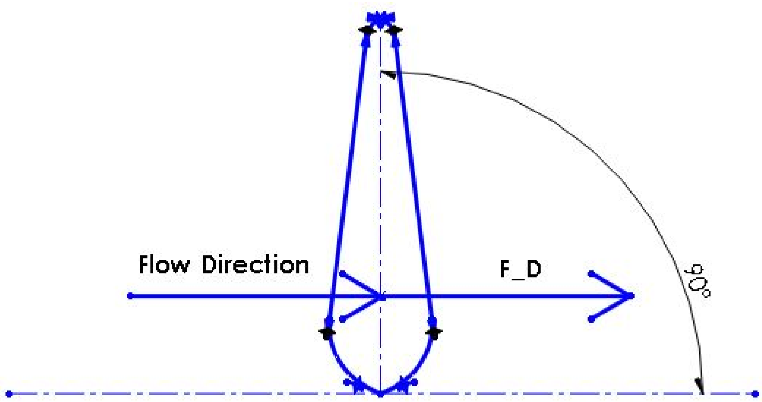

Figure 12: Resultant drag force vector F_D on the hydrofoil as a result of the flow direction.

Since the flipper rotates about a point, the velocity is a function of the position on the arm:

$$V = \omega \cdot r \tag{5.19}$$

With ω the angular velocity and r the length of the arm. The angular velocity can be determined using the fact that the flipper moves at a slow pace of 30 strokes per minute. The angular deflection is 60°, or 1.05 rad, thus the angular velocity can be calculated, assuming no difference in angular velocity between the power stroke and return stroke:

$$\begin{aligned} \omega &= \frac{d\phi}{dt} && (5.20) \\ &= \frac{1.05}{1} && (5.21) \\ &= 1.05\ rad/s \end{aligned}$$

The generated thrust is a function of the velocity, which on its turn is a function of the position on the arm r. Substituting $\bar{A} = r \cdot c \sin\alpha$, $\sin\alpha = 1$ for $\alpha = 90°$ and $c = \frac{1}{4}r$ as stated in section 5.1.2, and $V(r) = \omega \cdot r$, the thrust becomes:

$$\begin{aligned} T &= \frac{1}{2}\rho \bar{A} C_T V^2(r) && (5.22) \\ &= \frac{1}{8}\rho C_T \omega^2 r^4 && (5.23) \end{aligned}$$

The bending moment equation is used to determine the torque which is generated by the flipper on the axis of rotation:

$$\begin{aligned} \tau_{flipper} &= \int w \cdot r dr && (5.24) \\ &= \int_0^r \left(\frac{1}{8}\rho C_T \omega^2 r^4\right) \cdot r\ dr && (5.25) \\ &= \left[\frac{1}{48}\rho C_T \omega^2 r^6\right]_0^r \\ &= \frac{1}{48}\rho C_T \omega^2 r^6 \end{aligned}$$

Here w is the distributed load on the flipper, which is equal to the thrust. Now consider an ideal situation, in which the flipper during the return stroke has an angle of attack of 0°, complying with a drag- and lift coefficient equal to 0. This means that all energy during the return stroke can be stored in the spring attached to lever b (figure 10). Since this force was determined to be 86 N, the total force during the power stroke is $86 + 81 = 167$ N. Filling in the known values in equation 5.15:

$$\begin{aligned} \tau_{lever} &= \frac{(a \cdot F_{input} + b \cdot k\Delta x)\, c}{b} && (5.26) \\ &= \frac{(0.57 \cdot 81 + 0.1 \cdot 86) \cdot 0.1}{0.1} \\ &= 54.8\ Nm \end{aligned}$$

Since the torque generated by the user is equal but opposite to the torque generated by the flipper, the dimension r can be solved by setting both equations equal to each other. Using the values $C_T = 1.4$, $\omega = 1.05\ rad/s$ and $\rho = 998\ kg/m^3$, solving for r gives:

$$\frac{1}{48} \cdot 998 \cdot 1.4 \cdot (1.05)^2 \cdot r^6 = 54.8 \tag{5.27}$$

$$r^6 = 1.71 \tag{5.28}$$

$$\begin{aligned} r &= \sqrt[6]{1.71} \\ &= 1.09\ m \end{aligned}$$

Therefore the maximum size of the flipper, considering a uniform hydrofoil will be 1.09 x 0.27 m, which seems quite large, yet acceptable. Note that this situation considers a no-drag return stroke. An optimal configuration therefore leads to a maximum propulsion of 167 N normal to the flipper surface. The forward propulsion is a function of the angle θ the flipper makes with the horizontal, as is to be seen in figure 13. The vertical component of the force vector (2) can be calculated as follows:

$$F_{forward} = F_{thrust} \cdot \cos\theta \tag{5.29}$$

$$= 167 \cdot \cos\theta \tag{5.30}$$

The total amount of forward thrust during one stroke is the integral over the angular displacement:

$$F_{forward,total} = \int_{-\theta=-30}^{\theta=30} 167 \cdot \cos\theta\ d\theta \tag{5.31}$$

$$= 2 \cdot \int_{0}^{\theta=30} 167 \cdot \cos\theta\ d\theta \tag{5.32}$$

$$= [334 \cdot \sin\theta]_0^{\theta=30} \tag{5.33}$$

$$= 167\ N \tag{5.34}$$

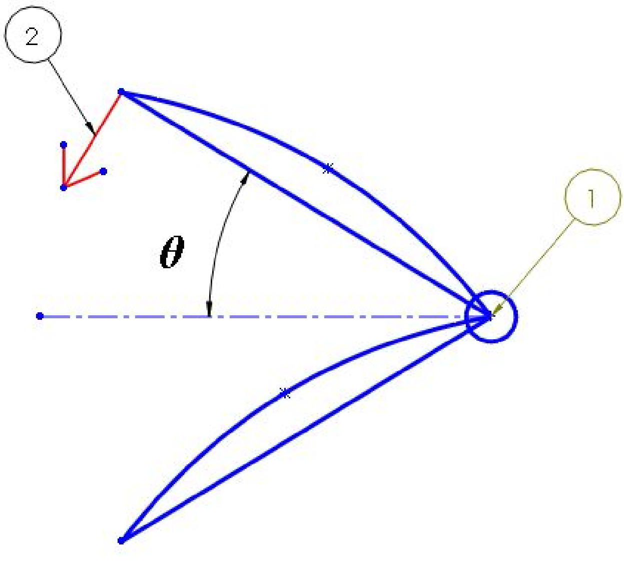

Figure 13: Flipper rotating about point (1) at an angle θ. The normal force (2) the flipper exerts on the water consists of both a forward and sideward component.

Spring The spring constant of the spring can be determined by using $F = k\Delta x$. Since F is known and Δx can be written as $\Delta x = \sin(2\alpha) \cdot b$, which are known values as well, the spring constant can be calculated accordingly:

$$F = k \cdot \sin(2\alpha) \cdot b \tag{5.35}$$
$$86 = k \cdot 0.087 \tag{5.36}$$
$$k = 993\ N/m \tag{5.37}$$

Return Stroke During the return stroke the flipper must be aligned such that the drag coefficient is as low as possible. For the hydrofoil considered in the calculations this is at an angle of attack of 0°, however the exact angle of attack has yet to be determined using the designed flipper. This shall be done in section 6.

Feathering Motion The angular displacement during the power stroke has been determined to be 90°. During the return stroke the angular displacement has been determined to be 0°. Therefore the fin must be able to rotate over a range of 90°. The mechanism to allow for this rotation shall be determined in section 6.

5.1.4 Concept 3

5.1.4.1 Force Profile, Angular Velocity and Angular Displacement

To determine the forces and velocities the mechanism is able to deliver, a closer look must be taken to its kinematic behavior. Figure 14(a) shows the mechanism; the red part of the arc shows when the power stroke is executed and the blue arc shows the quick return stroke. The maximum angle of the crank can be adjusted by positioning the point of rotation of the crank relative to the path the pin follows, as is to be observed in figure 14(b) and 14(c). By adjusting angle α, the length of the red and blue curve can be adjusted (i.e. when α increases the length of the quick return stroke decreases, but the angular velocity of the crank will increase). Since the kinematic equations are very cumbersome, SolidWorks is used to validate the model.

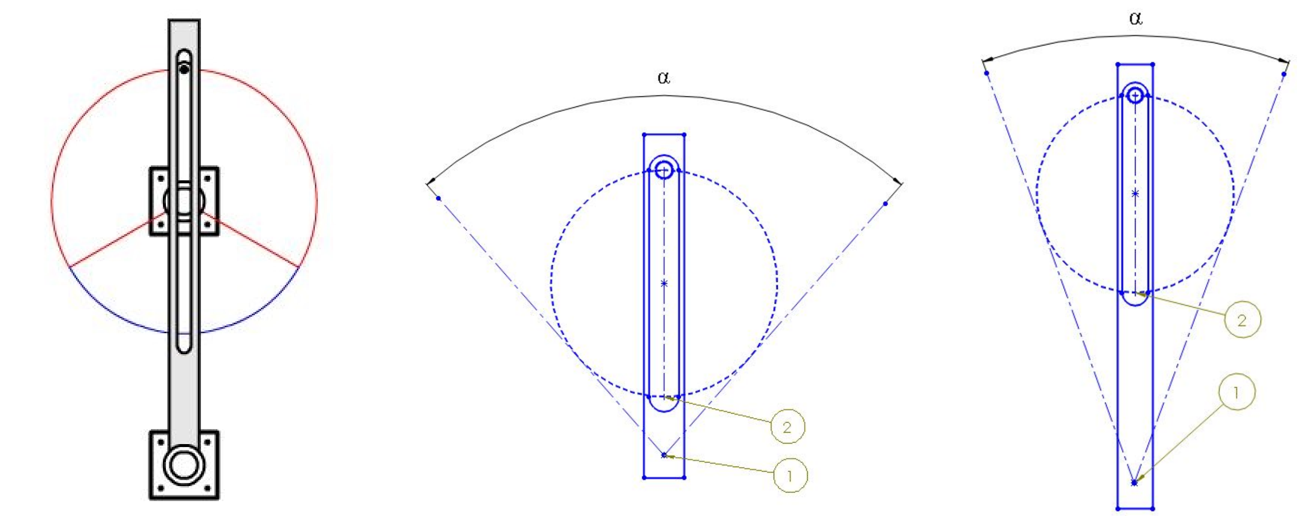

(a) Whitworth mechanism translating a rotational motion into an oscillating rotational motion. The red path represents the power stroke, the blue path represents the quick return stroke. [32]

(b) Maximum angle α for a small distance between point of rotation (1) and path (2)

(c) Maximum angle α for a large distance between point of rotation (1) and path (2)

Figure 14: Whitworth mechanism

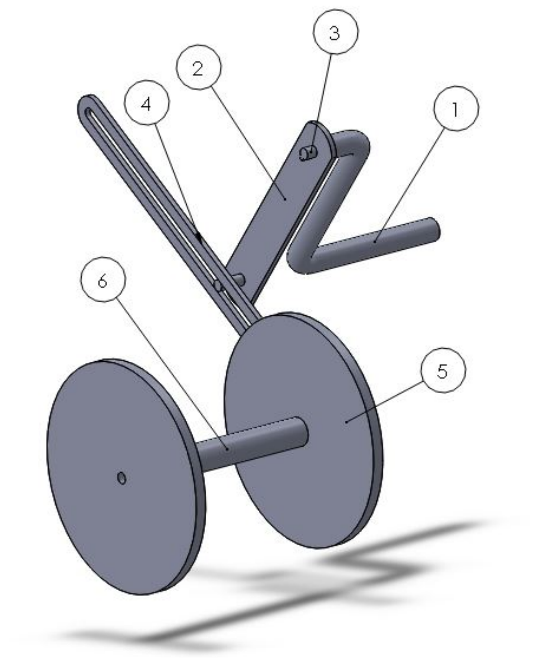

Figure 15: Model used for kinematic analysis. Bar (1) consists of a horizontal pedal and a vertical crank which rotates about axis (3); crank (1) and (2) have the same length; crank (2) rotates about point(3); the slitted crank (4) follows the pin attached to (2) and is attached to cylinder (5); both the slitted crank (4) and the cylinder (5) rotates about axis (6).

Validation in SolidWorks Figure 15 shows the model used in SolidWorks to validate the kinematic behavior of the Whitworth mechanism. The typical points of interest are the ratio between the radius of (2) and the distance between (1) and (2) as shown in figure 14(b) and 14(c). As a design choice the radius has been chosen to be equal to the length of a bicycle pedal crank, which typically is 170 mm for a bike, to keep a 1 : 1 force distribution. [33][34] The distance between point (1) and (2) has been chosen to be 60 mm in figure 14(b) and 210 mm in figure 14(c) to show the difference between the power stroke and return stroke in terms of angular velocity and angular deflection. The analysis has been done for the sides of the slitted crank with the beginning of the power stroke as the starting point. The results are plotted in figures 16 and 17.

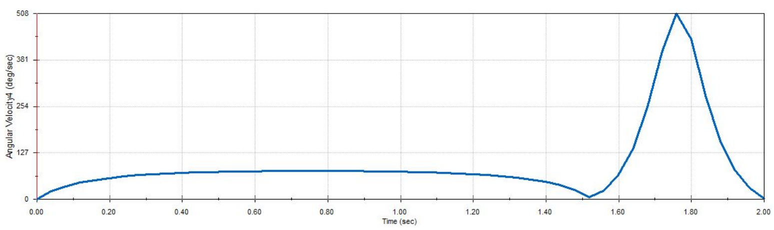

(a) Angular velocity in $degree/s$

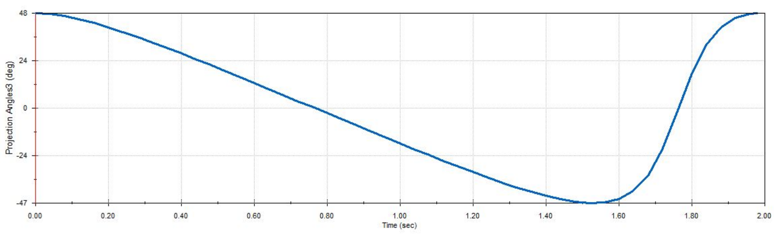

(b) Angular displacement in $degree$

Figure 16: Plots of the angular velocity and -displacement of the slitted crank for one rotation of a 30 r.p.m. motor and a 60 mm offset

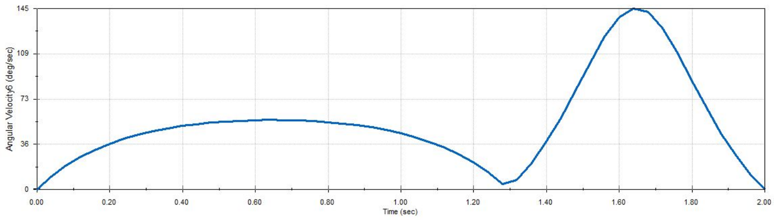

(a) Angular velocity in $degree/s$

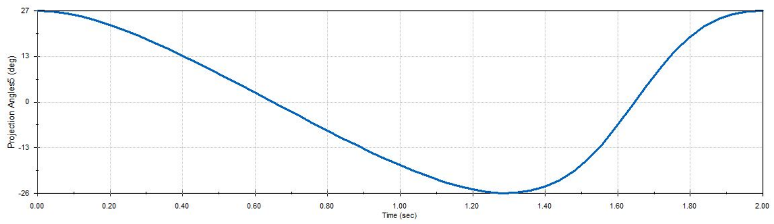

(b) Angular displacement in $degree$

Figure 17: Plots of the angular velocity and -displacement of the slitted crank for one rotation of a 30 r.p.m. motor and a 210 mm offset

As is to be observed there is a clear difference between the two configurations, even though both figures show a higly non-linear motion. The returning points are clearly visible in both configurations as the angular velocity is zero at those points: for the 60 mm offset configuration this occurs at $t = 1.52\ s$ and for the 210 mm offset configuration this occurs at $t = 1.27\ s$. Increasing the offset leads to a decrease of the difference in angular velocity during power stroke and return stroke. However it is to be observed that the power stroke shows a more linear behavior for the 60 mm offset than for the 210 mm offset. The values for both configurations are given in table 4.

	60 mm offset	**210 mm offset**
Variable	Value $[-]$	Value $[-]$
ω_{max} power stroke	1.34 rad/s	0.97 rad/s
Relative time power stroke	76 %	64 %
ω_{max} return stroke	8.87 rad/s	2.53 rad/s
Relative time return stroke	24 %	36 %
Max. angular displacement	48°	27°

Table 4: Quantitative results of the comparison between the two different configurations

5.1.4.2 Forward Propulsion

To compute the forward propulsion, a closer look must be taken at the pedaling behavior of a cyclist. Since the torque generated by the cyclist is nonlinear the input torque of the design is nonlinear as well. Figure 18 shows the radial- and tangential force distribution during one rotation of one pedal. As is to be observed the biggest forces occurs when the pedal is horizontal (0°) until the pedal reaches vertical position (−90°), which is to be expected since the force delivered by the cyclist's legs is oriented in downward direction. The torque generated by cyclists show a highly symmetrical and sinusoid pattern, as shown in figure 19 and as stated by [35][36]. Note that the graph represents the net torque generated by both pedals during one rotation.

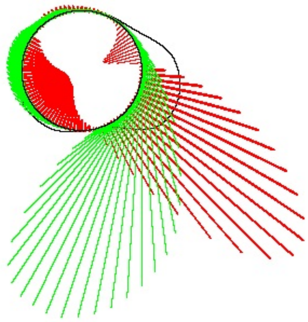

Figure 18: Radial force distribution (red) and tangential force distribution (green) during one clockwise rotation in cycling [37]

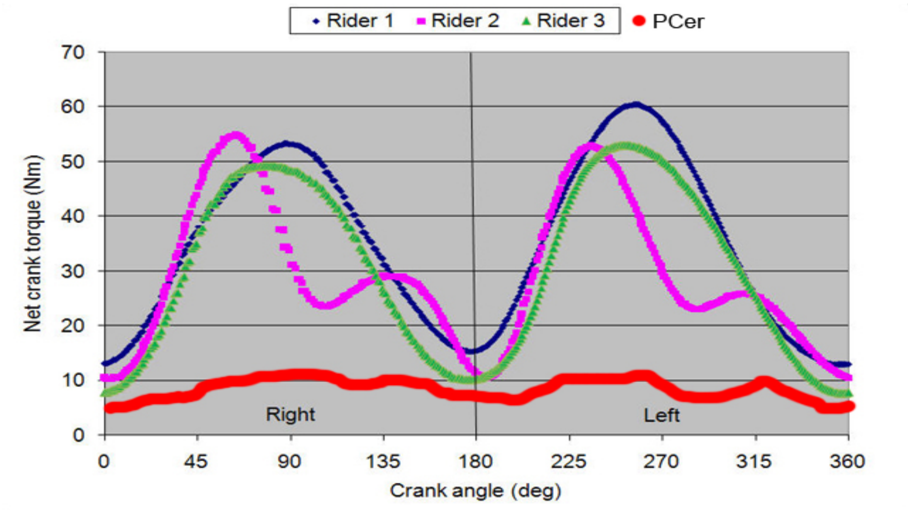

Figure 19: Net crank torque for 3 different riders shows a sinusoid pattern [36]

To approximate the torque profile consider the following trial function:

$$\tau = A \cdot \cos(n\theta + \phi) + B \tag{5.38}$$

Here A is the amplitude in Nm, n is a dimensionless integer number, θ is the phase in rad, ϕ is the phase shift in rad and B is the mean value of the torque in Nm. The power which a cyclist generates during easy cycling is 75 W and the power-torque relation is as follows: [38]

$$P = \tau_{pedal} \cdot \omega_{pedal} \tag{5.39}$$

Here, P is the power in W, τ_{pedal} is the torque in Nm and ω_{pedal} is the angular velocity in rad/s. Considering an angular velocity of π rad/s complying with a cycling frequency of 30 Hz the mean torque B generated is:

$$B = \frac{75}{\pi} = 24 \ N \cdot m \tag{5.40}$$

Rider 1 in figure 19 shows a mean torque of 35 $N \cdot m$ and an amplitude of 20 $N \cdot m$; rider 2 and 3 show a mean torque of 32.5 $N \cdot m$ and amplitude of 20 $N \cdot m$. The ratio between the amplitude A and mean torque B is:

$$\left.\begin{array}{lll} \text{rider 1}: & \frac{20}{35} & = 0.57 \\ \text{rider 2 and 3}: & \frac{20}{32.5} & = 0.62 \end{array}\right\} \text{mean: } 0.60 \tag{5.41}$$

The mean amplitude is 0.6 times the mean torque, in this case: $A = 0.6 \cdot 24 = 14.4\ N \cdot m$. Since the torque profile completes two cycles in 360° it follows that $n = 2$. With the torque profile starting at $\cos(\pi) = -\cos(0)$ the final function for the torque becomes:

$$\tau_{pedal} = -14.4 \cdot \cos(2\theta + \phi) + 24 \tag{5.42}$$

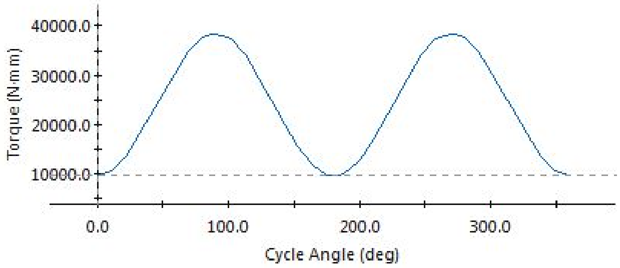

Figure 20: Plot of the trial function for the torque

Equation 5.42 shall be used as input torque on the mechanism and ϕ can be adjusted as desired to create the optimal force distribution.

During cycling motion the pedals show a non-uniform angular velocity, as shown in figure 21. It is chosen to use a chainring similar to the chainring in figure 21(b) to ensure a sinusoid angular velocity output, simplifying both the analytical calculations and the dynamic analysis in SolidWorks.

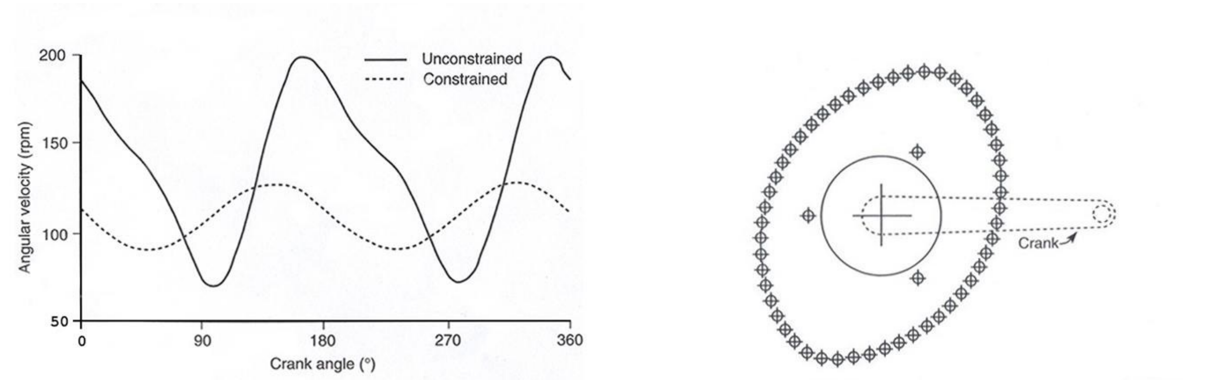

(a) Angular velocity profile for a cyclist for both a constrained and unconstrained angular velocity profile

(b) Chainring shape for a constrained angular velocity profile

Figure 21: Two different types of angular velocity profiles dependent on the chainring shape [39]

Figure 21(a) was used to determine the maximum amplitude as a function of the average angular velocity. Using the same method as for equation 5.42 an equation was found for the angular velocity:

$$\omega_{pedal} = A \cdot \cos(n \cdot t + \phi) + B \tag{5.43}$$

$$\omega_{pedal} = -0.69 \cdot \cos(2\pi t + \phi) + \pi \tag{5.44}$$

Variable	Symbol	Quantity
Amplitude	A	-0.69
Period	n	$2 \cdot \pi$
Phase shift	ϕ	$-$
Mean Value $\bar{\omega}$	B	π

Table 5: Quantities of the variables

To find the output torque of the oscillating point of rotation the Power Equality Law can be used, stating that no energy can be created or destroyed:

$$P = \tau \cdot \omega \tag{5.45}$$

$$P_{in} = P_{out} \rightarrow \tau_{in} \cdot \omega_{in} = \tau_{out} \cdot \omega_{out} \tag{5.46}$$

$$\tau_{out} = \tau_{pedal} \frac{\omega_{pedal}}{\omega_{crank}} \tag{5.47}$$

Both τ_{pedal} and ω_{pedal} are known functions and ω_{crank} can be determined using SolidWorks, hence τ_{out} can be determined. The torque applied by the flipper follows from equation 5.24 and has been determined to be:

$$\tau_{flipper} = 29.11 \cdot \omega^2 r^6 \tag{5.48}$$

It is desirable to have an output torque τ_{out} equal to the flippers torque $\tau_{flipper}$, as this will result in a smooth cycling motion without having any "dead" points or points in which extra force has to be generated. Having $\tau_{out} > \tau_{flipper}$ will result in having less resistance, leading to a possible "overshoot"; $\tau_{out} < \tau_{flipper}$ on the other hand will lead to the cyclist having to excert extra force, also leading to an uncomfortable motion. Since the only variables are the flipper length r and phase shift ϕ in the angular velocity ω_{pedal}, those are the variables to be optimized. Figure 22 shows 4 different configurations for which r has been optimized while keeping $\phi = 0$. It has been chosen for $\tau_{flipper}$ not to exceed τ_{out} and the sizes have been chosen as 60 mm is roughly $\frac{1}{3}^{rd}$ the crank length, 170 mm is equal to the crank length, 340 mm is twice the crank length and 600 mm is roughly 3.5 times the crank length.

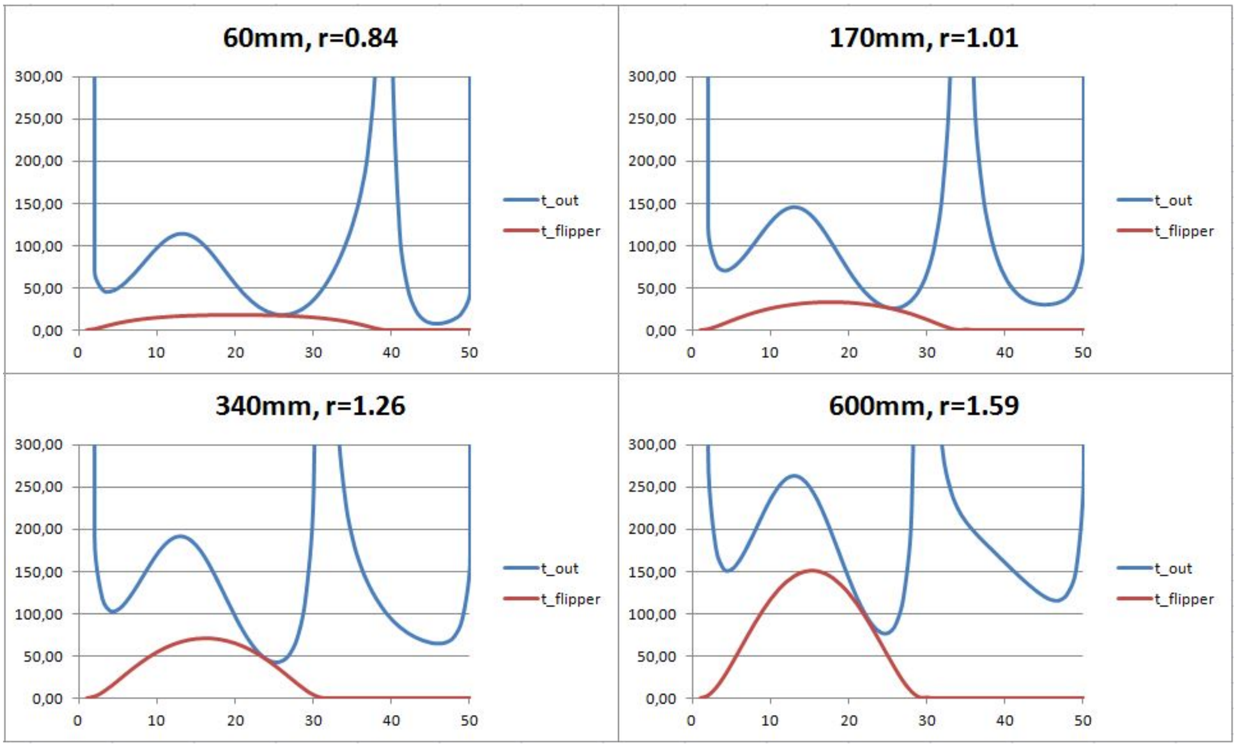

Figure 22: 4 Different configurations for which the flipper length r has been optimized. The vertical axis shows the torque in Nm and the horizontal axis shows one full rotation in 50 steps.

It is to be observed that due to a drag coefficient $C_D = 0$ for the symmetric hydrofoil the torque $\tau_{flipper}$ is equal to 0 during the return stroke; this of course is not realistic and has to be taken into consideration in the detailed design. The output torque τ_{out} shows values going to ∞ as the angular velocity of the crank ω_{crank} goes to 0 in equation 5.45. Obviously this shall not happen for a real mechanism as forces such as momentum and inertia forces will be present and work on the mechanism. The 4 different configurations show a difference in the output torque. It can be explained that having a lower angular velocity as a result of a lower angular deflection leads to a higher torque, as $P = \tau \cdot \omega$ and P has a non-zero value and is the same for all 4 configurations.

The fourth configuration with a length of 600 mm between point (1) and (2) in figure 14(c) leads to the best fitting torque profile, yet still shows a big difference between τ_{out} and $\tau_{flipper}$. It is chosen not to increase this length as this will lead to an undesirably large mechanism.

Feathering Motion Similar to concept 2, the angular displacement during the power stroke has been determined to be 90°. During the return stroke the angular displacement has been determined to be 0°. Therefore the fin must be able to rotate over a range of 90°. The mechanism to allow for this rotation shall be determined in section 6.

6 Detailed Design

6.1 Flipper Morphology

Little research has been done concerning sea turtles' front flipper morphology. Sun, X. et al. have designed a prosthetic left flipper for an injured sea turtle *(species: Caretta Caretta)* of which the projected top area is presented in their paper, see figure 23; Davenport, J. et al. have done some research into the cross sectional area of the front flipper. [5][20] Furthermore photos and videos of swimming sea turtles are used to give more insight into the contour and cross-sectional area of the front flipper. [40][41] This knowledge shall be used to design a flipper used for the concepts presented.

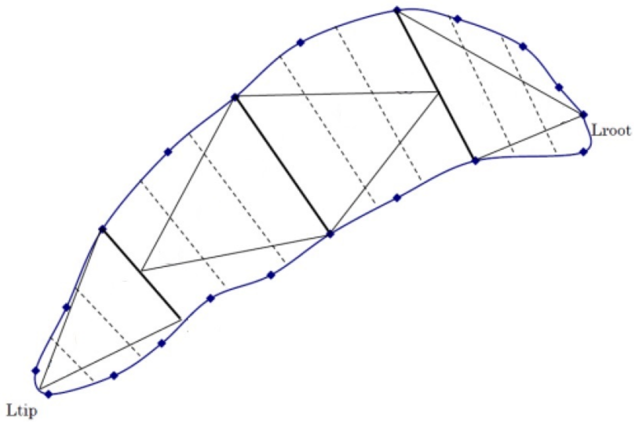

Figure 23: Projected top area of the left front flipper for a *Caretta Caretta* species sea turtle [20]

6.1.1 Flipper Design in SolidWorks

The image of the projected top area of the left front flipper was imported in CorelDraw X6 and converted to a vector image. This image subsequently was imported in SolidWorks. The vector image was used to trace the contour of the flipper which then was used as a base to design the artificial flipper. Different cross-sections of the flipper were designed for different parts of the flipper, after which a loft was used to smoothly fill in the contour of the entire flipper. Different cross-sections are to be found in figure 24 to give an idea of the morphology.

As is to be observed the proximal part of the flipper has a heavily cambered cross-section, as seen in figure 24(b) and 24(c). This corresponds with the sea turtle's front flipper morphology and follows from the presence of the humerus and radius/ulna together with the muscles involved. The distal part of the flipper consists mainly of the phalanx bones, which are much smaller in diameter and do not show any muscular tissue. [42][43] Hence, the cross-section of this part is more symmetrical and less cambered in shape, as seen in figure 24(d) and 24(e).

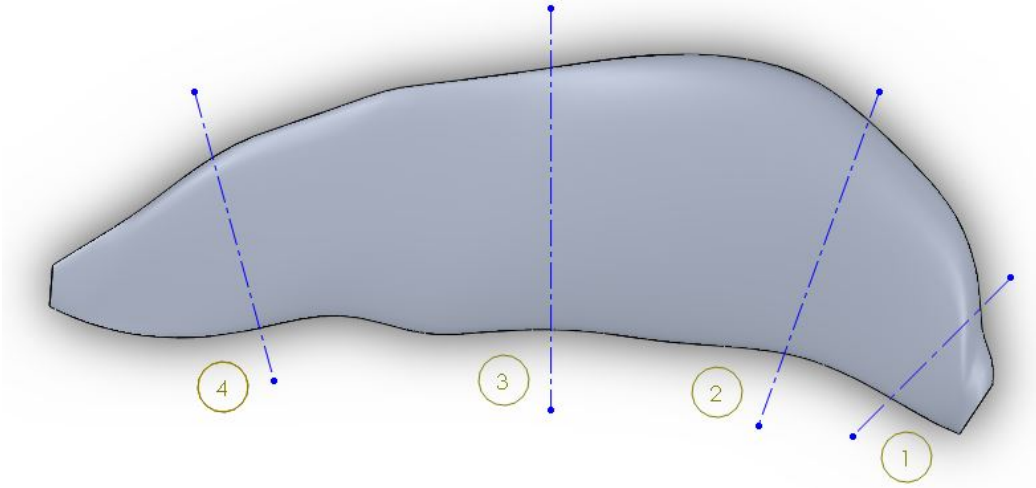

(a) Top area of the flipper with corresponding positions of the cross-sections

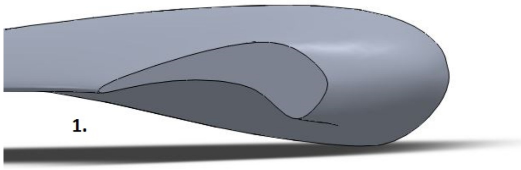

(b)

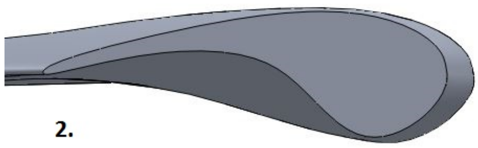

(c)

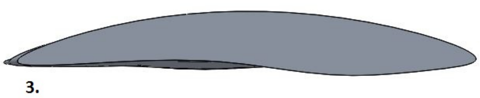

(d)

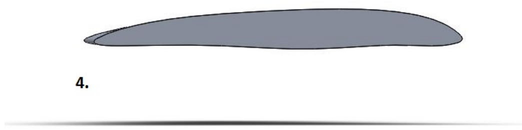

(e)

Figure 24: 4 Cross-sections of the flipper design

6.2 Feathering Mechanism

In order to decrease work, a feathering mechanism feasible for all three concepts has been thought of. By changing the dimensions the mechanism can be altered to fit for each concept. Figure 25 shows the mechanism which enables the feathering motion.

Hole (1) is where the rotating axis of the flipper is to be attached and might consist of a bearing to reduce friction; the angular deflection is limited by the two bars (2) and can be adapted depending on the desired angular deflection. Boss extrude (3) can either be present or not, for concept 1 this plate can be used to protect the leg from the user during rotation of the flipper, as a pin will be moving up an down between the two bars (2), close to the leg. Boss extrude (4) can be used to attach to either the leg of the user in concept 1 or to the oscillating axis of rotation in concept 2 and 3.

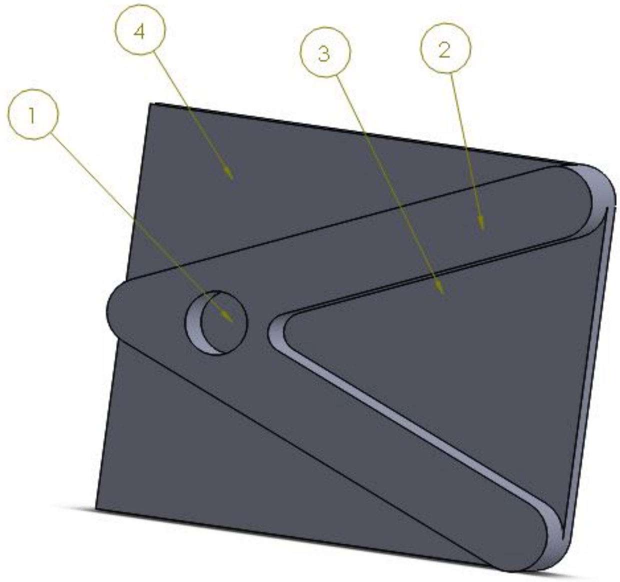

Figure 25: The feathering mechanism. The hole (1) is the point of rotation for the flipper; the inclined bars (2) restrict the movement of the flipper.

To be able to control in which direction the flipper rotates during the power- and return stroke, the hydrodynamic center of the flipper has to be determined. For a symmetrical airfoil this point is approximately at $1/4^{th}$ chord length, measured from the leading edge. [44] For a non-symmetrical hydrofoil this is only an approximation, as is the case for the flipper. It is therefore chosen to have the point of rotation either near the leading edge or at 1/2 chord length, depending on which way the flipper should rotate. Should the point of rotation be at 1/2 chord length the flipper is likely to rotate in the wrong direction during the return stroke, putting the trailing edge forward instead of the leading edge. This can be prevented by adding a weak torsional spring at the point of rotation, helping the flipper to rotate in the right direction.

The mechanism as a whole is presented in figure 26, showing the flipper (1), a metal strip to which the flipper is attached (2) which in this example ensures that the point of rotation (3) lies in front of the hydrodynamic center. This strip then is attached to the feathering mechanism (4).

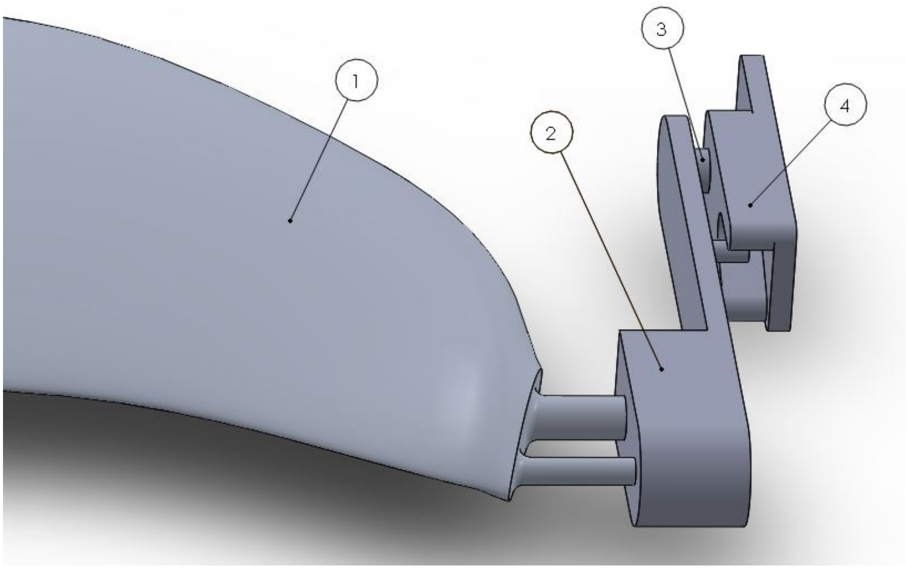

Figure 26: The flipper (1) attached to a strip (2) ensuring that the point of rotations (3) lies near the leading edge. The strip is attached to the feathering mechanism (4).

6.3 Analysis in SolidWorks

The flipper as designed shall be analyzed in SolidWorks to determine the lift and drag coefficient. The shear stress as a result of the fluid shall be determined as well to see if the flipper shows susceptible points.

The analytical calculations of the concepts shall be redone with the new found values; the stresses in the mechanisms of each concept shall be determined to see whether the concepts are feasible or if adaption of the design is needed.

6.3.1 Computational Fluid Dynamics

A computational fluid dynamics analysis will be carried out in SolidWorks. The results will be discussed in this section.

6.3.1.1 Lift and Drag Coefficient

To find the lift- and drag coefficient of the artificial flipper a CFD-analysis has been carried out in SolidWorks. To give accurate results the following assumptions were made:

- Following from the results in section 5 a flipper with a length of 1.1 m is assumed.
- Following from the assumptions in section 5 the chord length is $\frac{1}{4}r$, complying with a length of 0.275 m.
- Since the flipper motion is rotational, the mean velocity occuring at $\frac{1}{2}r$ with $\omega = 1.05\ rad/s$ is taken as the free stream velocity. This complies with a free stream velocity of 0.58 m/s.
- The device is assumed to be used in water temperatures of $20°C$, hence the kinematic viscosity of water at this temperature is used. [45]

The Reynolds Number used in the analysis follows from:

$$Re = \frac{V \cdot c}{\mu} \tag{6.1}$$

$$= \frac{0.58 \cdot 0.275}{1.004 \cdot 10^{-6}} \tag{6.2}$$

$$= 158\ 865$$

The analysis was carried out with SolidWorks Flow Simulation for angles of attack ranging from $\alpha = -40°$ to $\alpha = 100°$ with a step size of 4°. Since the applied method is not straightforward, explanation of the exact methods used are to be found in Appendix A. The result of the analysis are to be found in figure 27.

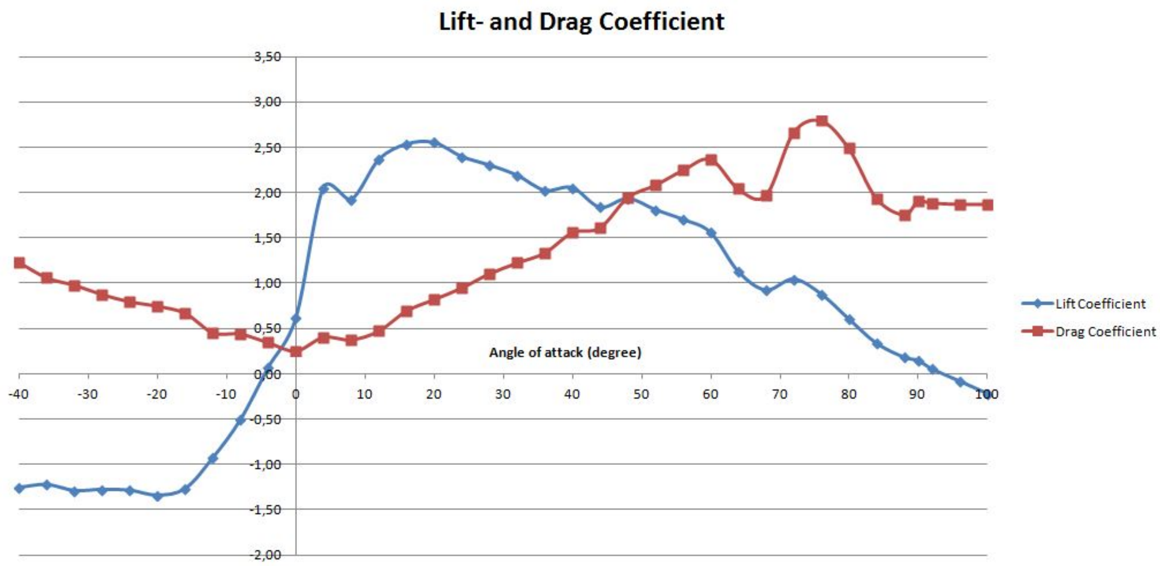

Figure 27: The lift and drag coefficient as a function of the angle of attack

It is to be observed that for the lift coefficient a small dip is present at 8°. A similar dip is to be observed for both the lift- and drag coefficient at 64° and 68°. Those dips might be present either as a possible error due to the limitations of the accuracy of the software or as a result of the highly non-uniform shape of the hydrofoil. The foil does not behave like the foil assumed in section 5.1.1, figure 7, which is a uniform and symmetrical foil and thus shows a symmetrical drag- and lift profile. Furthermore this foil generates zero lift at $-5°$ and stalls at 20°. When considering a negative angle of attack, the lift coefficient remains stable from $\alpha = -16°$ while the drag coefficient increases.

A velocity profile and pressure profile are given in figure 28 for angles of attack of 0°, maximum lift at 20° and maximum drag at 76° at the cross section where the hydrofoil has the biggest camber.

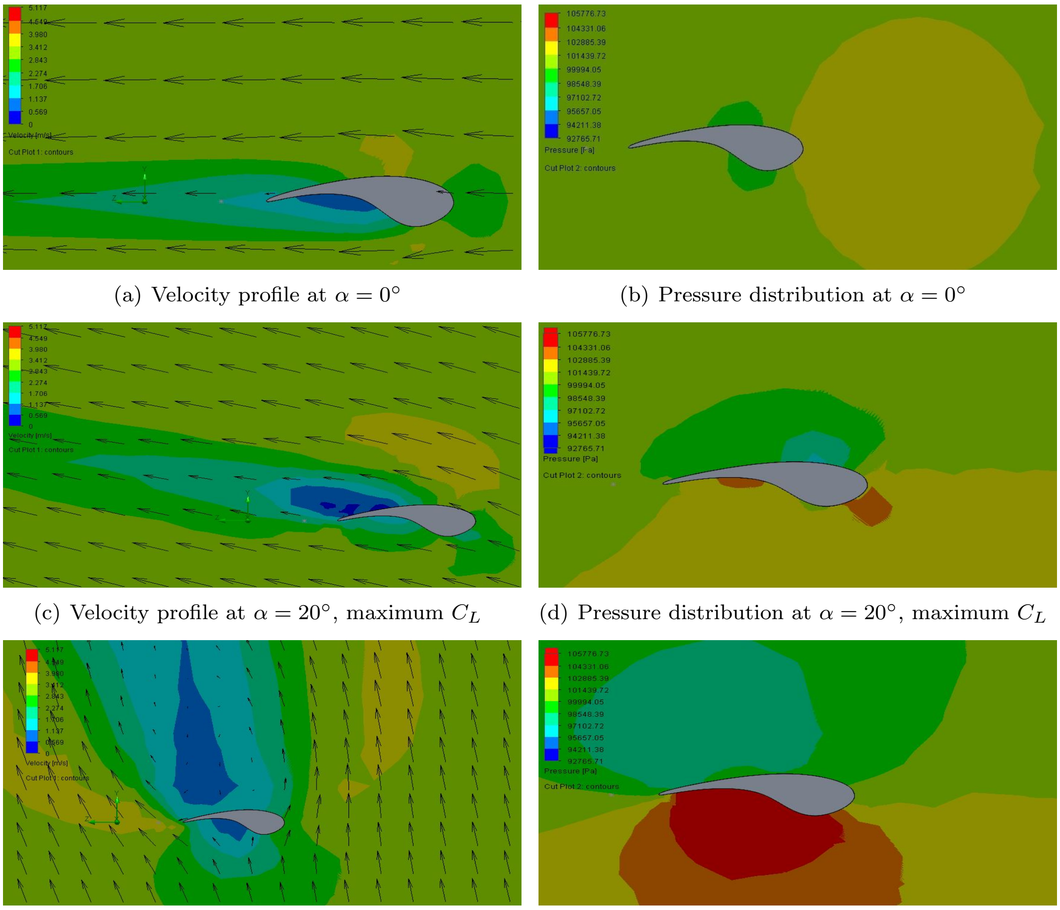

(a) Velocity profile at $\alpha = 0°$

(b) Pressure distribution at $\alpha = 0°$

(c) Velocity profile at $\alpha = 20°$, maximum C_L

(d) Pressure distribution at $\alpha = 20°$, maximum C_L

(e) Velocity profile at $\alpha = 76°$, maximum C_D

(f) Pressure distribution at $\alpha = 76°$, maximum C_D

Figure 28: Velocity profiles and pressure distribution at zero angle of attack, maximum C_L and maximum C_D

It is clearly visible that the hydrofoil section shows a wake even at an angle of attack of $\alpha = 0°$, which is to be explained by having a heavily cambered hydrofoil. The same holds for the non-symmetrical pressure distribution, which is to be explained as a result of the camber.

6.3.1.2 Shear Stress on the Flipper

The artificial flipper experiences shear stresses as a result of the forces acting upon it. Figure 29 shows the maximum shear stress occuring at an angle of attack of $\alpha = 76°$, at which the cumulative forces acting upon the flipper are the highest.

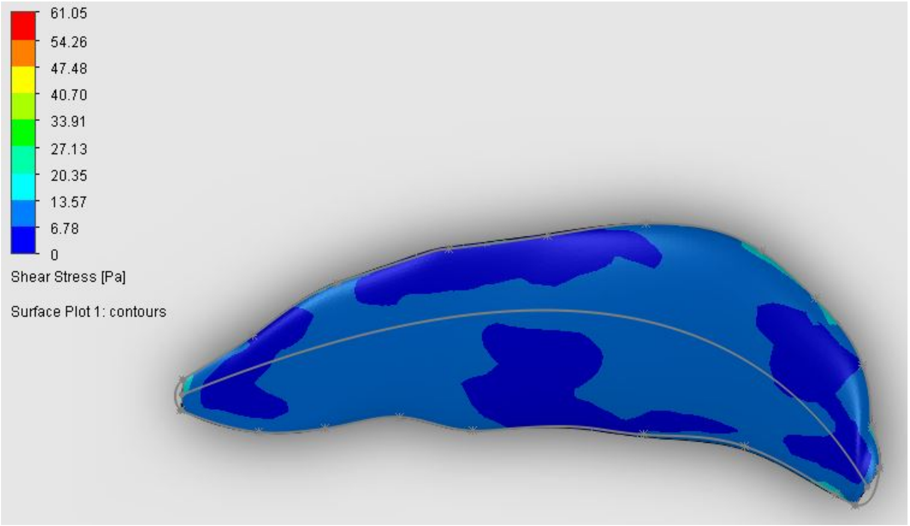

(a) Shear stress acting upon the top of the flipper

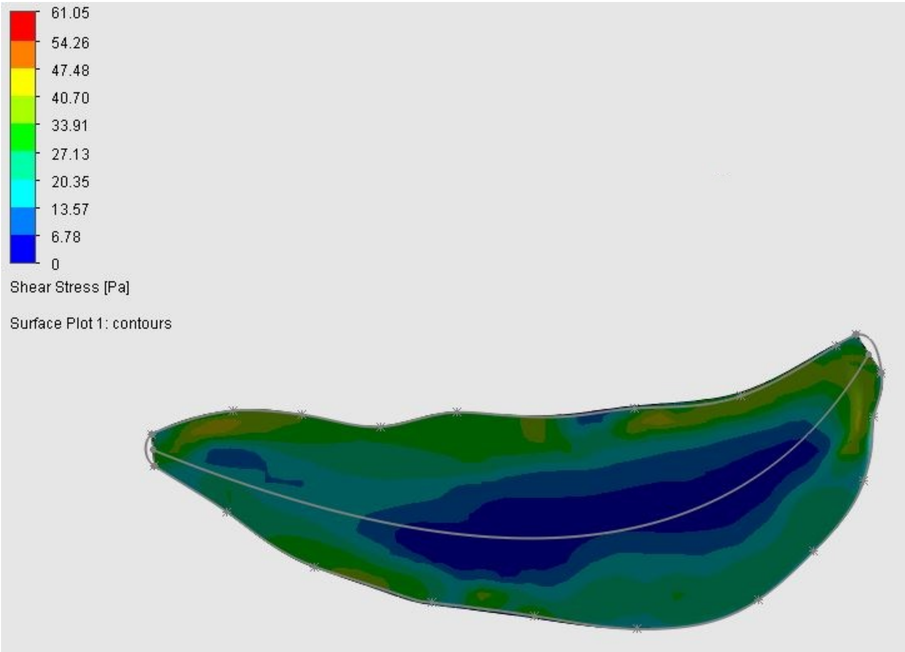

(b) Shear stress acting upon the bottom of the flipper

Figure 29: Shear stress profile of the flipper at an angle of attack of 76°

The maximum shear stresses as a result of the free stream are present at the bottom of the flipper, located on the trailing edge near the attachment to the mechanism. This can be explained due to the fact that the pressure has the highest value at this point (see figure 28(f)) and the flipper is thin at the trailing edge, thus leading to higher shear stresses. This simulation considers a uniform free stream velocity, whereas the free stream velocity of a rotating flipper is a function of the width of the flipper. However the shear stresses as a result of the free stream are considered small enough to cause no problems in the design.

6.3.2 Analytical Calculations

Using the data acquired from the SolidWorks analysis, the values for the torque, thrust and drag and flipper dimensions can be calculated.

6.3.2.1 Concept 1 The calculations from section 5.1.2 can be redone with the found values to find the maximum amount of thrust generated as well as the torque acting upon the legs of the user. The same design criteria are used as in section 5.1.2.

Torque Using the lift coefficient calculated in the previous section and equations 5.10 and 5.11 derived in section 5.1.2, the force profile of the flipper as a function of the angle of attack can be determined. Figure 30 shows that only a small range of angles of attack lead to a positive value for the thrust, with a maximum at $\alpha = 20°$.

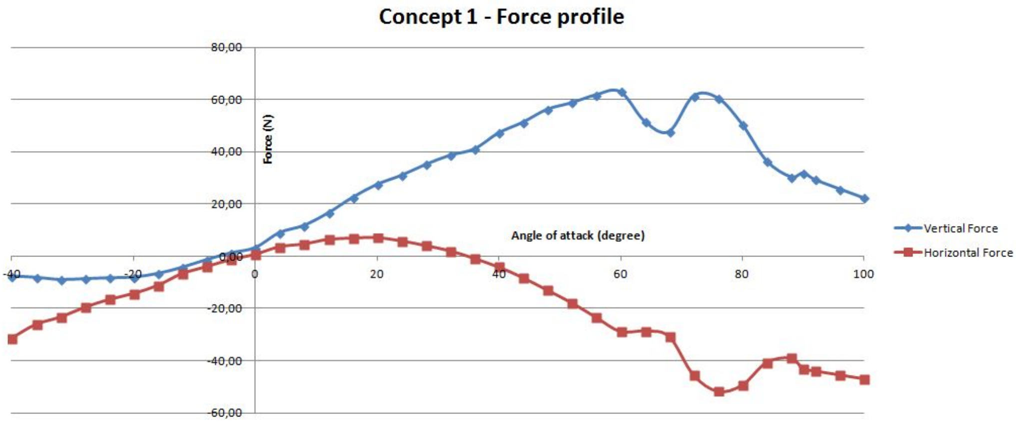

Figure 30: Force profile for the flipper. A negative horizontal force indicates drag.

The vertical force at $\alpha = 20°$ is 27.6 N. The expected torque becomes:

$$\tau = \frac{1}{2}\omega l^2 \tag{6.3}$$
$$= \frac{1}{2} \cdot 27.6 \cdot 0.5^2$$
$$= 3.45\ Nm \tag{6.4}$$

The found torque is roughly 10 times as big as the torque calculated in section 5.1.2 and might be explained by having both a higher lift- and drag force, leading to a higher vertical force component.

Forward Propulsion The forward propulsion can be derived from figure 30 and is equal to 6.97 N per leg. This value is lower than the values found in section 5.1.2 and can be explained by having a higher horizontal component in the drag force, leading to a lower net horizontal force vector.

The force needed to propel the device can be calculated as follows. As the horizontal- and vertical force vector are orthogonal the total force can be calculated using Pythagoras' law:

$$F_{tot} = \sqrt{6.97^2 + 27.6^2} = 28.5\ N \tag{6.5}$$

Drag and Feathering Motion The free stream velocity during the return stroke has an equal velocity but at a negative inclination of $\gamma = -32°$. To minimize the drag during the return stroke the horizontal force and thus the drag should be 0. According to figure 30 this occurs at an angle of attack of $\alpha = 0°$. The upward force at this angle of attack as a result of the generated lift is 3.37 N, thus slightly reducing the force needed for the return stroke.

The range of the feathering motion is the difference in angle of attack during the power stroke and the return stroke. During the power stroke the angle of attack relatively to the horizontal is $32 - 20 = 12°$; the angle of attack during the return stroke is equal to the inclination of the free stream velocity vector and therefore is 32°. The total rotational movement thus needs to be $12 + 32 = 44°$.

The point of rotation for the flipper should be behind the hydrodynamic center, as a positive angle of attack is desired during the power stroke. A torsional spring in the axis of rotation can ensure that the leading edge rotates forward during the return stroke.

6.3.2.2 Concept 2

The calculations from section 5.1.3 can be done with the found values to find the maximum amount of thrust generated during the power stroke as well as the drag force generated during the return stroke.

Power Stroke The maximum thrust occurs at an angle of attack of $\alpha = 76°$ with a thrust coefficient of $C_T = 2.80$. Equations 5.22 and 5.24 are used to calculate the amount of torque as a function of the flipper size, substituting $\bar{A} = r \cdot c \sin\alpha$, $\sin\alpha = 0.970$ for $\alpha = 76°$ and $V(r) = \omega r$. Using SolidWorks it is determined that the ratio between the chord length and the length of the flipper is $c = 0.249 \cdot r$. The thrust and torque now become:

$$\begin{aligned} T &= \frac{1}{2}\rho\bar{A}C_T V^2(r) \qquad (6.6)\\ &= \frac{1}{2} \cdot 998 \cdot 0.242 \cdot r^2 \cdot 2.8 \cdot (1.05 \cdot r)^2 \\ &= 372.17 \cdot r^4 \end{aligned}$$

$$\begin{aligned} \tau_{flipper,thrust} &= \int T \cdot r \ dr \\ &= 365.21 \int_0^r \left(r^4\right) \cdot r \ dr \\ &= 365.21 \ |_0^r \frac{1}{6} r^6 \\ &= 62.03 \cdot r^6 \qquad (6.7) \end{aligned}$$

Variable	Symbol	Quantity [-]
Fluid Density	ρ	$998 \ kg/m^3$
Projected Area	$\bar{A}$	$0.237 \cdot r^2 \ m^2$
Thrust Coefficient	C_T	2.8
Velocity	$V(r) = \omega r$	$1.05 \cdot r \ rad/s$

Table 6: Quantities of the variables

Return Stroke It is desirable to have a drag- and lift coefficient which are as low as possible during the return stroke, as this will be in favor of the amount of energy which can be stored in the spring. The drag coefficient is lowest at an angle of attack of $\alpha = 0°$ being $C_D = 0.25$, however the flipper does generate lift at this angle of attack with a lift coefficient of $C_L = 0.62$. It is thought of that the flipper's connection to the axis of rotation is rigid in this dimension, thus only the drag has to be overcome during the return stroke. The projected area $\bar{A}$ is dependent on the flipper width r and thickness t; using SolidWorks it was found that the projected area $\bar{A}$ can be determined as $\bar{A} = 4.54 \cdot 10^{-2} \cdot r^2$. The drag force and torque now become:

$$\begin{aligned} D &= \frac{1}{2}\rho\bar{A}C_D V^2(r) \qquad (6.8)\\ &= \frac{1}{2} \cdot 998 \cdot 4.54 \cdot 10^{-2} \cdot r^2 \cdot 0.25 \cdot (1.05 \cdot r)^2 \\ &= 6.25 \cdot r^4 \end{aligned}$$

$$\begin{aligned} \tau_{flipper,drag} &= \int D \cdot r \ dr \\ &= 6.25 \int_0^r \left(r^4\right) \cdot r \ dr \\ &= 6.25 \ |_0^r \frac{1}{6} r^6 \\ &= 1.04 \cdot r^6 \qquad (6.9) \end{aligned}$$

What	Symbol	Quantity [-]
Fluid Density	ρ	$998 \ kg/m^3$
Projected Area	$\bar{A}$	$9.17 \cdot 10^{-3} \cdot r^2 \ m^2$
Thrust Coefficient	C_D	0.25
Velocity	$V(r) = \omega r$	$1.05 \cdot r \ rad/s$

Table 7: Quantities of the variables

Flipper Dimension The energy which can be stored in the spring is equal to the torque which is delivered by human force minus the torque as a result of the drag. Using the equilibrium equation (equation 5.15) for this mechanism together with the input force the energy which can be stored in the spring can be calculated. For the return stroke, using the values found in section 5.1.3, the deliverable torque becomes:

$$\tau_{return\ stroke} = \frac{(a \cdot F_{input})\,c}{b} \tag{6.10}$$

$$= \frac{(0.57 \cdot 86) \cdot 0.1}{0.1} \tag{6.11}$$

$$= 49.0\ Nm$$

Combining with τ_{spring} and $\tau_{flipper,drag}$ gives the amount of torque which can be delivered by the spring:

$$\tau_{spring} = \tau_{return\ stroke} - \tau_{flipper,drag} \tag{6.12}$$

$$= 49.0 - 1.04 \cdot r^6 \tag{6.13}$$

The torque delivered by the spring in equation 5.15 is defined as $0.1 \cdot k\Delta x$. By substituting equation 6.13 in equation 5.15 the torque during power stroke can be determined:

$$\tau_{power\ stroke} = \frac{(a \cdot F_{input} + b \cdot k\Delta x)\,c}{b} \tag{6.14}$$

$$= \frac{\left(0.57 \cdot 81 + 49.0 - 1.04 \cdot r^6\right) \cdot 0.1}{0.1} \tag{6.15}$$

$$= 95.2 - 1.04 \cdot r^6\ Nm \tag{6.16}$$

Since the torque generated by the user is equal but opposite to the torque generated by the flipper, the length r can be solved by setting both equations equal to each other:

$$62.03 \cdot r^6 = 95.2 - 1.04 \cdot r^6 \tag{6.17}$$

$$r^6 = 1.56 \tag{6.18}$$

$$r = \sqrt[6]{1.56} \tag{6.19}$$

$$= 1.08\ m$$

The maximum size of the flipper would be 1.08 x 0.27 m, which complies accurately with the dimensions found in section 5.1.3. Reasonings that the results are comparable can be found in the 6^{th} order power in r; $\sqrt[6]{x}$ converges quickly to 1 for small values of x. Furthermore is the torque needed during the return stroke small compared to the torque needed for the power stroke. As a result the energy stored in the spring is just a little less than the found value in section 5.1.3 and hence the total available torque and thus the length r is similar.

It must be taken into consideration that the force distribution in the integral of equations 6.7 and 6.9 consider a uniform force distribution. However, due to the non-uniform shape of the foil the force distribution is also non-uniform and hence the calculated torque remains an approximation.

Forward Propulsion The force available during the power stroke is equal to the force applied by human hand plus the force applied by the spring. In equation 6.10 it has been determined that the available torque is 49.0 Nm. The torque as a result of the drag is equal to $1.04 \cdot r^6 = 1.65\ Nm$. This means that 47.35 Nm is available to store in the spring, which is 96.6% of the total torque, hence of the force applied. As stated in section 5.1.3 the available force during the return stroke is 86 N, substracting the force needed to pull the flipper through the water leaves 83.1 N to store in the spring. This force will be available during the powerstroke as the spring releases the stored energy. The total force during power stroke therefore becomes $81 + 83.1 = 164.1\ N$. As the direction of this force is normal to the flipper surface, the vertical component of the force leading to forward propulsion has to be calculated as follows:

$$F_{forward} = F_{thrust} \cdot \cos\theta \tag{6.20}$$
$$= 164.1 \cdot \cos\theta \tag{6.21}$$

The total amount of forward thrust during one stroke is the integral over the angular displacement:

$$F_{forward,total} = \int_{-\theta=-30}^{\theta=30} 164.1 \cdot \cos \; d\theta\theta \tag{6.22}$$
$$= 2 \cdot \int_{0}^{\theta=30} 164.1 \cdot \cos\theta \; d\theta \tag{6.23}$$
$$= [328.2 \cdot \sin\theta]_0^{\theta=30} \tag{6.24}$$
$$= 164.1 \; N \tag{6.25}$$

Spring Constant The spring constant of the spring can be determined by using $F = k\Delta x$. Since both F and Δx are known, the spring constant can be calculated accordingly:

$$F = k \cdot \sin(\alpha) \cdot b \tag{6.26}$$
$$83.1 = k \cdot 0.087 \tag{6.27}$$
$$k = 960 \; N/m \tag{6.28}$$

Variable	Symbol	Quantity [-]
Force	F	83.1 N
Angular Deflection	α	30 °
Lever length	b	0.1 m

Table 8: Quantities of the variables

Feathering Motion The total angular deflection is the difference in angle of attack during the power stroke and the return stroke. During the power stroke the flipper has an angle of attack of $\alpha = 76°$ and during the return stroke the angle of attack is $\alpha = 0°$. The flipper therefore must be able to rotate over a range of 76°.

As the leading edge of the flipper rotates downwards during the power stroke and upwards during the return stroke, the point of rotation should be in front of the hydrodynamic center. During the return stroke the leading edge automatically returns to the right position, so no additional torsional spring is needed in the axis of rotation.

6.3.2.3 Concept 3 The results from the analysis in SolidWorks will be combined with the values found for the designed flipper to calculate the torque, thust and drag and flipper dimensions.

Forward Propulsion Similar to concept 2, the maximum thrust coefficient is achieved at an angle of attack of $\alpha = 76°$. By optimizing the flipper length r using this thrust coefficient the dimensions of the flipper for the 4 different configurations have been found, as is to be observed in figure 31. It has been chosen for $\tau_{flipper}$ not to exceed τ_{out}.

It is clearly visible that the 600 mm configuration shows the best resemblance between $\tau_{flipper}$ and τ_{out}, although the differences are still significant.

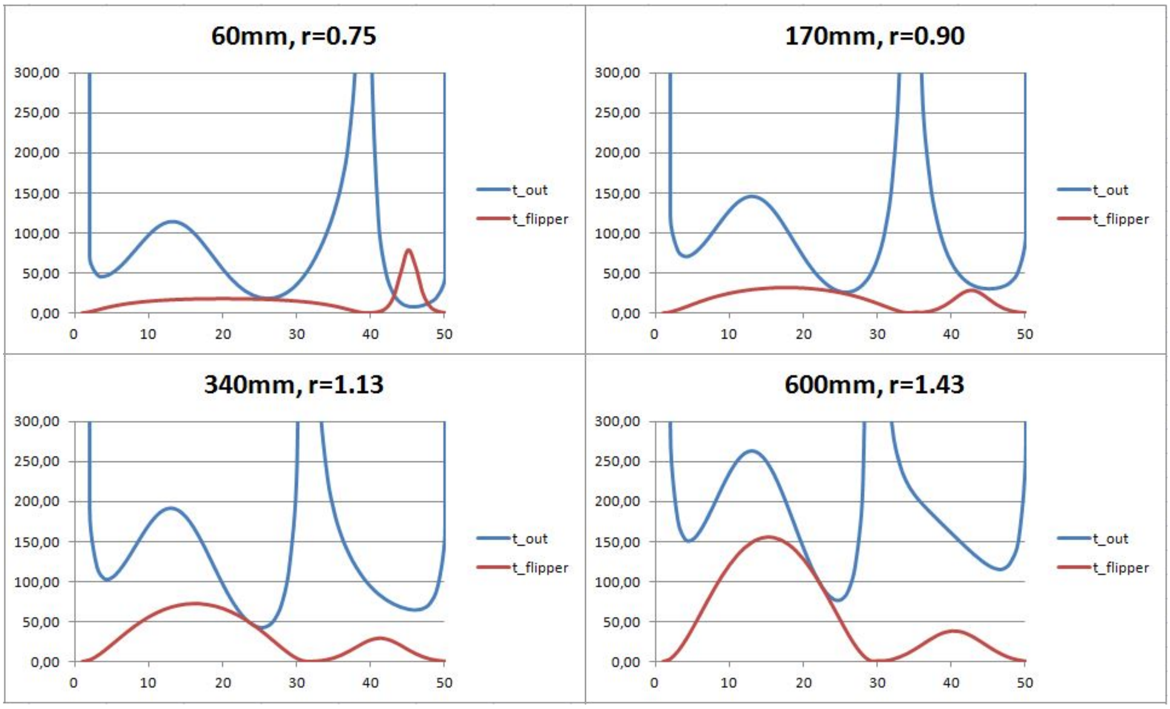

Figure 31: 4 Different configurations for which the flipper length r has been optimized. The vertical axis shows the torque in Nm and the horizontal axis shows one full rotation in 50 steps.

By changing the phase shift ϕ (and thus the initial position of the slitted crank) with 10% from 0 to 0.2π for τ_{out} in order to have a better fit between the two curves, not only a phase shift is present, but both the shape of the curve of τ_{out} and $\tau_{flipper}$ change as well, as is to be observed in figure 32. This is likely due to the fact that both $\tau_{flipper}$ and τ_{out} are dependent on the initial configuration of the mechanism, thus changing ϕ leads to a change in both τ_{out} and $\tau_{flipper}$. Optimization of the system therefore proves to be difficult and cumbersome and is considered outside the scope of this project.

Since this concept shows many difficulties in optimizing, it has been decided to discard this concept for further analysis.

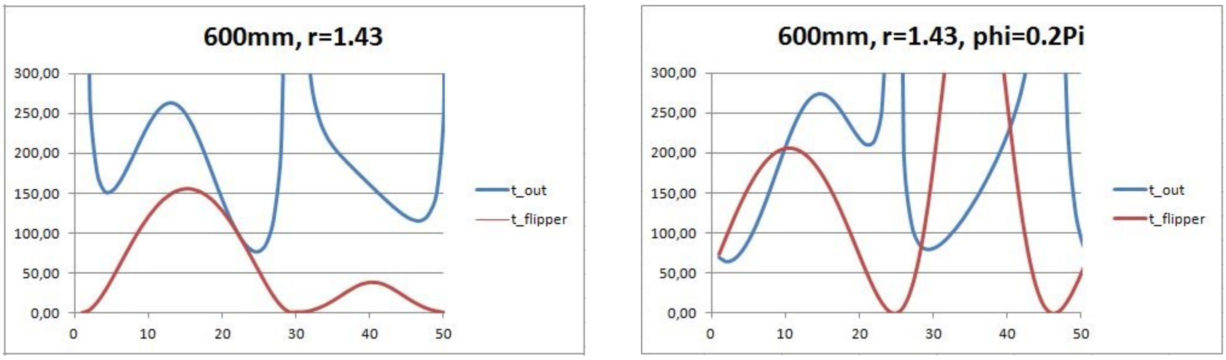

(a) τ_{out} and $\tau_{flipper}$ with no phase shift

(b) τ_{out} and $\tau_{flipper}$ with a phase shift of $\phi = 0.2\pi$

Figure 32: Difference between $\tau_{flipper}$ and τ_{out} by only changing ϕ for the 600 mm configuration

Feathering Motion The total angular deflection is the difference in angle of attack during the power stroke and the return stroke. During the power stroke the flipper has an angle of attack of $\alpha = 76°$ and during the return stroke the angle of attack is $\alpha = 0°$. The flipper therefore must be able to rotate over a range of $\alpha = 76°$.

As the leading edge of the flipper rotates downwards during the power stroke and upwards during the return stroke, the point of rotation should be in front of the hydrodynamic center. During the return stroke the leading edge automatically returns to the right position, so no additional torsional spring is needed in the axis of rotation.

6.3.3 Finite Element Analysis

The Finite Element Analysis shall be carried out on the mechanisms to evaluate the stresses involved during usage. This knowledge shall then be used to optimize the dimensions of the mechanisms and to finally choose a material of which the mechanisms can be produced. For each mechanism the biggest expected force is taken into consideration. The mechanism will be analyzed on stress, deformation and buckling. The flipper will be discussed independently in section .

Materials For each concept three different materials are taken into consideration: two metals for the mechanisms and flipper and a composite for only the flipper. It has been chosen to use relatively cheap and widely available materials. The materials of choice are 5454-H112 aluminum and AISI-316L stainless steel. 5454-H112 Aluminum consists of 94.5-97.14% Al; 2.4 - 3.0% Mg; 0.5-1.0% Mn; 0-0.4%Fe; 0-0.25%Si; 0-0.25% Zn; 0.05-0.2% Cr; 0-0.2% Ti; 0-0.15% residuals and 0-0.1% Cu. [46] AISI-316L stainless steel consists of 65% Fe; 17% Cr; 12% Ni; 2.5% Mo; 2% Mn; 1% Si; 0.045% P; 0.03% S and 0.03% C. [47] Both materials have excellent sea water resistance, are cheap and are easy to process; steel usually is stronger but aluminum has a lower density thus reducing weight. [48][49][50]

For the flipper it is desirable to have a hollow product, as this will greatly reduce the weight. Furthermore the shape is highly non-linear, thus the flipper either has to be casted from aluminum or steel or has to be produced with use of composites. For the composite the widely used and available glass fiber reinforced epoxy composite shall be used. Table 9 shows the material properties of both metals and the glass fiber reinforced epoxy composite. [51][52][53][54][55]

Property	5454-H112 Aluminum	AISI-316L Steel	E-glass/Epoxy Composite
Elastic Modulus	70 GPa	200 GPa	80 GPa
Shear Modulus	26 GPa	82 GPa	39 GPa
Yield Strength	125 MPa	170 MPa	1080/470 MPa*
Density	2690 kg/m^3	8027 kg/m^3	2100 kg/m^3
Fiber/resin ratio	-	-	0.55-0.45
Price per kg.	USD $1.00 - 3.50 per kg.	USD $ 1.00 - 3.50 per kg.	USD $0.25 - 1.25 per kg.

*Unidirectional/multidirectional [56]

Table 9: Material properties for both metals

6.3.3.1 Concept 1

The expected forces working on the flipper are modeled as shown in figure 33(a). Point (1) is the part which is to be attached to the swimmer's leg and therefore is constrained in all directions. The forces have been chosen to be equal to the forces calculated in section 6.3.2 and are 27.6 N in upward direction and 6.97 N in forward direction, as shown by the purple arrows.

As it is undesirable to have a solid flipper due to the weight, a hollow model is used instead. SolidWorks is unable to create a shell of the solid flipper due to the geometry. However SolidWorks is able to create a shell mesh with a prescribed thickness, using thin shell elements. The model is meshed as shown in figure 33(b); the gray mesh represents a solid structure and the orange mesh represents a shell structure.

As a choice of design the thickness of the flipper has been chosen to be 3 mm; the details of the dimensions of the other parts are to be found in Appendix B.

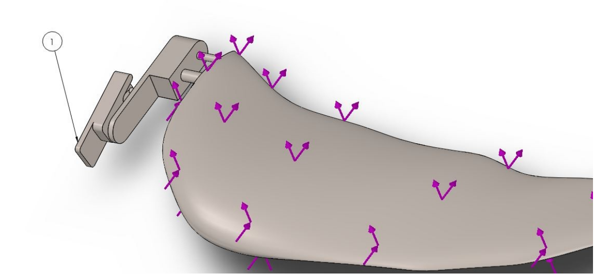

(a) Force distribution on the flipper. Point (1) is constrained in all directions.

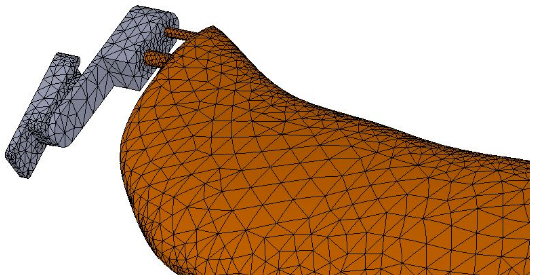

(b) Visualization of the mesh. The gray mesh is a solid mesh and the orange mesh indicates a thin shell mesh.

Figure 33: Model used in SolidWorks for the static analysis

Stress Figure 34 shows the stress distribution as a result of the applied force. It can be seen that the biggest stress occurs at the metal strip, connecting the flipper to the feathering mechanism and at the feathering mechanism. This was to be expected, as the torque as a result of the force acting upon the flipper is large at this point. The point of rotation (1) shows the largest stress being 88 MPa; which remains well below the yield strength of both aluminum and steel.

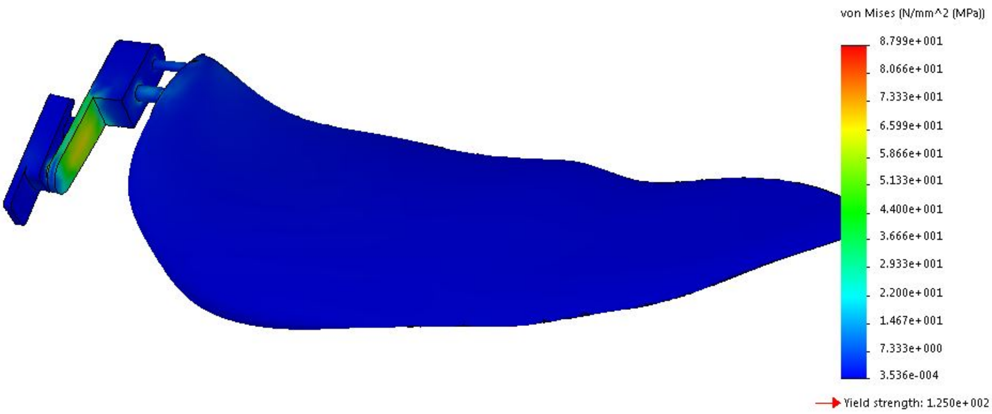

(a) Stress distribution along the mechanism

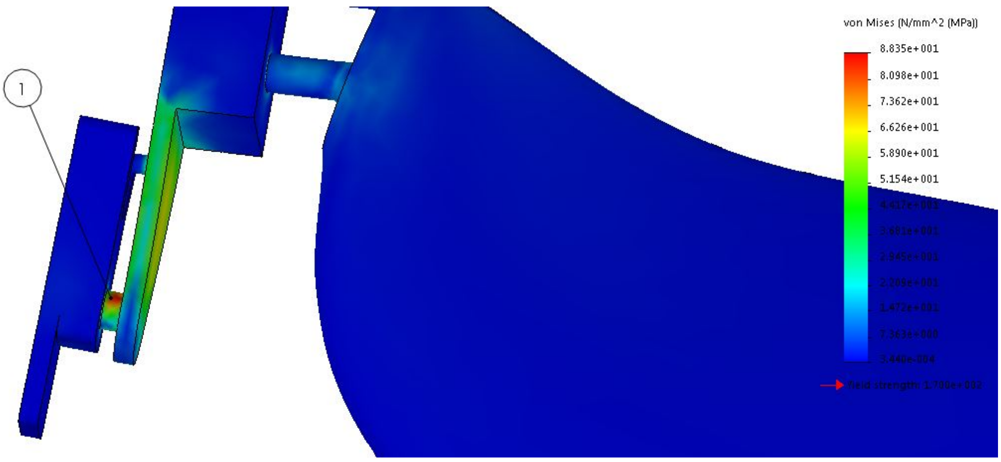

(b) Local stress distribution showing the highest stresses

Figure 34: Stress distribution in the mechanism

Deformation Figure 35 shows the displacement as a result of the deformation of the mechanism. It is clearly visible that the tip of the flipper has the highest deflection; this however is as a result of the strain occurring at the strip connecting the flipper to the feathering mechanism, as is to be observed in figure 35(c). The aluminum mechanism shows a deflection of 10 mm and the steel mechanism shows a deflection of 3 mm, both in vertical direction. This can be explained by the torsion shown by the strip. Thickening the material should decrease the deformations. However, the deformations fall within the limit of max. 10 mm and the design appears to be feasible. As calculated by SolidWorks, all deformations are expected to be elastic.

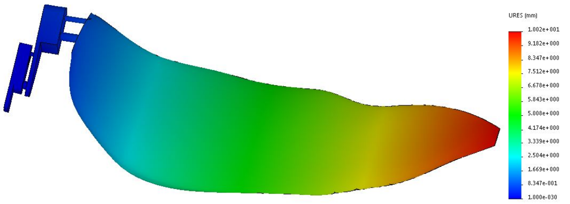

(a) Displacement as a result of the deformation of the aluminum mechanism

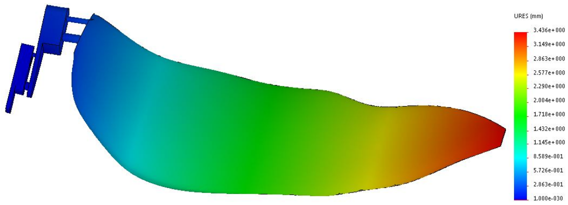

(b) Displacement as a result fo the deformation of the steel mechanism

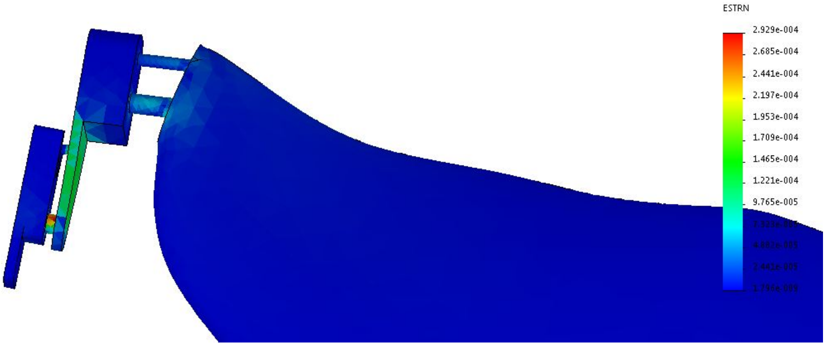

(c) Strain in the aluminum mechanism

Figure 35: Displacement of the mechanism as a result of the applied force

Buckling As buckling is considered as undesirable behavior, a buckling analysis has been performed in SolidWorks. Figure 36 shows the result for both the aluminum mechanism and the steel mechanism. SolidWorks has a threshold for the Buckling Load Factor (BFL), which has to be larger than 1 to prevent buckling. The calculated BLF for the different materials are as follows: aluminum (78.3), steel (227.7). The mechanism therefore is considered safe enough to prevent buckling.

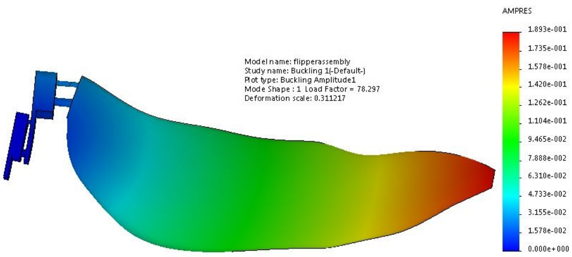

(a) Buckling analysis for the aluminum mechanism

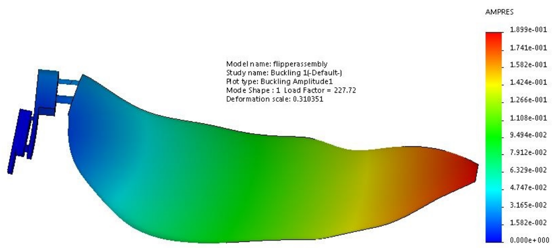

(b) Buckling analysis for the steel mechanism

Figure 36: Buckling analysis for both materials

6.3.3.2 Concept 2

Even though the mechanism is designed for low-frequency high-repetitive motions, it is to be expected that users will try to go as fast as possible, exerting forces up to 330 N. [29] During the power stroke the energy stored in the spring is released which is, following from equation 6.28, equal to a force of 83 N. Besides the forces during regular usage, a maximum expected force of 500 N is modeled in SolidWorks: 400 N for the human force and 100 N for the spring force; this ensures that the mechanism is able to withstand the forces. The stress analysis shall be carried out for the maximum forces; the deformation analysis shall be carried out for the forces during normal usage, as the mechanism is designed for normal usage.

Figure 37(a) shows the setup of the analysis. As the stresses and deformation of the handlebar and horizontal bar are the points of interest, both points of rotation (1) and (2) are fixed to the ground. Point (1) provides the point of rotation and point (2) in this case has been constrained in all directions. The purple arrows show the direction of the force; during the pushing phase the direction of the arrows on the handlebar are reversed, but the force of the spring keeps acting in the same direction. Note that the spring is not modeled as a part, but as a force instead. The model is meshed as shown in figure 37(b).

As a choice of design the bars are modeled as $3x1$ cm solid bars; the handlebar has a length of 20 cm and is a 3 cm diameter solid bar. The hinge point (1) is designed as a 1 cm diameter hole with a 1 cm diameter pin. For the technical drawings, see Appendix C.

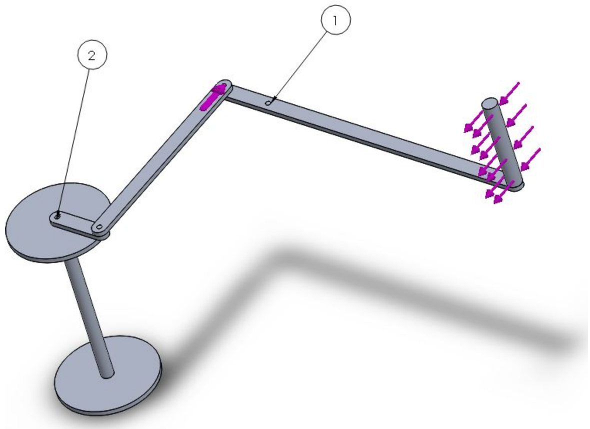

(a) Setup for the static analysis. Points (1) and (2) are fixed and the purple arrows indicate the direction of the force.

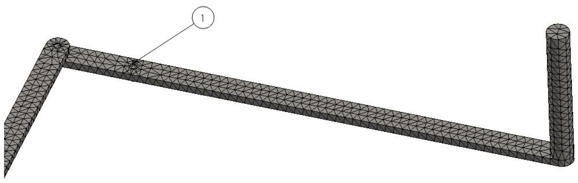

(b) Visualization of the mesh of the region near point (1)

Figure 37: Model used in SolidWorks for the static analysis

Stress Figure 38 shows the stress distribution as a result of the applied force. It is to be observed that even though the bars are able to withstand the maximum stresses for both the aluminum and steel configuration, the pin at (1) in figure 37 shows significant stresses well exceeding the maximum yield stress for both aluminum (125 MPa) and steel (170 MPa), whereas stress values of the handlebar and horizontal bar remain lower than the yield stress. Adaptation of either the dimensions of the pin or the choice of material has to be done in order to prevent failure of the component.

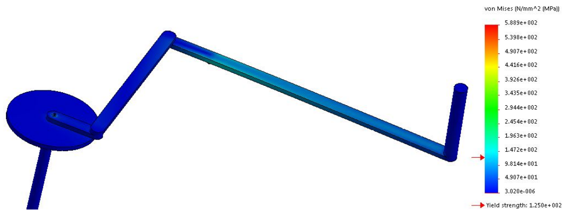

(a) Stress distribution during pulling action

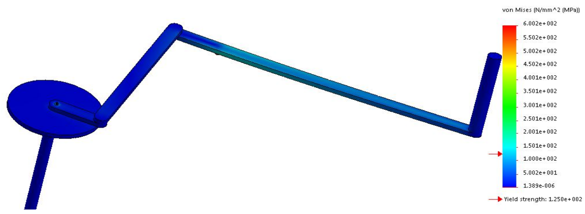

(b) Stress distribution during pushing action

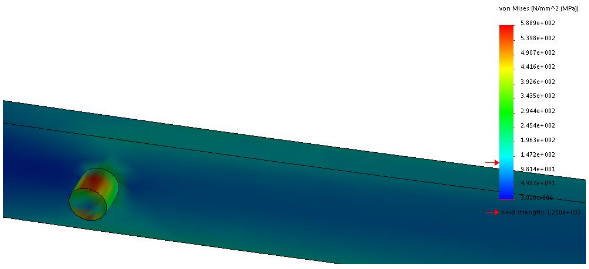

(c) Close-up of maximum stress during pulling action

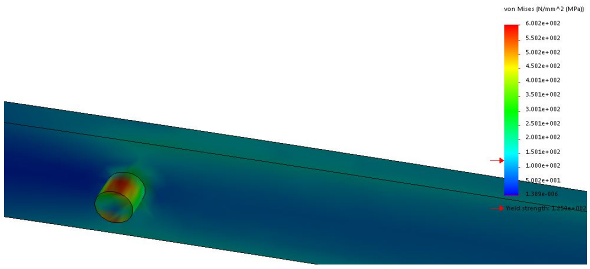

(d) Close-up of maximum stress during pushing action

Figure 38: Stress distribution in the mechanism during pulling- and pushing action

Deformation Figure 39 shows the deformation as a result of the maximum applied force of 400 N. It is to be observed that the deformation is considerably large for both materials: 67 mm for the aluminum mechanism and 23 mm for the steel mechanism, occurring at the tip of the handle bar and both slightly larger during the pushing action than during the pulling action. The displacement of the tip of the horizontal bar is approximately half the size of the maximum displacement, leading to a displacement of 33 mm for the aluminum mechanism and 11 mm for the steel mechanism. As calculated by SolidWorks, all deformations are expected to be elastic. This however does not hold for the pin (1), which has to be redesigned. The deformations occur uniformly along the horizontal bar, as the strain is uniformly distributed; the displacement of the tip of the handlebar is mainly due to torsion of the horizontal bar.

When simulated with a force of 81 N, as is to be expected during regular usage, the deformation decreases to 6 mm at the tip of the handlebar and 3 mm at the tip of the horizontal bar for the steel mechanism, which complies well with the requirement of a maximum deflection of 10 mm. For the aluminum mechanism the deflection however is 17 mm at the tip of the handlebar and 8 mm at the tip of the horizontal bar, which is still considered to be too large, and the dimensions of the mechanism have to be adapted.

By changing the dimensions of the horizontal bar from $3x1$ cm to $6x2$ cm and the diameter of the handlebar to 4 cm, the deflections for the aluminum mechanism decrease to 9 mm for the tip of the handlebar and 6 mm for the tip of the horizontal bar, which are well within the boundaries of the required 10 mm.

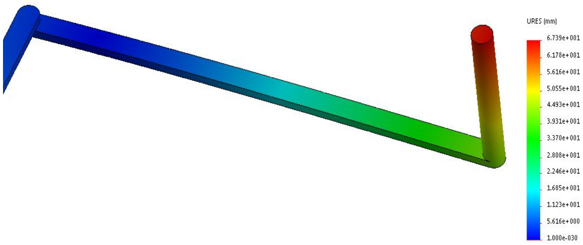

(a) Displacement as a result of the deformation during pulling action for the aluminum mechanism

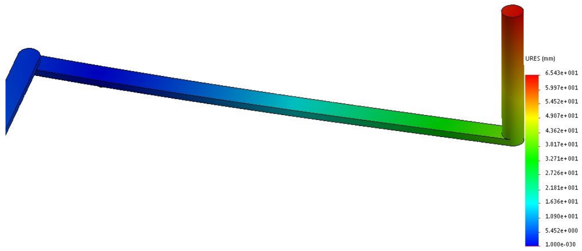

(b) Displacement as a result of the deformation during pushing action for the aluminum mechanism

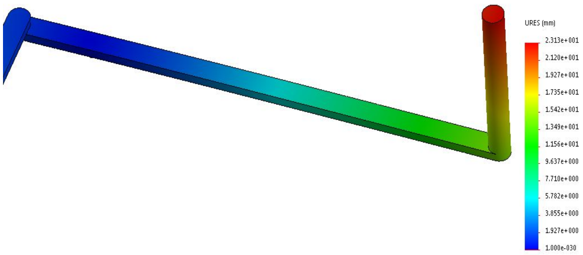

(c) Displacement as a result of the deformation during pulling action for the steel mechanism

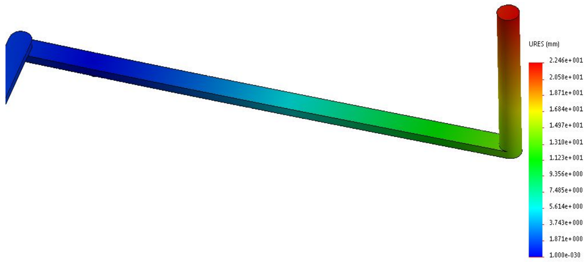

(d) Displacement as a result of the deformation during pushing action for the steel mechanism

(e) Strain as a result of the deformation during pushing action for the aluminum mechanism

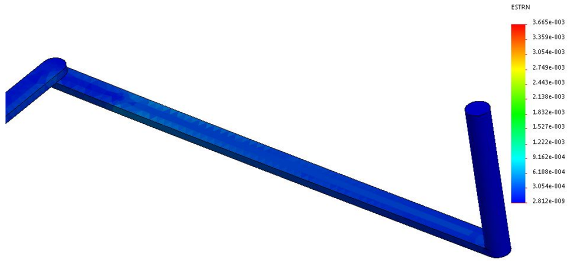

(f) Strain as a result of the deformation during pushing action for the steel mechanism

Figure 39: Displacement and strain rate of the mechanism during pulling- and pushing action

Buckling As buckling is considered as undesirable behavior, a buckling analysis has been performed in SolidWorks. Figure 40 shows the result for both the aluminum mechanism and the steel mechanism. SolidWorks has a threshold for the Buckling Load Factor (BLF), which has to be larger than 1 to prevent buckling. The buckling analysis has been carried out for the pushing action, as the stresses are largest during pushing action and the components are under tension during pulling action. The calculated BLF for the different materials are as follows: aluminum (5.8), steel (16.8). The mechanism therefore is considered safe enough to prevent buckling.

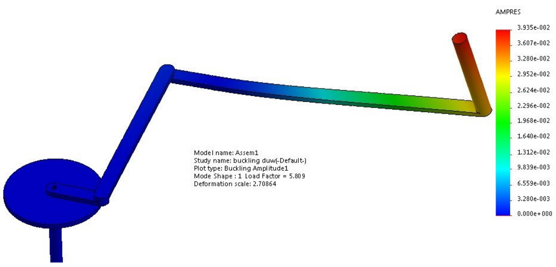

(a) Buckling analysis for the aluminum mechanism

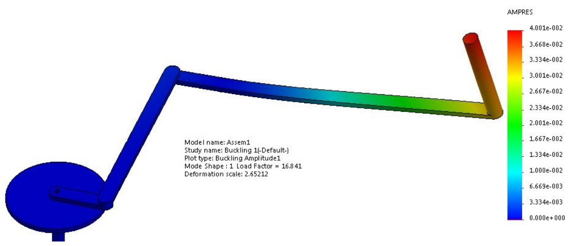

(b) Buckling analysis for the steel mechanism

Figure 40: Buckling analysis during pushing action

6.3.3.3 Flipper

The flipper has a highly nonuniform shape and is therefore very suitable for producing with composite materials. The E-glass/epoxy composite shall therefore be included in the analysis.

As concept 2 shows the largest forces acting upon the flipper, those values shall be used in the analysis. The water exerts a distributed force of 500 N upon the flipper. As the flipper has an angle of attack of 76° the force vector is split in a vertical component of $500 \cdot \sin 76 = 476$ N and a horizontal component of $500 \cdot \cos 76 = 155$ N. The flipper has been designed with a wall thickness of 5 mm such that the maximum stresses are below the yield stress criteria. Figure 41 shows the model used in the analysis. The end point of the flipper has been fixed as indicated by (1); the red arrows indicate the direction of the force. The flipper has been meshed with thin shell elements. For the technical drawing, see Appendix D.

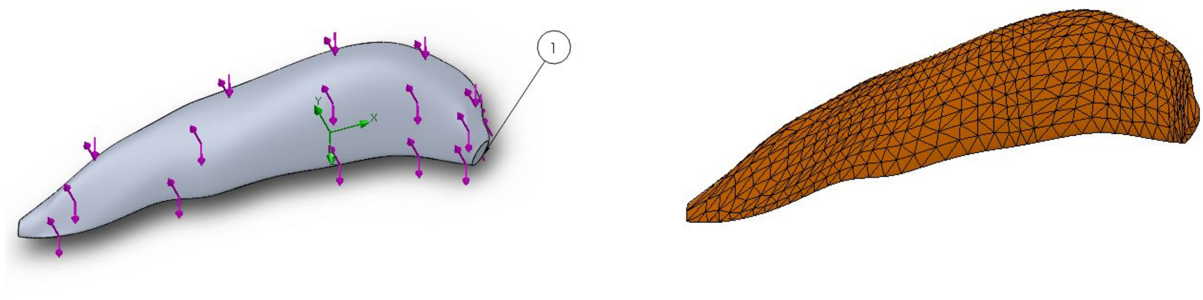

(a) Force distribution on the flipper. Point (1) is constrained in all directions.

(b) Visualization of the mesh. The orange mesh indicates a thin shell mesh.

Figure 41: Model used in SolidWorks for the static analysis

Stress Figure 42 shows the stress distribution as a result of the applied force. It is to be observed that the stresses are highest near the constrained side. This is to be expected as the torsional forces are highest at that point, inducing the high stresses. The stress however remains well below the maximum yield stress of aluminum (125 MPa), steel (170 MPa) and composite (470 MPa). It has to be stated that SolidWorks does not take interlaminar failure into account between composite layers, thus no qualitative conclusions can be made about this subject.

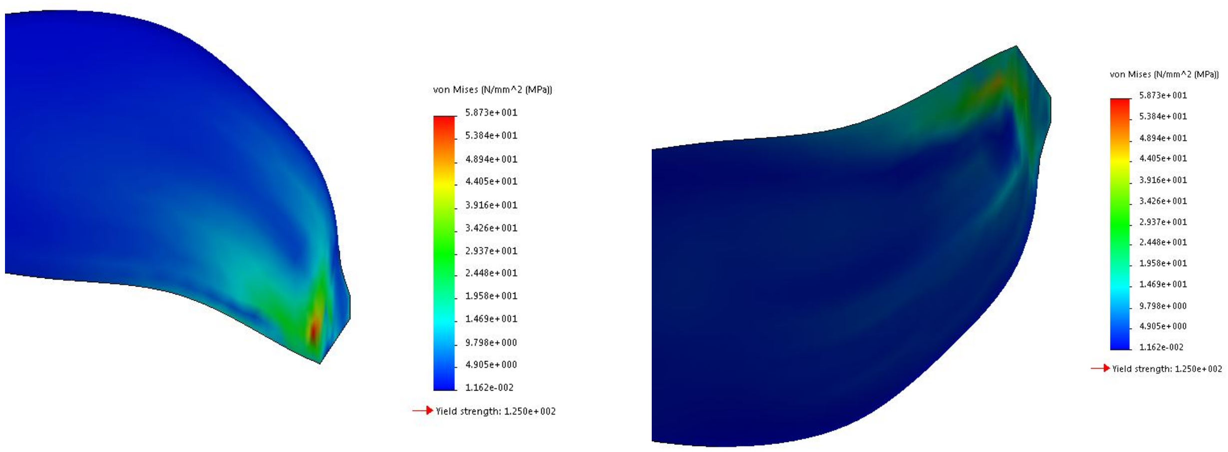

(a) Stress distribution on the top side of the flipper

(b) Stress distribution on the bottom side of the flipper

Figure 42: Stress distribution in the flipper

Deformation Figure 44 shows the displacement as a result of the forces acting on the flipper during normal usage. It is clearly visible that the tip of the flipper has the highest deflection; this is a result of the strain occurring near the constrained side, as is to be observed in figure 43(d). The aluminum flipper shows a deflection of 7 mm, the steel flipper shows a deflection of 2 mm and the composite flipper shows a deflection of 6 mm, all in vertical direction. As calculated by SolidWorks, all deformations are expected to be elastic.

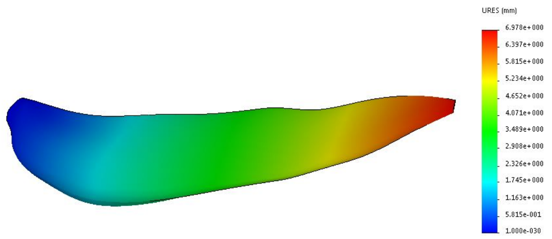

(a) Displacement as a result of the deformation of the aluminum flipper

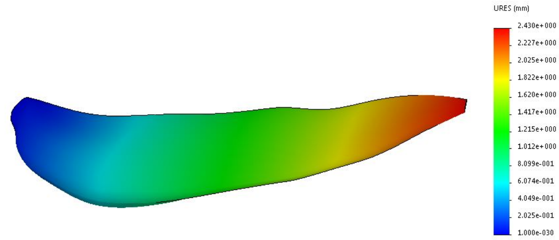

(b) Displacement as a result of the deformation of the steel flipper

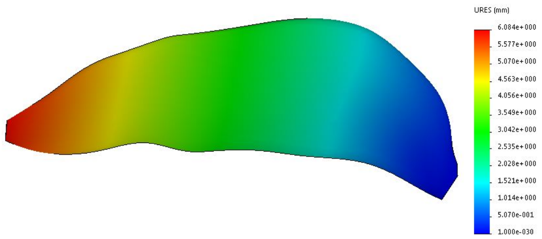

(c) Displacement as a result of the deformation of the composite flipper

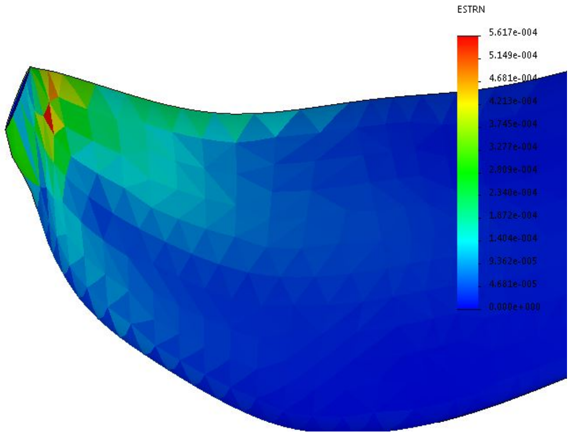

(d) Strain in the flipper

Figure 43: Displacement as a result of the deformation in the flipper

Buckling As buckling is considered as undesirable behaviour, a buckling analysis has been performed in SolidWorks. Figure 44 shows the result for the aluminum, steel and composite flipper. SolidWorks has a threshold for the Buckling Load Factor (BLF), which has to be larger than 1 to prevent buckling. The calculated BLF for the different materials are as follows: aluminum (60.2), steel (166.8), composite (67.2). The mechanism therefore is considered safe enough to prevent buckling.

The analysis shows in all three materials a strange deformation near the constrained part of the flipper. It is unknown why this deformation is shown by SolidWorks, as the flipper has been considered safe in terms of buckling.

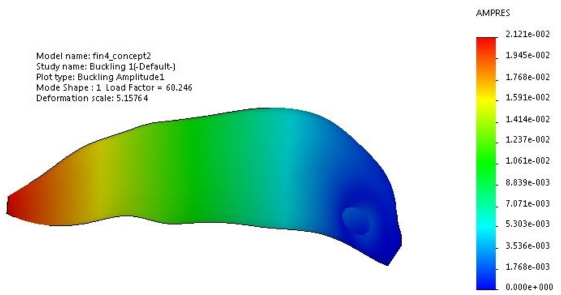

(a) Buckling analysis for the aluminum flipper

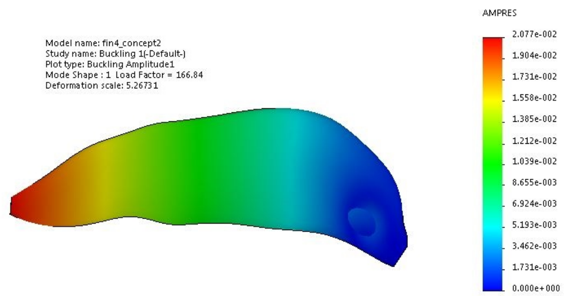

(b) Buckling analysis for the steel flipper

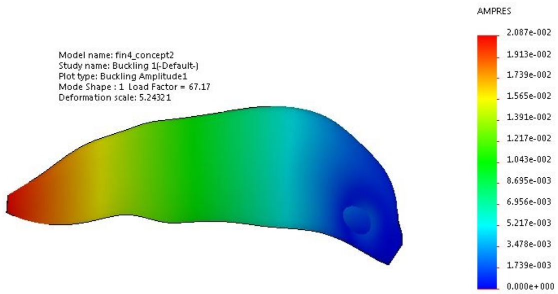

(c) Buckling analysis for the composite flipper

Figure 44: Buckling analysis for the flipper

6.4 Material Selection

As it is desirable to have both a stiff and lightweight mechanism, it is advisable to not only choose one material, but to choose different materials for the different components. Components requiring high strength and susceptible to high forces shall be made out of AISI-316L steel; the other components shall be made of 5454-H112 aluminum to reduce weight. Since it is to be expected that the flipper makes up for a large part of the weight, it is desirable to have this component made from a lightweight material. Considering the mechanical properties, the E-glass/Epoxy composite appears to be superior to the aluminum and shall be chosen as material of choice for the flipper.

Reasoning to choose aluminum over composites for the other components requiring low weight is that aluminum components can be processed in many different ways such as casting, milling and forging and therefore can consist of more complex shapes, whereas composite components usually are produced by pultrusion, impregnation infusion or by using molds [56]. These production technologies not only limit the complexity the components can consist of, but also increase the price of the components as special methods have to be used or molds have to be produced.

7 Final Design

7.1 Concept Selection

The choice of the concept is based upon the key requirement: increasing efficiency. As concept 3 has shown to be too complicated for optimization during this project, further development of this concept has been discarded in the preceding section. This leaves only concept 1 and concept 2, and as the efficiency has to increase as much as possible, concept 2 is expected to be more promising. Concept 1 has a very high vertical force vector of 27.6 N and a horizontal force vector of 6.97 N. The fraction of the total useful force thus becomes $\frac{6.97}{27.6+6.97} \cdot 100 = 20\%$, leading to a relatively low efficiency.

It is to be expected that concept 2 is more efficient than concept 1, even though energy losses as a result of friction are not taken into account in the calculations. Part of the energy during the power stroke shall be converted to sideward thrust as the flipper rotates around an axis, and part of the energy during the power stroke shall be converted to forward thrust. The forward thrust has been calculated to be 164.1 N in section 6.3.2; the sidewards thrust can be calculated via:

$$F_{sideward,total} = \int_{-\theta=-30}^{\theta=30} 164.1 \cdot \sin\theta \; d\theta \tag{7.1}$$

$$= 2 \cdot \int_{0}^{\theta=30} 164.1 \cdot \sin\theta \; d\theta \tag{7.2}$$

$$= [-328.2 \cdot \cos\theta]_0^{\theta=30} \tag{7.3}$$

$$= 44.0 \; N \tag{7.4}$$

The fraction of the total useful force thus becomes $\frac{164.1}{164.1+44.0} \cdot 100 = 79\%$, leading to a much higher efficiency than concept 1. Therefore concept 2 shall be further optimized into a final design.

7.2 Dimensional Optimization

To minimize the weight while meeting the requirements a closer look must be taken into the deformations of the mechanism. The mechanism shows significant deformation regarding the horizontal bar (2), see figure 45. Not only bending appears to be a problem, but also torsion is shown as a form of deformation. Therefore it is desirable to have a circular geometry, as this is known to be torsional resistant.

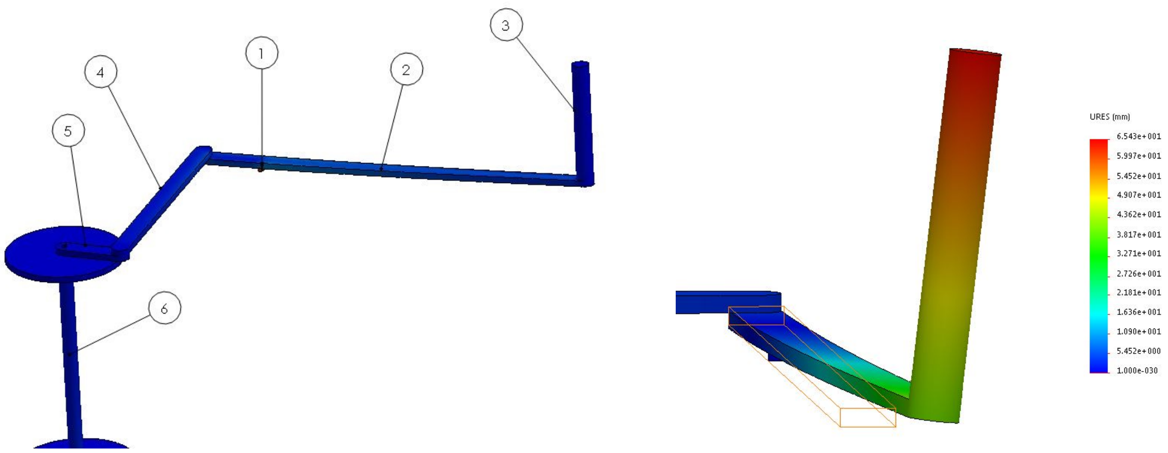

(a) Recapitulation of the model used in section 6

(b) Deformation of the horizontal bar as a result of bending and torsion. The orange contour shows the initial shape.

Figure 45: Stress and deformation of the mechanism

The handlebar (2) has shown to be fairly rigid; low stresses and strains lead to the fact that the dimensions of this part can be reduced to reduce weight. The pin used as a point of rotation (1) shall be left out in the finite element analysis in SolidWorks; the materials chosen have relatively low E-moduli and yield strengths, and other materials for these parts can be chosen to ensure that the pin meets the yield stress criteria. This shall be discussed in section 7.2.3. Also part (4) and (5) have shown to be rigid and show very little strain. The dimensions of these parts therefore can be reduced as well, and a closer look into the material shall be taken. The vertical axis of rotation (6) to which the fin is to be attached is susceptible to torsional forces, thus a circular geometry is desirable to cope with the deformations. The discs at the ends of bar (6) shall be left out, as they do not add to the purpose nor strength of the mechanism.

Using the requirements set up in section 3.3 the dimensions shall be optimized in SolidWorks. The technical drawings with the final dimensions are to be found in Appendix E, including a mechanism to connect the flipper to the axis of rotation. The lengths of the levers and flipper shall be kept as determined earlier, see figure 46 and table 10.

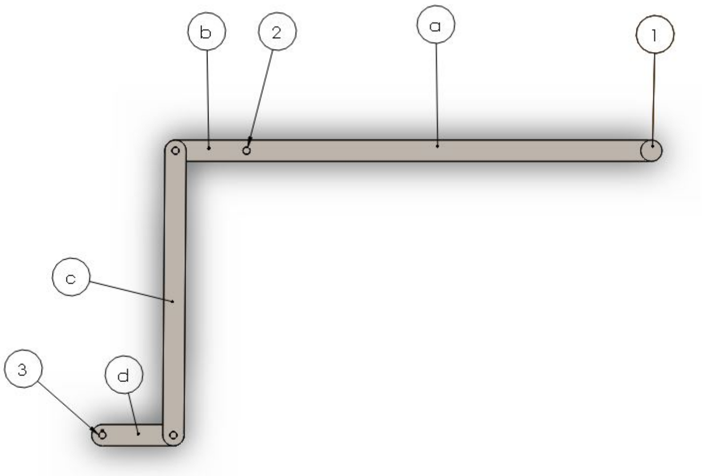

Figure 46: Overview of the levers with (1) handlebar; (2) point of rotation for the horizontal bar; (3) point of rotation of the flipper

Variable	**Dimension [-]**
a	0.57 m
b	0.10 m
c	0.40 m
d	0.10 m
Flipper length	1.08 m

Table 10: Dimensions of the components for the final design

7.2.1 Analysis in SolidWorks - Mechanism

The first part of the optimization shall be done for the mechanism by constraining the movements of the flipper. SolidWorks is used for the optimizations of the dimensions, ensuring to comply with the requirements. Figure 47 shows the setup used in the analysis. Again the yield stress criteria for the maximum expected force delivered by the user (400 N) shall be used as threshold for the optimization, as well as the maximum deformation of 10 mm during regular usage (81 N during pulling action and 86 N during pushing action). The force delivered by the spring is taken to be 83 N for both cases, as calculated in equation 6.28. The minimum dimensions shall be optimized such that the yield stress criteria and maximum deflection requirement are met.

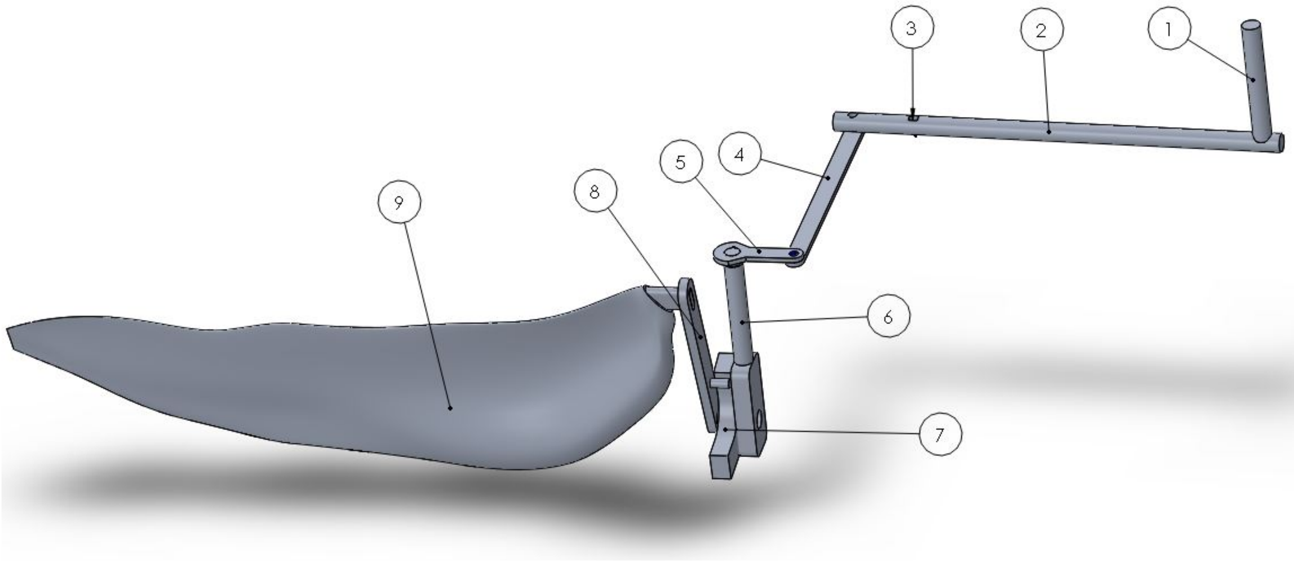

Figure 47: Model used for the Finite Element Analysis in SolidWorks

The numbers in figure 47 comply with the following parts of the mechanism:

1. Handlebar with circular cross section
2. Horizontal bar with circular cross section
3. Point of rotation for the horizontal bar
4. Flat bar transferring mainly tensional forces
5. Small bar translating translational motion to rotational motion
6. Axis of rotation for the flipper
7. Feathering mechanism
8. Strip which determines the point of rotation for the feathering motion of the flipper
9. Flipper

Figure 48(b) shows the setup of the analysis. Point of rotation (1) of the horizontal bar has been fixed to the ground and point of rotation (2) of the axis is only able to rotate; the other degrees of freedom are constrained. The largest forces are to be expected when the flipper has no initial velocity and the handlebar is pushed or pulled. The resistance of the water will lead to the fact that the flipper doesn't move in the first moment after a force is applied. After the flipper starts moving through the water the internal stresses will decrease; the point of interest thus lies in the first moment when a force is applied. For the analysis this means that the flipper is constrained in every degree of freedom, as is to be observed in figure 48(a). The green arrows show the constraints of the flipper; point (1) and (2) are fixed hinges and the purple arrows show the direction of the forces. In this case a pulling action is simulated.

After analyzing and optimizing, the final dimensions of each of the components has been determined. The final dimensions of each of the components is to be found in the technical drawings in Appendix E.

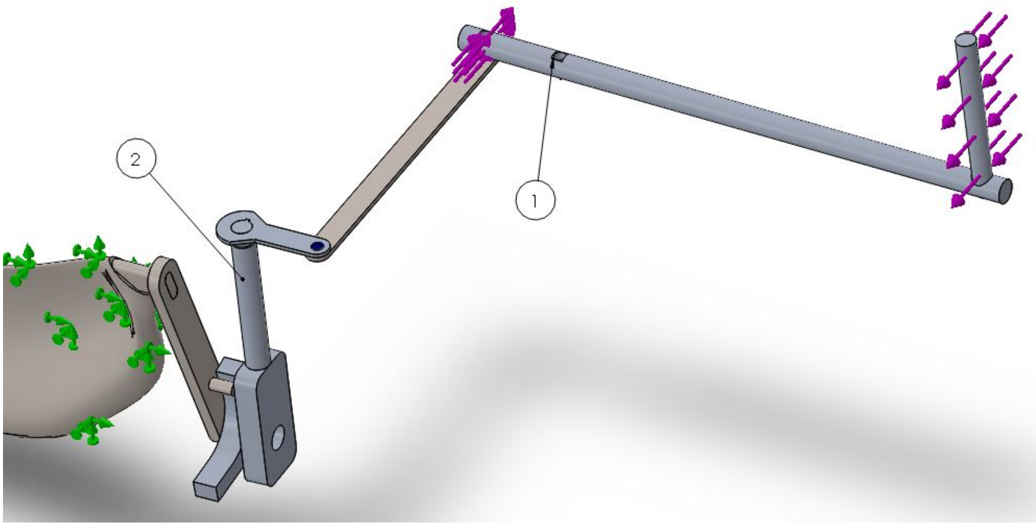

(a) Setup for the static analysis. Points (1) and (2) are fixed and the purple arrows indicate the direction of the force.

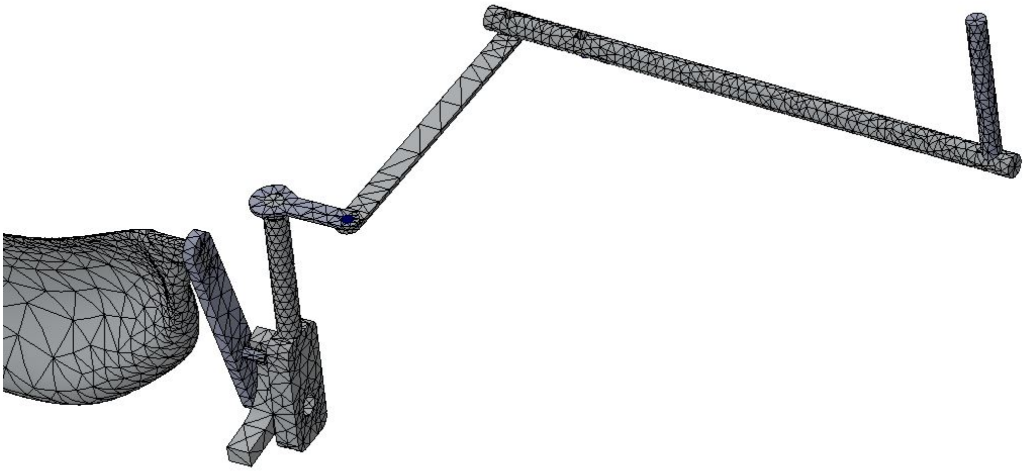

(b) Visualization of the mesh of the mechanism

Figure 48: Model used in SolidWorks for the static analysis

Stress Figure 49 shows the stress distributions as a result of the applied force. The different components have been analyzed with the two different metals and have been optimized for their weight as a function of the maximum stress. Components (1), (2), (5), (6) and (7) in figure 47 have been chosen to be made from aluminum; optimizing their dimensions for steel increases their weight. Components (4) and (8) have been chosen to be made from steel, as they are susceptible to high stresses or deformations and thus need a high E-modulus and yield strength. Optimizing the dimensions for those components for aluminum will only increase their weight.

The stresses all fall within the yield stress criteria, with the highest stress being 149 MPa located on the flat bar, see figure 49(c), falling within the 170 MPa yield stress criteria for steel. The maximum stress in the aluminum components are within the horizontal bar and is determined to be 99 MPa, falling within the 125 MPa yield stress criteria. All other stresses are lower and thus the mechanism can be considered safe.

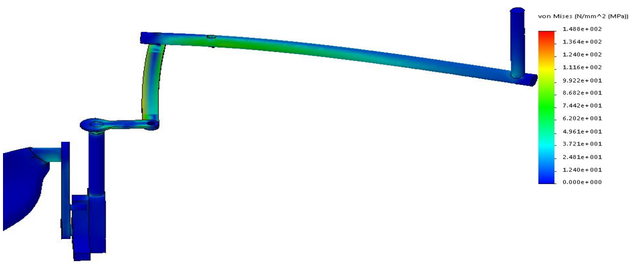

(a) Stress distribution during pulling action

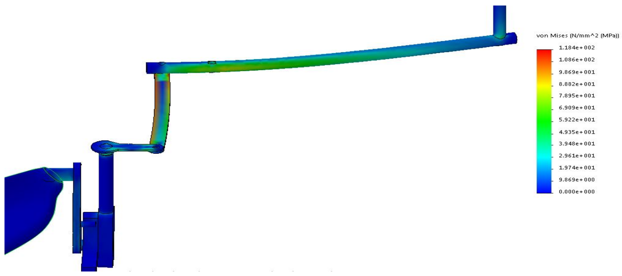

(b) Stress distribution during pushing action

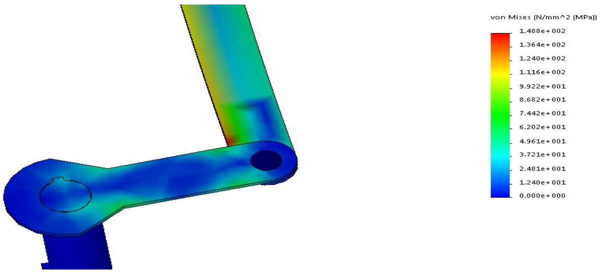

(c) Close-up of maximum stress during pulling action

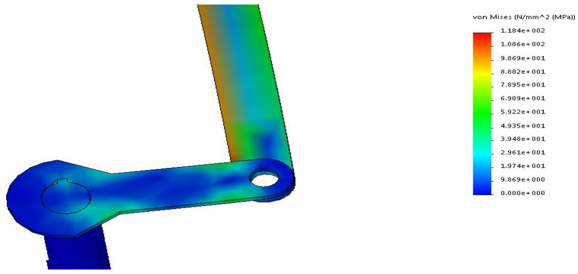

(d) Close-up of maximum stress during pushing action

Figure 49: Stress distribution in the mechanism during pulling- and pushing action

Deformation Figure 50 shows the deformations as a result of the maximum applied force of 81 N during pulling motion and 86 N during pushing action. It is to be observed that the biggest deformation occurs during pushing action, being 4.0 mm and located at the tip of the handlebar. This falls well within the 10 mm threshold and thus the mechanism complies with the requirement.

As is to be observed, the locations of the high strain values comply with the locations of the high stress values, mostly occurring in the horizontal bar. Those strains are normative for the displacements and hence the handlebar shows the largest displacement as the highest strains occur left of the handlebar.

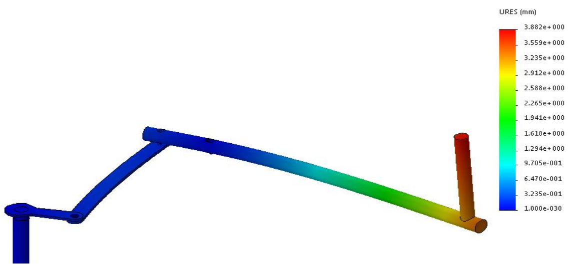

(a) Displacement as a result of the deformation during pulling action

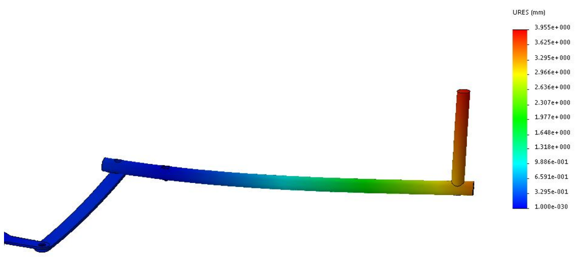

(b) Displacement as a result of the deformation during pushing action

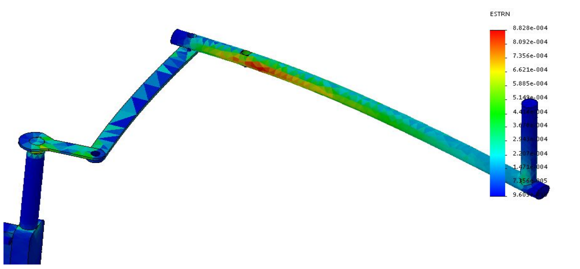

(c) Strain as a result of the deformation during pulling action

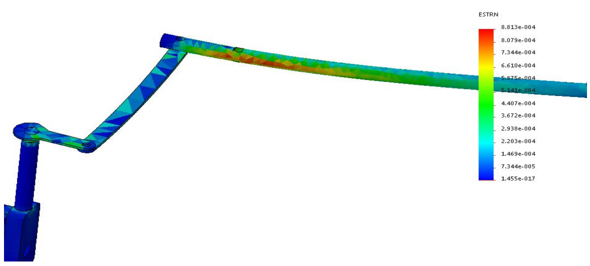

(d) Strain as a result of the deformation during pushing action

Figure 50: Displacement of the mechanism during pulling- and pushing action

Buckling As buckling is considered as undesirable behavior, a buckling analysis has been performed in SolidWorks. Figure 51 shows the result for the buckling analysis. Buckling is likely to occur at the flat bar, as this component has the most susceptible geometry for buckling. Only pushing action has been taken into consideration, as during pulling action the flat bar is under tension. SolidWorks has a threshold for the Buckling Load Factor (BLF), which has to be larger than 1 or smaller than -1 to prevent buckling, The calculated BLF is -1.02, which is just slightly larger than the threshold, therefore the mechanism is considered safe enough to prevent buckling.

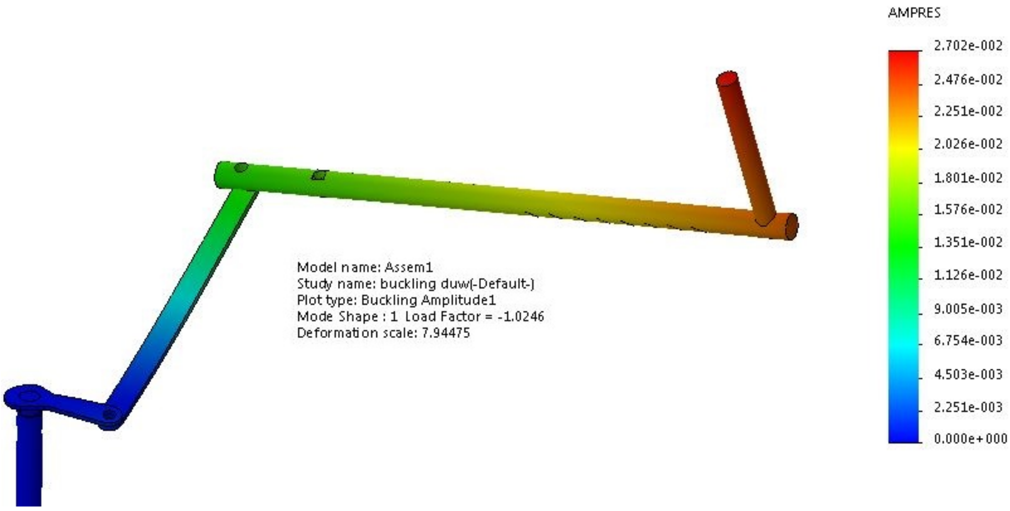

Figure 51: Buckling analysis during pushing action

7.2.2 Analysis in SolidWorks - Flipper

As the flipper is susceptible to the water resistance as a result from the force applied by the user, the flipper is exposed to internal stress, deformation and possible buckling. The optimization of the thickness of the shell of the flipper is point of interest in this case, as the other dimensions are determined earlier in the report. Again the stress- and buckling analysis shall be done with an applied force of 400 N, the deformation analysis shall be carried out for an applied force of 81 N for pulling action, as the flipper then is orientated at an angle of attack of $\alpha = 76°$, thus having the largest forces acting upon the flipper.

Figure 52 shows the setup of the analysis. Similar to the analysis performed on the flipper in section 6.3.3.3 the end part of the flipper is constrained and the force is split in a horizontal component of 155 N and a vertical component of 476 N. The flipper has been meshed using thin shell elements.

The final dimensions of the flipper are to be found in Appendix E.

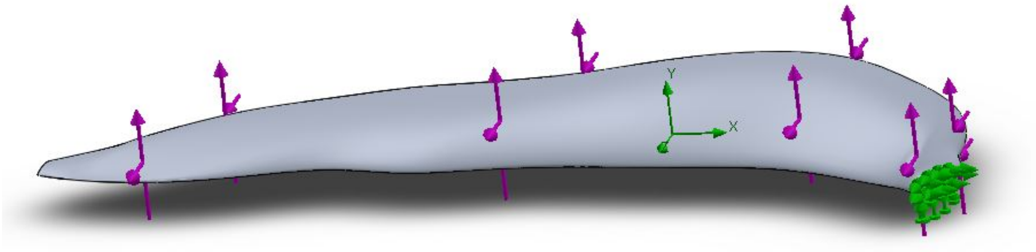

(a) Setup for the static analysis. The green arrows show the constrained part and the purple arrows indicate the direction of the force.

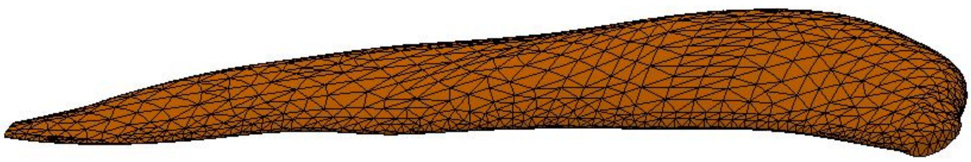

(b) Visualization of the mesh of the flipper. The orange mesh indicates the use of a shell element

Figure 52: Model used in SolidWorks for the static analysis

Stress Figure 53 shows the stress distribution as a result of the applied force for a shell thickness of 1.7 mm. It is to be observed that the stresses are highest on the bottom side of the flipper near the constrained side. This is to be expected as the torsional forces increase when close to the constrained point, inducing high stresses. The stress however remains below the maximum yield stress of the composite (470 MPa), with a maximum stress of 452 MPa. It has to be stated that SolidWorks does not take interlaminar failure into account between composite layers, thus no qualitative conclusions can be made about this point.

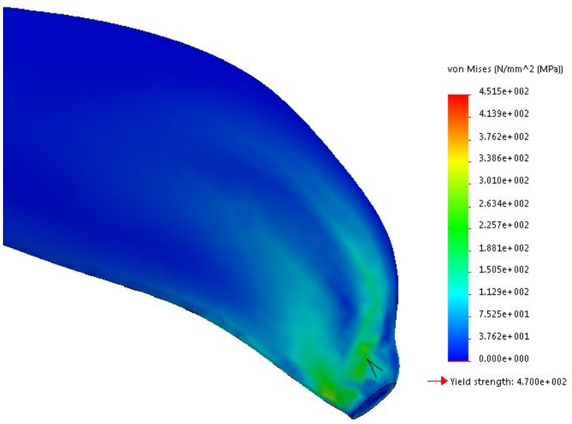

(a) Stress distribution on the top side of the flipper

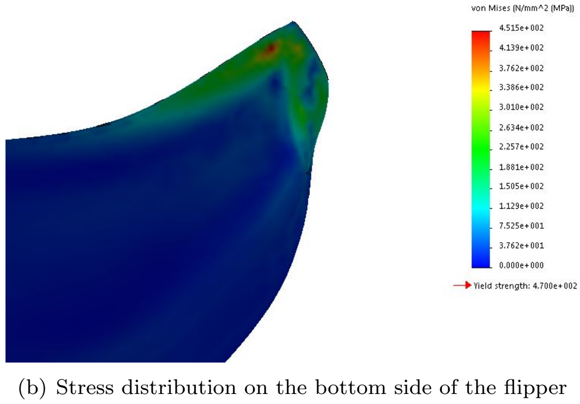

(b) Stress distribution on the bottom side of the flipper

Figure 53: Stress distribution in the flipper

Deformation Figure 54 shows the displacement as a result of the forces acting on the flipper during normal usage, using a shell thickness of 2.1 mm. It is clearly visible that the tip of the flipper has the largest deflection; this is however a result of the strain occurring near the constrained side, as is to be observed in figure 54(b) and 54(c). The maximum deflection is 9.3 mm in the vertical direction. As calculated by SolidWorks, all deformations are expected to be elastic.

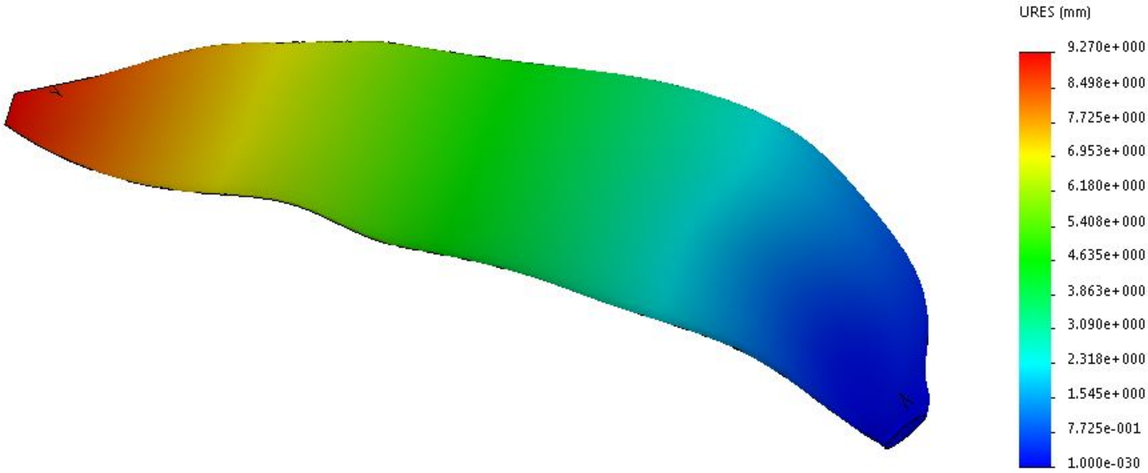

(a) Displacement as a result of the deformation of the flipper

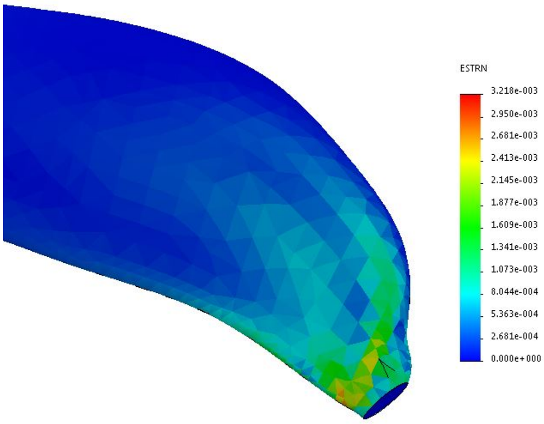

(b) Strain in the top side of the flipper

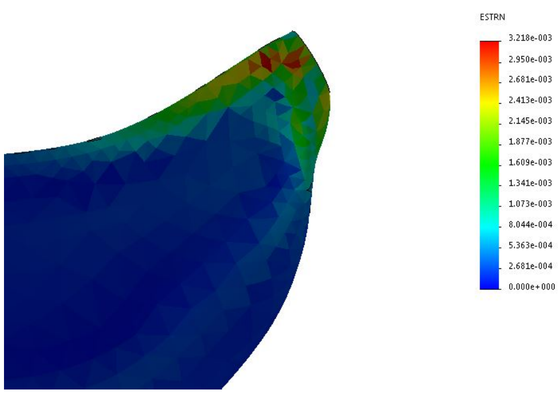

(c) Train in the bottom side of the flipper

Figure 54: Displacement as a result of the deformation in the flipper

Buckling As buckling is considered as undesirable behavior, a buckling analysis has been performed in SolidWorks. Figure 55 shows the result for the buckling analysis when a force of 400 N is applied on the flipper with a shell thickness of 2.1 mm. SolidWorks has a threshold for the Buckling Load Factor (BLF), which has to be larger than 1 to prevent buckling. The calculated BLF for the flipper is 7.2, the flipper therefore is considered safe enough to prevent buckling.

Again the analysis shows a strange deformation near the constrained part of the flipper. It is unknown why this deformation is shown by SolidWorks, as the flipper is considered safe in terms of buckling.

As the deformation analysis requires the shell elements to have a thickness of at least 2.1 mm, this thickness shall be used as the minimum thickness of the composite.

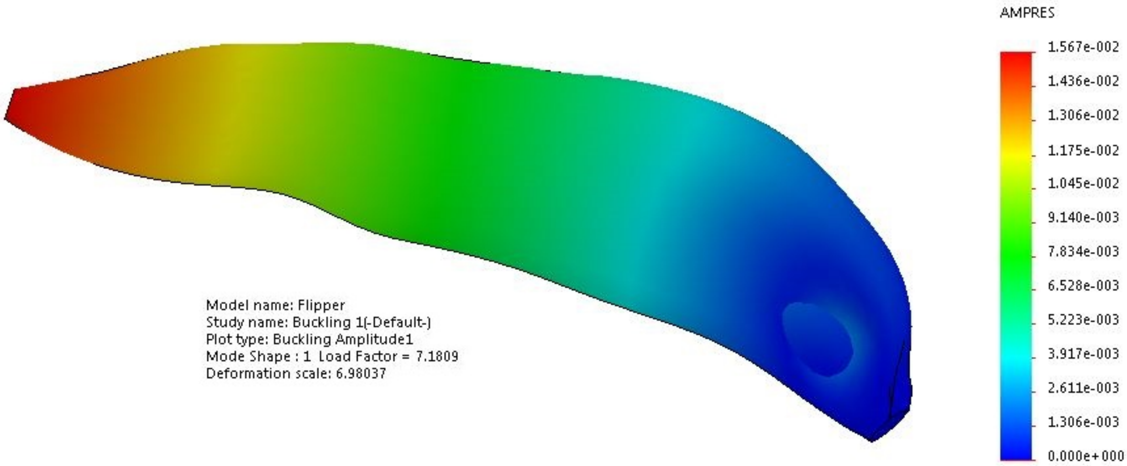

Figure 55: Buckling analysis for the flipper

7.2.3 Material Justification

As the weight is to be reduced as much as possible, it has been chosen to use certain materials for certain components. The handlebar and horizontal bar have been chosen to be made out of aluminum; even though the deflection increases and the yield strength is lower than for steel, the components would have been heavier when dimensionally optimized for steel. However the flat bar has shown to be lighter when made of steel instead of aluminum. The same holds for the steel strip between the flipper and the feathering mechanism.

The flipper has been made of epoxy/e-glass because it has excellent material properties, can be shaped in complex shapes and is very lightweight. The reason that only the flipper is made of this material is that a mold is needed to produce the parts, which is expensive. Since a mold is needed for the flipper regardless of the material of which it is produced, it might as well be made of a composite material. The other components can either be extruded or cut; the feathering mechanism has to be cast or milled due to its complex shape.

The fasteners such as the pins acting as point of leverage have to be made of a stronger material to be able to resist the high stresses. Those materials are often more expensive, however the parts are small compared to the other components and hence costs are not likely to increase much when chosen for stronger materials.

7.3 Mass and Material Costs

The mass and material costs of the mechanism shall be determined per component using SolidWorks. Note that the costs are the material costs and not the production costs. As SolidWorks is unable to create a shell model of the flipper to determine the mass, the mass has been calculated by multiplying the flippers area with the thickness and the specific weight. The results are shown in table 11.

Component	**Mass [gram]**	**Material Costs [USD]**
Handlebar	247	0.25 - 0.86
Horizontal bar	1345	1.35 - 4.71
Flat bar	595	0.60 - 2.08
Small bar	60	0.06 - 0.21
Feathering mechanism	1805	1.80 - 6.32
Strip	2068	2.07 - 7.24
Flipper	3480	0.87 - 4.35
Total	**9600**	**7.00 - 25.77**

Table 11: Mass and material costs of each of the components

As this is the mass for one mechanism, and two mechanisms are needed for the concept, the total mass and price has to be doubled: 19200 gram and \$14.00 - \$51.54.

7.4 Assembly

The assembled mechanism is shown in figure 56(a). An exploded view of the assembly is shown in figure 56(b). The numbers show the positions to which fasteners are to be used; those fasteners are not designed, but a brief overview of the fastening methods will be given.

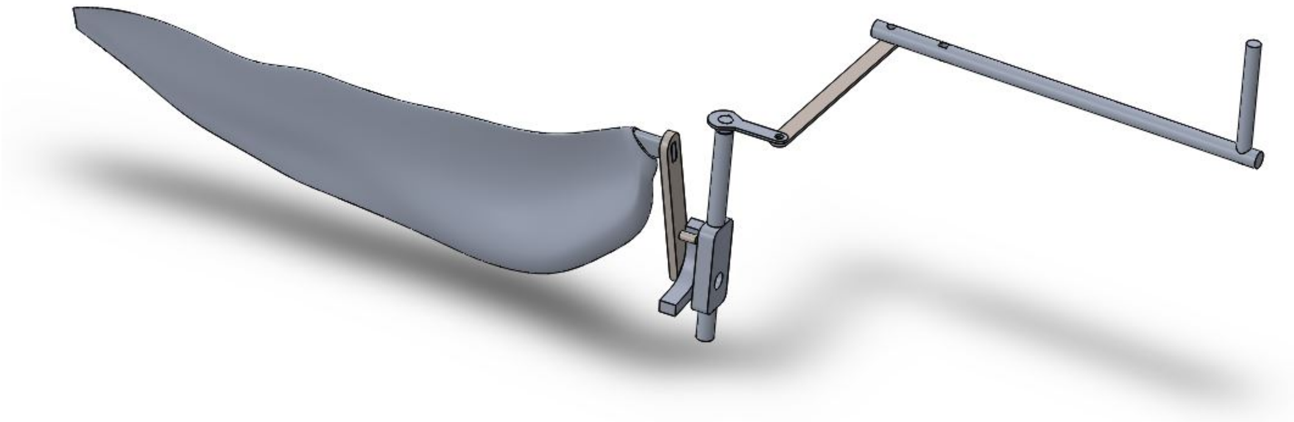

(a) Assembled mechanism of the final design

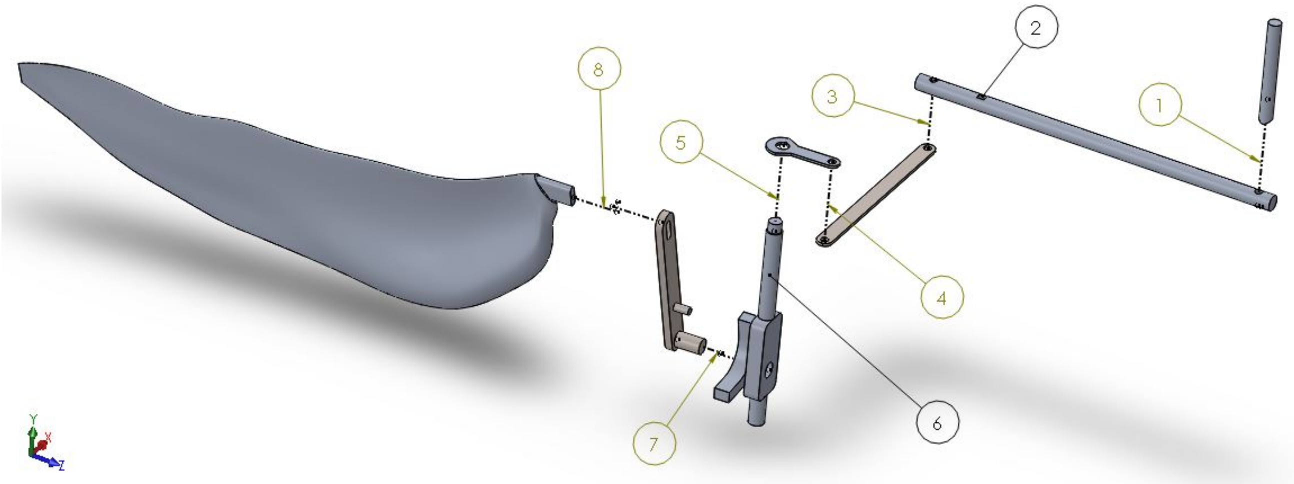

(b) Exploded view of the assembly

Figure 56: Overview of the assembly of the final design

Fastener 1 The handlebar has to be attached rigidly to the horizontal bar, this can be achieved by tapping a thread in the handlebar and bolting the two parts together.

Fastener 2 This point is the point of rotation for the horizontal bar; the pin going through (2) therefore must be able to rotate freely. The pin has to be attached to the ground, in this case the bodyboard.

Fastener 3 The horizontal bar and the flat bar must be able to rotate freely; this can be achieved by using a nut and a partially blank bolt or a clevis fastener. A spring also must be able to be connected to this fastener.

Fastener 4 Similar to (3), the flat bar and small bar must be able to rotate, to be achieved by using a nut and a partially blank bolt or a clevis fastener.

Fastener 5 The connection between the axis of rotation (6) and the small bar has to be rigid; a key pin is used to ensure that the rotation is locked. The two components can be fixed together to prevent vertical movement using bolting or clamping. Welding is undesirable as aluminum is difficult to weld.

Fastener 6 The axis of rotation to which the flipper is attached has to be fixed to the body board. This can be achieved by using a bearing, but as the axis is not allowed to move in vertical direction, including a slit in the axis might be necessary to constrain this degree of freedom.

Fastener 7 The axis of the strip must be able to rotate freely within the feathering mechanism. However, the axis must be kept in place. This can be achieved by having a bearing holder at the axis.

Fastener 8 The connection between the strip and the flipper must be rigid, but since the flipper is made of a composite, welding cannot be used. Clamping or bolting is a possible way of attaching both components to each other.

7.5 Artist's impression

Figure 57 gives a rendered image of the final design implemented on a body board.

Figure 57: Artist's impression of the final design

8 Conclusion

Three different concepts were generated in which a distinction was made between flapping- and lemniscate motion. The final design has been chosen based upon feasibility and locomotion efficiency, in which the body board has shown to be most feasible and energy efficient. The maximum amount of thrust generated by the mechanism is estimated to be 164 N, distinguished in a part delivered by a spring and a part delivered directly by the user. Drag from the mechanism and body board in the water has not been taken into account and might be a point of interest in the future.

Regarding the requirements 12 out of 15 are met; reasoning will be given in the discussion. The requirements not met are:

1. The artificial flippers must mimic the sea turtles' flippers physical properties as close as possible
2. The motion of the mechanical model must resemble either of the swimming motions of the sea turtle
3. The mechanical device must be safe to use

9 Discussion and Remarks

The swimming behavior of sea turtles has been proven to be very complex; mimicking their motion therefore is very difficult to achieve with mechanical linkages only. The proposed design only covers a small part of their swimming behavior, looking only at a 2 degree of freedom system: back-and-forth motion and feathering motion. Other research has shown that mimicking the swimming behavior is very difficult and even with use of motorized parts the swimming is still often mimicked as a 2 degree of freedom system. [6][7][9][57][58]

This project is a 2-year masters project at the University of the South Pacific; this report therefore only scrapes off the surface of this subject and hence can be used as a base for further research. General points of interest which need further research are:

- During the change from power stroke to return stroke, it takes time for the flipper to feather even though the return motion already has started. Energy is lost during this process, but might be overcome by using a rotational spring with a small k-value.
- By determination of the torque generated by the flipper in concept 2 and 3 as well as during determination of the lift and drag coefficient of the flipper in SolidWorks a uniform free stream velocity has been taken into consideration. However as the flipper rotates about an axis, the lift and drag force are dependent on the position on the flipper. It has shown to be difficult and time-consuming to do the analysis in SolidWorks for the uniform free stream velocity, so no further time was spent for a non-uniform free stream velocity. Further research might include the simulation of a non-uniform free stream velocity to acquire a more accurate result.
- Although the scope of the project was to mimic the sea turtles' flippers as closely as possible, enhancements can be made by for example adding tubercles on the trailing edge of the flipper to reduce vortex shedding and thus decrease drag. Further investigation is needed to confirm this.
- No energy losses due to friction and deformations of the components have been determined, as well as energy loss due to drag of the mechanism and body board in the water. This leads to a higher expected forward thrust than the actual forward thrust. Further research might include energy losses due to these reasons.
- The Finite Element Analysis of concept 2 and 3 consider no initial velocity of the mechanism, leading to a lower flipper drag than calculated. The forces acting upon the mechanism however are largest when there is no initial velocity and the power stroke is assessed, as the flipper will meet the largest resistance at that point. Future research might include both a static and a dynamic analysis to cover this part.
- As the flipper is very light-weight and watertight, the flipper will have some positive buoyancy, which might lead to a unstable device. This has not been taken into consideration, and adaption of the mechanism to reach neutral buoyancy might be necessary in the future.
- Regarding the efficiency, only mechanical efficiency has been taken into account for the concepts, whereas the sea turtles' swimming efficiency is measured in VO_2-saturation. However it is to be expected that the use of a mechanical device as proposed in this report will lead to an increase in the 3% swimming efficiency in humans.

Concept related points of interest are:

- Concept 1 is not likely to work as the lift vector is oriented mostly in vertical direction. The reason why sea turtles are able to make use of lift-based motion is because their flapping speed is higher during the power stroke, leading to a higher angle of attack of the free stream relative to the horizontal and therefore to a more horizontal lift vector.
- Concept 1 might have problems with the attachment to the legs; it might be possible that the mechanism starts rotating around the leg due to the torsional forces. Further research is needed to cover this part.

Requirement related points of interest are:

- It has been chosen to create a flipper which is as stiff as possible instead of a flipper which mimics the sea turtles' flippers physical properties as close as possible, as no information has been found concerning the physical properties of real flippers. Having a more flexible flipper might lead to energy losses; it is however known that feathering of the tip decreases vortex shedding and thus drag. Further investigation is needed to optimize the artificial flippers physical properties.
- Mimicking the sea turtles swimming motion has been proven to be very hard; therefore it has been chosen to approximate the lemniscate motion by a feathered back-and-forth motion.
- Safety has not specifically taken into consideration when designing the mechanism, however surface finish of the materials, proper location of the leverages and instruction before use might help to improve safe usage.

In general it can be stated that even though a lot of research has been done in this report, there is still a lot of research left to be done to find an optimal device for increasing swimming efficiency in humans using sea turtle biomimetics.

10 Acknowledgement

I would like to thank Dr. David Aitchison for his supervision and help in every possible manner during my internship. I would like to thank the University of the South Pacific for providing the necessary means for me to do my research, the University of Twente for their support in organizing my internship in Fiji and the Twente Mobility Fund for providing me of an allowance to cover part of my expenses.

Furthermore I would like to thank my colleagues, host family and all other people who've made it possible for me to be able to have this incredible experience.

References

[1] Pereira, C. (2014). Swimming ability in sea turtle hatchlings: a comparison between species. *Thesis - School of Biological Sciences, University of Queensland*, p. 1-121.

[2] Zamparo, P. et al. (2002, June 8). How fins affect the economy and efficiency of human swimming. *The Journal of Experimental Biology 205*, p. 2665-2676.

[3] *Navy SEALs could turn superhuman with Pentagon's PowerSwim* (2009, September 30). Available at: http://www.popularmechanics.com/military/a2126/4223354/ (accessed: 16 April 2015)

[4] *Total Immersion Swimming* (2012). Available at: http://totalimmersion.net/blog/swim-farther-and-faster-by-saving-energy/ (accessed: 16 April 2015)

[5] Davenport, J. et al (1983, May 24). A comparison of the swimming of marine and freshwater turtles. *Proc. R. Soc. Lond*, p. 447-457.

[6] Font, D. et al. (2011, November 28). Design and Implementation of a Biomimetic Turtle Hydrofoil for an Autonomous Underwater Vehicle. *www.mdpi.com/journal/sensors*, p. 1-20.

[7] Font, D. et al. (2011, June 9). Experimental determination of the hydrofoils angle of attack in the case of a turtle-like Autonomous Underwater Vehicle. *OCEANS, 2011*, p. 1-5.

[8] Rivera, A. et al. (2012, October 15). Forelimb kinematics during swimming in the pig-nosed turtle, Carettochelys insculpta, compared with other turtle taxa: rowing versus flapping, convergence versus intermediacy. *The Journal of Experimental Biology 216*, p. 668-680.

[9] Xu, J. et al. (2011, August 10). Analysis of Bionic Hydrofoil Propulsive Performance. *International Conference on Mechatronics and Automation*, p. 1-5.

[10] Zhang, M. et al. (2008, December 20). The Principle of Turtle Motion and Bio-mechanism of Its Four Limbs Research. *Computational Intelligence and Industrial Application, vol. 2*, p. 573-578.

[11] Prange, H. (1975, March 26). Energetics of swimming of a sea turtle. *The Journal of Esperimental Biology 64*, p. 1-12.

[12] *Wikipedia page: Propeller_(aeronautics)* (2015). Available at: http://en.wikipedia.org/wiki/Propeller_%28aeronautics%29#Feathering (accessed: 23 April 2015)

[13] FAA (2015). Chapter 2: Aerodynamics in Flight. *faa.gov handbook manuals*, p. 1-28.

[14] Licht, S. et al. (2009, September 16). In-line motion causes high thrust and efficiency in flapping folls that use power downstroke. *The Journal of Experimental Biology 213*, p. 63-71.

[15] Renous, S. et al. (2009, January 10). Locomotion in marine Chelonia: Adaptation to the aquatic habitat. *Historical Biology: An International Journal of Paleobiology 14:1-2*, p. 1-13.

[16] *Wikihow* (2015). Available at: http://www.wikihow.com/Swim-Free-Style-Correctly#/Image:Swim-Free-Style-Correctly-Step-8.jpg (accessed: 27 April 2015)

[17] *Wikipedia Page: Kutta-Joukowski Theorem* (2015). Available at: http://en.wikipedia.org/wiki/Kutta%E2%80%93Joukowski_theorem (accessed: 30 April 2015)

[18] *Nasa: The Lift Equation* (2014). Available at: https://www.grc.nasa.gov/www/k-12/airplane/liftco.html (accessed: 30 April 2015)

[19] *Nasa: The Drag Equation* (2015). Available at: https://www.grc.nasa.gov/www/k-12/airplane/dragco.html (accessed: 8 May 2015)

[20] Sun, X. et al. (2013, February 22). Three-dimensional Hydrodynamic Analysis of Forelimb Propulsion of Sea Turtle With Prosthetic Flippers. *Journal of Aero Aqua Bio-mechanisms, Vol. 3 (2013) No. 1*, p. 36-44.

[21] Samimy, S. et al. (2005, March). A theoretical and experimental analysis of diver technique in underwater fin swimming. *Sports Engineering, vol. 8, issue 1 (2005)*, p. 27-38.

[22] *Wikihow page: Swim Free Style Correctly* (2015). Available at: http://www.wikihow.com/Swim-Free-Style-Correctly (accessed: 27 April 2015)

[23] *Correct finninf technique for freediving* (2015). Available at: http://freediveuk.com/correct-finning-technique-for-freediving/ (accessed: 11 May 2015)

[24] *Wikipedia page: Airfoil* (2015). Available at:http://en.wikipedia.org/wiki/Airfoil (accessed: 14 May 2015)

[25] American Wood Council (2005). Beam Design Formulas With Shear And Moment Diagrams. *ANSI/AF&PA NDS*, p. 1-20.

[26] Pendergast, D. et al. (2003). Evaluation of fins used in underwater swimming. *UHM 2003, Vol. 30, No. 1 - Fins used in underwater swimming*, p. 55-71.

[27] *Wikipedia page: Small-angle Approximation* (2015). Available at: http://en.wikipedia.org/wiki/Small-angle_approximation (accessed: 13 May 2015)

[28] *Body Segment Data* (2015). Available at: http://www.exrx.net/Kinesiology/Segments.html (accessed: 18 May 2015)

[29] Karwowski, W. (2006). International Encyclopedia of Ergonomics and Human Factors, Vol. 1, 2nd edition. *Google Books*, p. 499-500.

[30] *Researchgate* (2012). Available at: http://www.researchgate.net/post/Whats_the_link_between_maximal_force_one_repetition_and_endurance_force_several_repetitions_with_light_loads1 (accessed: 20 May 2015)

[31] *SpeedEndurance - Weight Training: Strength, Muscle Mass and Endurance* (2013). Available at:http://speedendurance.com/2013/10/09/weight-training-strength-muscle-mass-and-endurance/ (accessed: 20 May 2015)

[32] *Principle of Whitworth quick return mechanism* (2015). Available at: http://jeanlouis.blanchard.pagesperso-orange.fr/english_swf/ppe_fst_quick_return.html (accessed: 14 May 2015)

[33] *Bike Dynamics - Bike Fitting Specialists* (2015). Available at: http://bikedynamics.co.uk/FitGuidecranks.htm

[34] *Crank Length - Which One?* (2011). Available at: https://www.stevehoggbikefitting.com/bikefit/2011/06/crank-length-which-one/

[35] Balbinot, A. et al. (2014, December 3). A New Crank Arm-Based Load Cell for the 3D Analysis of the Force Applied by a Cyclist. *Sensors 14(12), 2014*, p. 22924-22939.

[36] *SlowSwitch: Triathlon Forum* (8 January 2008). Available at: http://forum.slowtwitch.com/gforum.cgi?do=post_view_printable;post=1625728; (accessed: 26 May 2015)

[37] *Analytic Cycling: Forces at Pedals* (2001). Available at: http://www.analyticcycling.com/PedalForcesAt Pedal_Page.html

[38] *Pedal Power: Spinning for the Future at CCAT* (2015). Available at: http://www.green-trust.org/2000/humanpower.htm (accessed: 26 May 2015)

[39] *Cycling Optimization Analysis* (1996). Available at: http://www.veelberg.dk/uddrag/uddrag.html (accessed: 3 June 2015)

[40] emphMailOnline - Science & Tech (2014). Available at: http://www.dailymail.co.uk/sciencetech/article-2891080/Rarest-turtles-world-wash-British-beaches-5-000-miles-Gulf-Mexico-cold-weather-leaves-weak-swim-against-ocean-currents.html (accessed: 22 May 2015)

[41] *Wall Monkeys* (2015). Available at: http://www.wallmonkeys.com/hawksbill-sea-turtle-isolated-on-white-background-wall-decal-32858.html (accessed: 22 May 2015)

[42] Wyneken, J (2001, December). The Anatomy of Sea Turtles. *NOAA Technical Memorandum NMFS-SEFSC-470*, p. 1-60.

[43] *Pixgood - Turtle Muscle Anatomy* (2015). Available at: http://pixgood.com/turtle-muscle-anatomy.html (accessed: 22 May 2015)

[44] *Wikipedia page: Aerodynamic Center* (2015). Available at: http://en.wikipedia.org/wiki/Aerodynamic_center (accessed: 10 June 2015)

[45] *Water - Dynamic and Kinematic Viscosities* (2015). Available at: http://www.engineeringtoolbox.com/water-dynamic-kinematic-viscosity-d_596.html (accessed: 27 May 2015)

[46] *5454-H112 Aluminum* (2015). Available at: http://www.makeitfrom.com/material-properties/5454-H112-Aluminum/ (accessed: 9 Juni 2015)

[47] *ASM Aerospace Specification Metals Inc.* (2015). Available at: http://asm.matweb.com/search/Specific Material.asp?bassnum=MQ316P (accessed: 9 June 2015)

[48] 316/316L Stainless Steel (2007). Product Data Sheet. *AK Steel Datasheet*, p. 1-2.

[49] North American Stainless (2015). Long Product Stainless Steel Grade Sheet. *NAS Datasheet*, p. 1-8.

[50] *Charleston Aluminum Marine Products* (2015). Available at: http://www.charlestonaluminum.com/ marine_products.php (accessed: 8 June 2015)

[51] Fadhil, B.A. (2013). Effect of Plies Stacking Sequence and Tube Geometry on The Crush Behavior of Tube under Low Velocity Impact Numerical Study. *Petroleum Engineering Department, Koya University, Erbil, 964, Iraq*

[52] *Tianjin Tiangang Weiye Steel Tube CO., LTD* (2015). Available at: http://tjtgwy.en.alibaba.com/product/1910806681-218166599/aluminum_alloy_plate_grade_5454_H112.html (accessed: 9 June 2015)

[53] *Alibaba - AISI 316L stainless teel sheet & plate price* (2015). Available at: http://www.alibaba.com/product-detail/aisi-316L-stainless-steel-sheet-plate_60241408932.html?s=p (accessed: 9 June 2015)

[54] *Alibaba - Epoxy Resin Reinforced Fiber Glass Composite Rod* (2015). Available at: http://www.alibaba.com/showroom/glass-epoxy-composites.html (accessed: 9 June 2015)

[55] *AZO Materials - E-Glass Fibre* (2013). Available at: http://www.azom.com/article.aspx?ArticleID=764 (accessed: 9 June 2015)

[56] Warnet, L. (2014). Design, Production and Materials - Composite: Material and Production. *University of Twente.*

[57] Konno, A. et al. (2005, October 28). Development of Turtle-like Submergence Vehicle. *Proceedings on the 7th International Symposium on Marine Engineering*, p.1-5.

[58] Seo, K. et al. (2010 January 22). CPG-based control of a turtle-like underwater vehicle. *Auton Robot 28*, p. 247-269.

A Determination of C_L and C_D in SolidWorks

To be able to calculate the lift- and drag coefficient of the flipper, the SolidWorks Flow Simulation has been used, see figure 58. The wizard will help to complete all the necessary information to do the analysis.

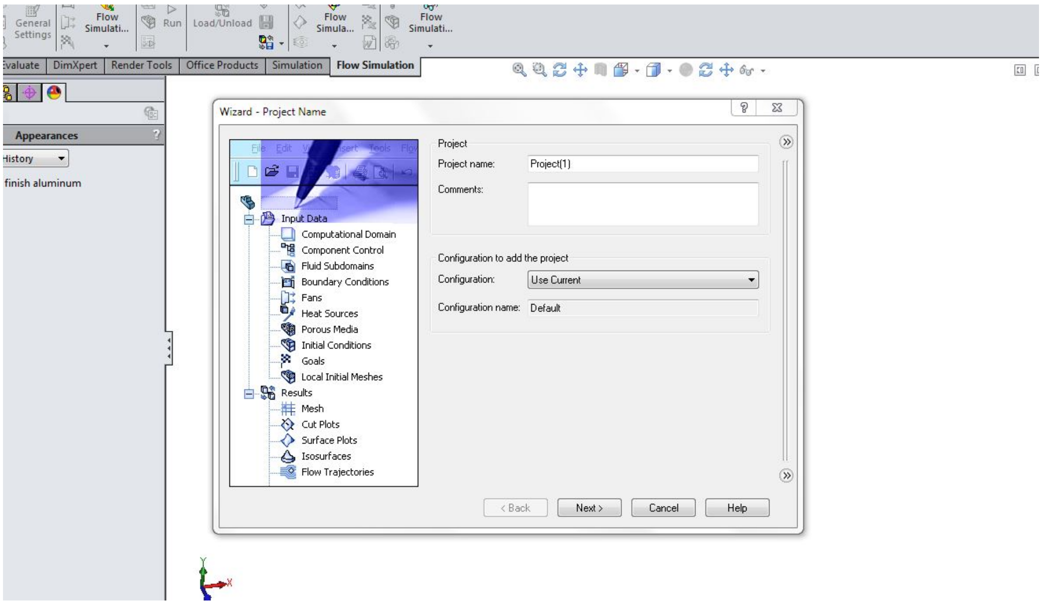

Figure 58: Flow Simulation Wizard

The analysis type has been set to ”external”, as the point of interest is the flow around the flipper. No heat conduction, radiation, time-dependency, gravity or rotation has been used in the analysis. The fluid used is water, no surface roughness has been taken into account. For the ”Initial and Ambient Conditions” the standard settings were used.

The Reynold’s number of the flipper in concept 1 - 3has been determined to calculate the flow velocity in the analysis. In this analysis the flow speed is 3.15 m/s. The leading edge points in the y-direction; for a angle of attack of $\alpha = 0°$ an y-velocity of $\cos(0) \cdot 3.15 = 3.15\ m/s$ and z-velocity of $\sin(0) \cdot 3.15 = 0\ m/s$ has been used, see figure 59. For different angles of attack the y- and z-component of the velocity can be calculated.

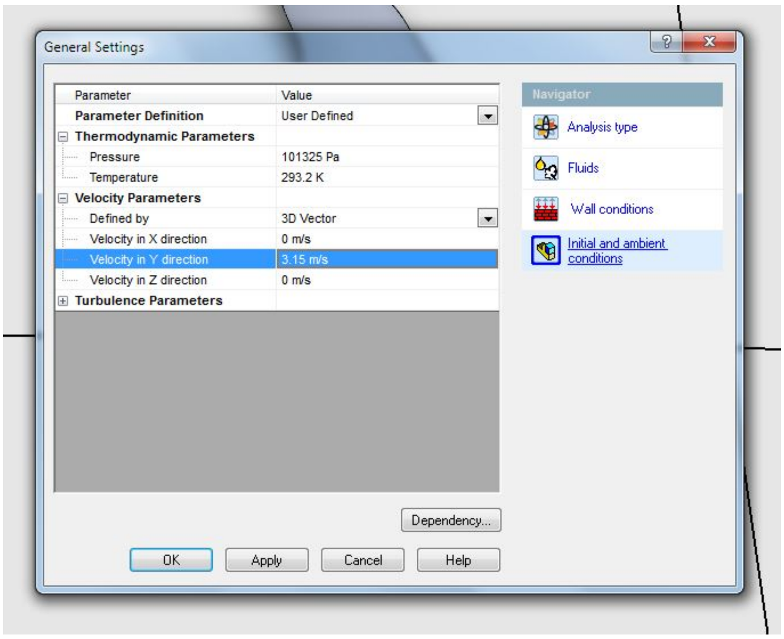

Figure 59: Wizard in which the velocities can be adjusted

SolidWorks will now determine the computational domain, and the analysis is ready to be executed.

To determine the lift- and drag coefficient, the lift and drag must be determined. These forces act upon the flipper, and thus a "goal" can be inserted to measure these forces. Right-click on the "goals"-button gives a menu, select "insert global goals...", see figure 60.

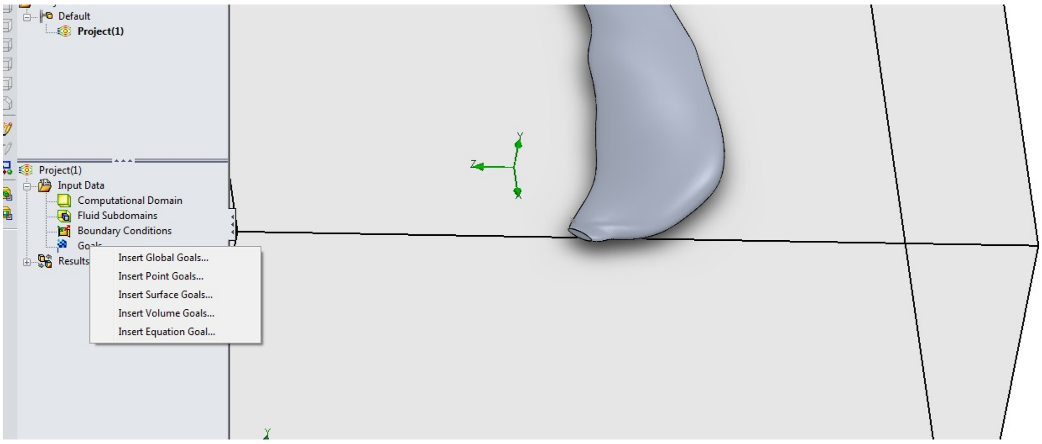

Figure 60: Menu where a goal can be inserted

Check the "Force (y)" and "Force(z)" boxes, as those determine the drag and the lift, see figure 61. Then click the green "check"-mark to apply the goals.

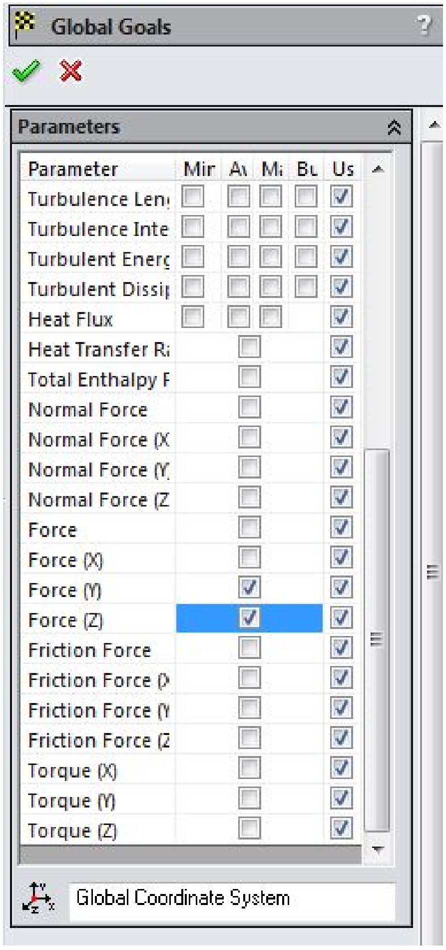

Figure 61: Menu showing the different goals which can be set

To solve the analysis, go to "Flow Simulation>Solve>Run", see figure 62.

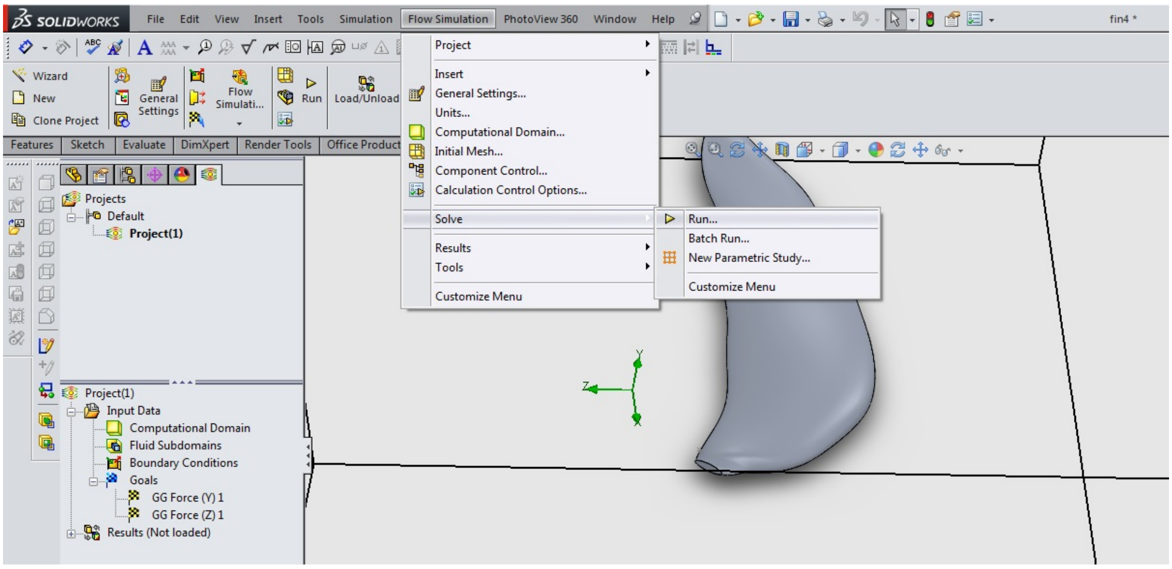

Figure 62: Menu to solve the analysis

SolidWorks will now open the solver, click on "Run". To show the y- and z-force, click on "Insert>Goal Table" in the solver. A bar with the results for the y- and z-force will pop-up, see figure 63.

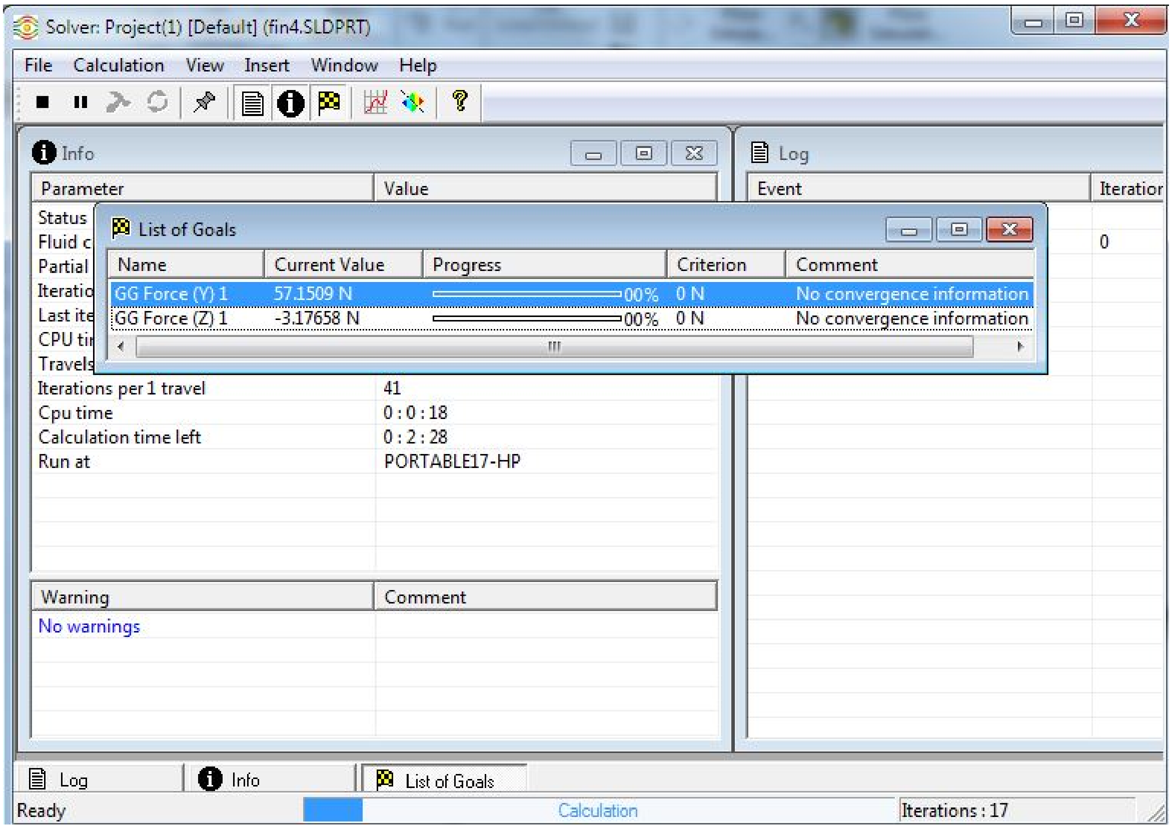

Figure 63: Goal Table with corresponding values for the forces

This data can now be inserted in a table in Microsoft Excel, MatLab or similar program.

As the calculated force is in the y- and z-direction, whereas the lift- and drag vector are perpendicular respectively parallel to the flow direction, the forces must be corrected accordingly:

$$Drag = \cos\alpha \cdot F_y + \sin\alpha \cdot F_z \tag{A.1}$$

$$Lift = \sin\alpha \cdot F_y + \cos\alpha \cdot F_z \tag{A.2}$$

The lift coefficient can now be calculated using:

$$C_L = \frac{2L}{\rho V^2 \bar{A}} \tag{A.3}$$

Where L is the lift, ρ is the fluid density, V is the *general* fluid velocity and $\bar{A}$ is the projected area, which can be calculated as explained in section 5.1.2. As all the variables are known, both the lift- and drag coefficient can be calculated for $\alpha = 0°$. This process can be redone for different angles of attack and a graph can be made from the resulting values.

B Technical Drawing Concept 1

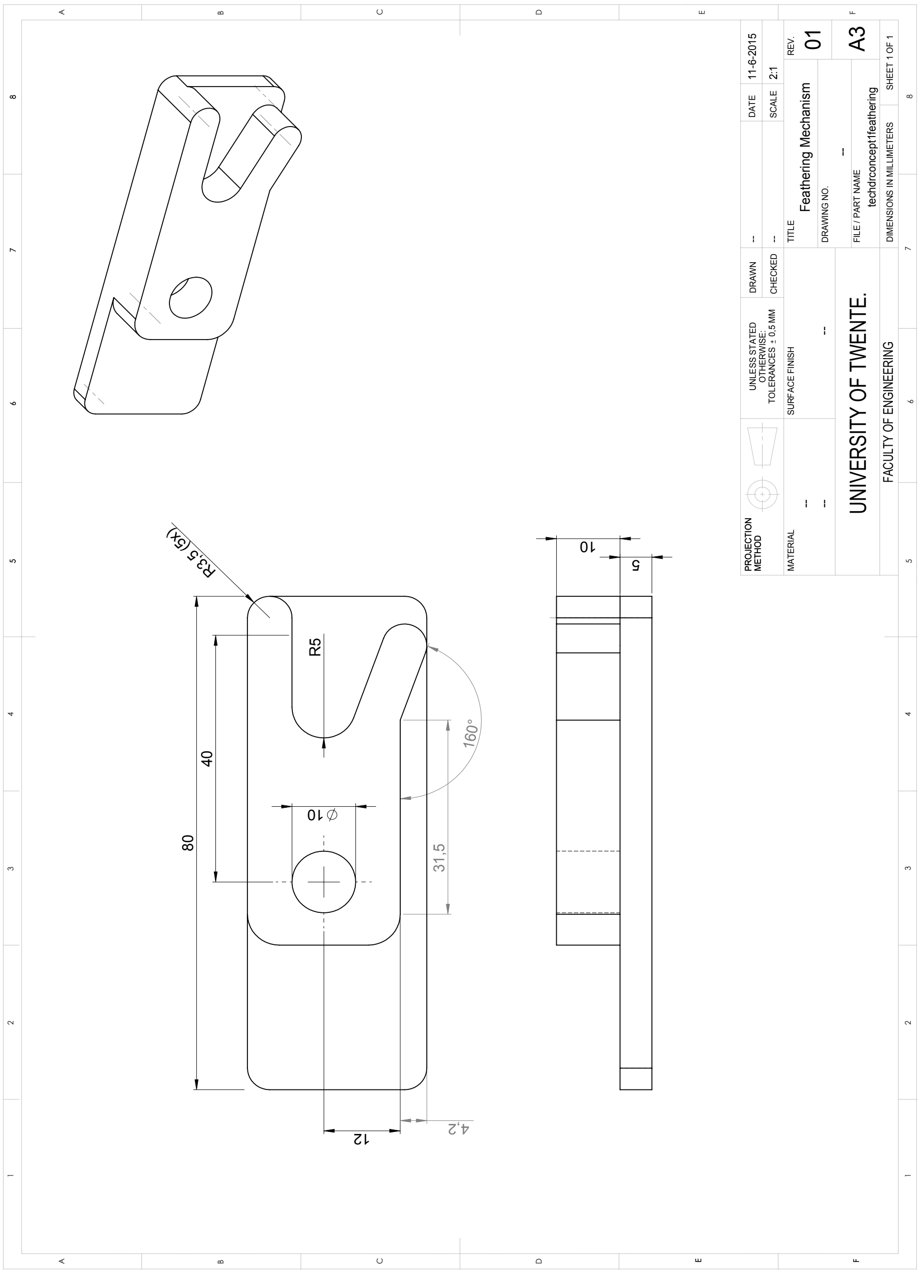

Figure 64: Technical drawing of the feathering mechanism

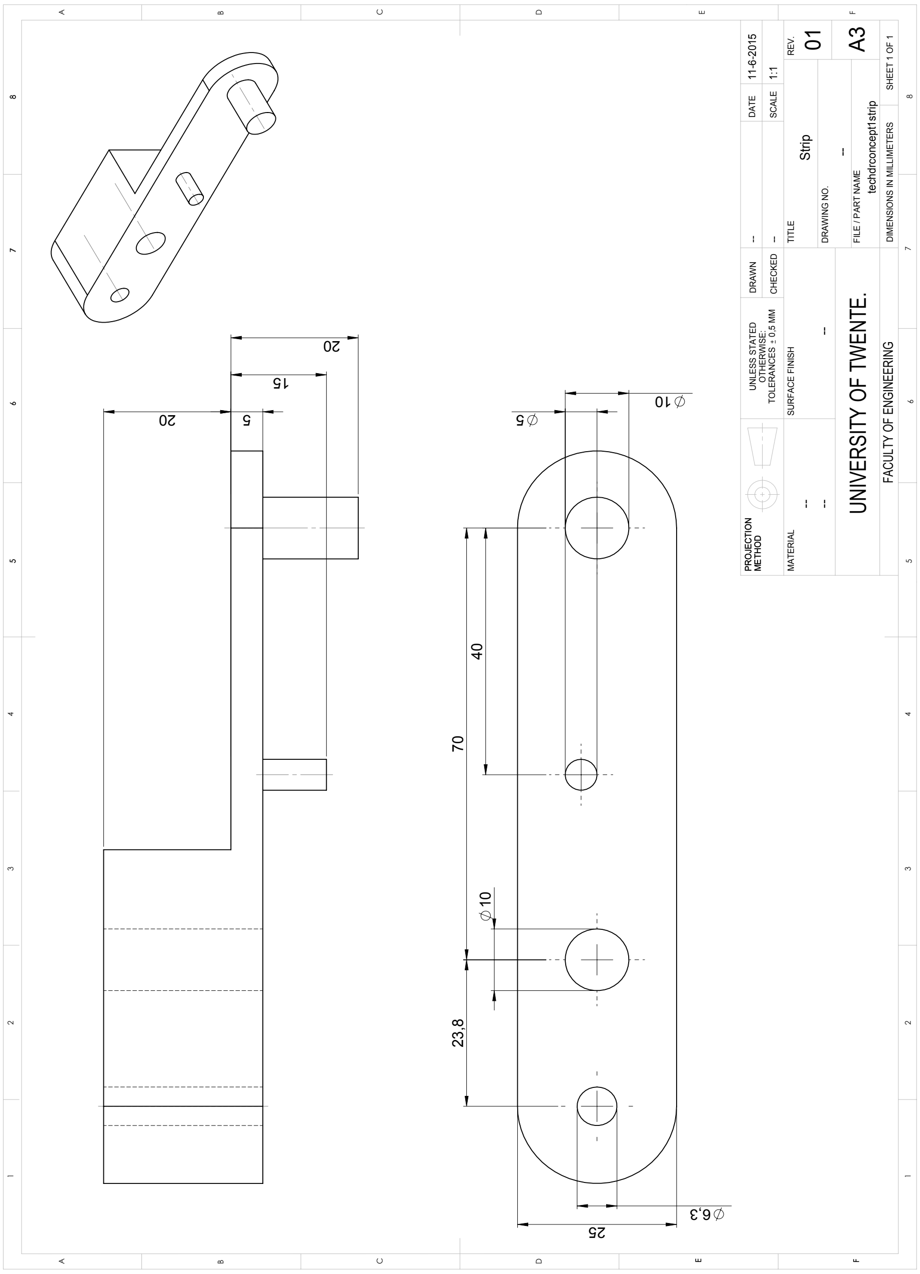

Figure 65: Technical drawing of the strip connecting the flipper and the feathering mechanism

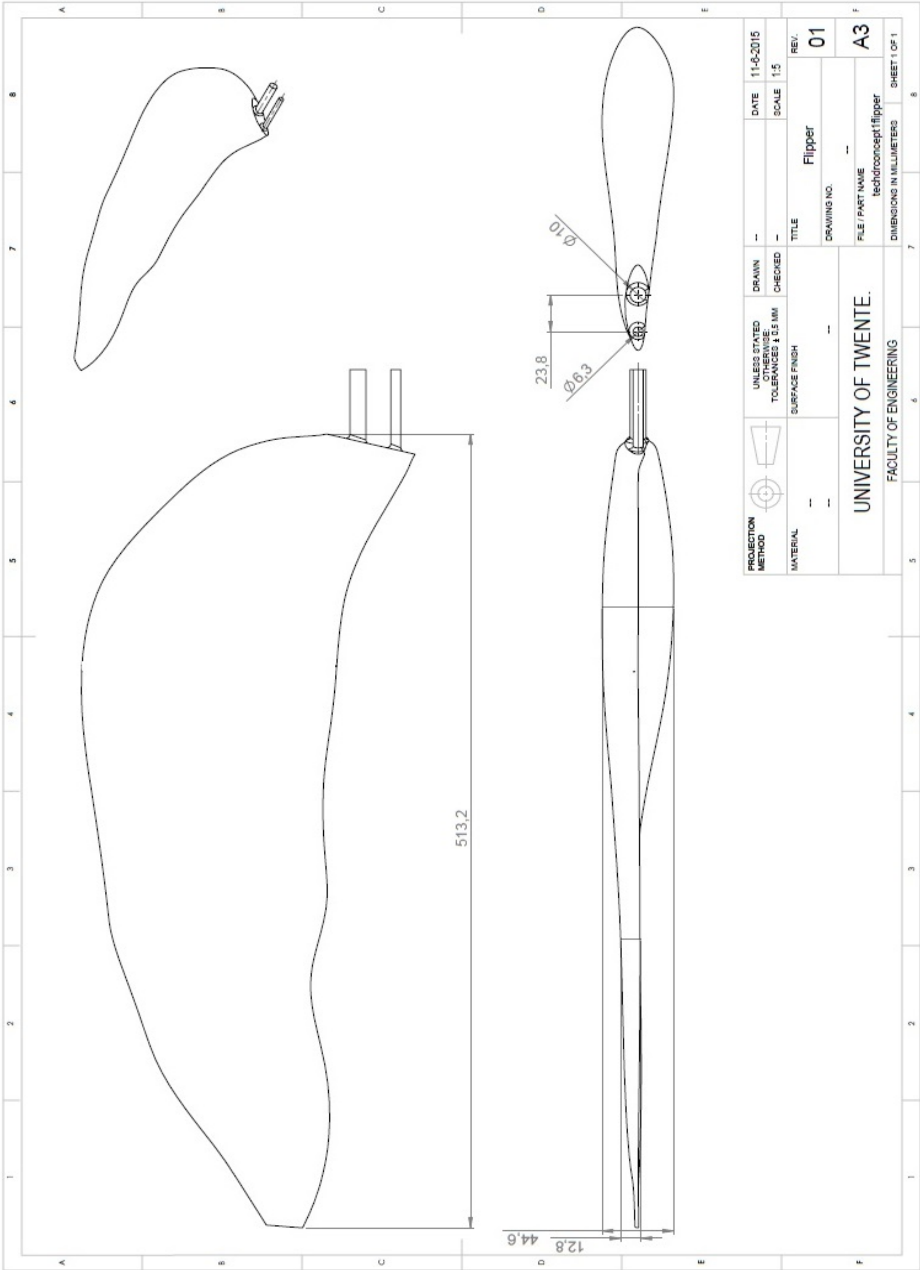

Figure 66: Technical drawing of the flipper

C Technical Drawing Concept 2

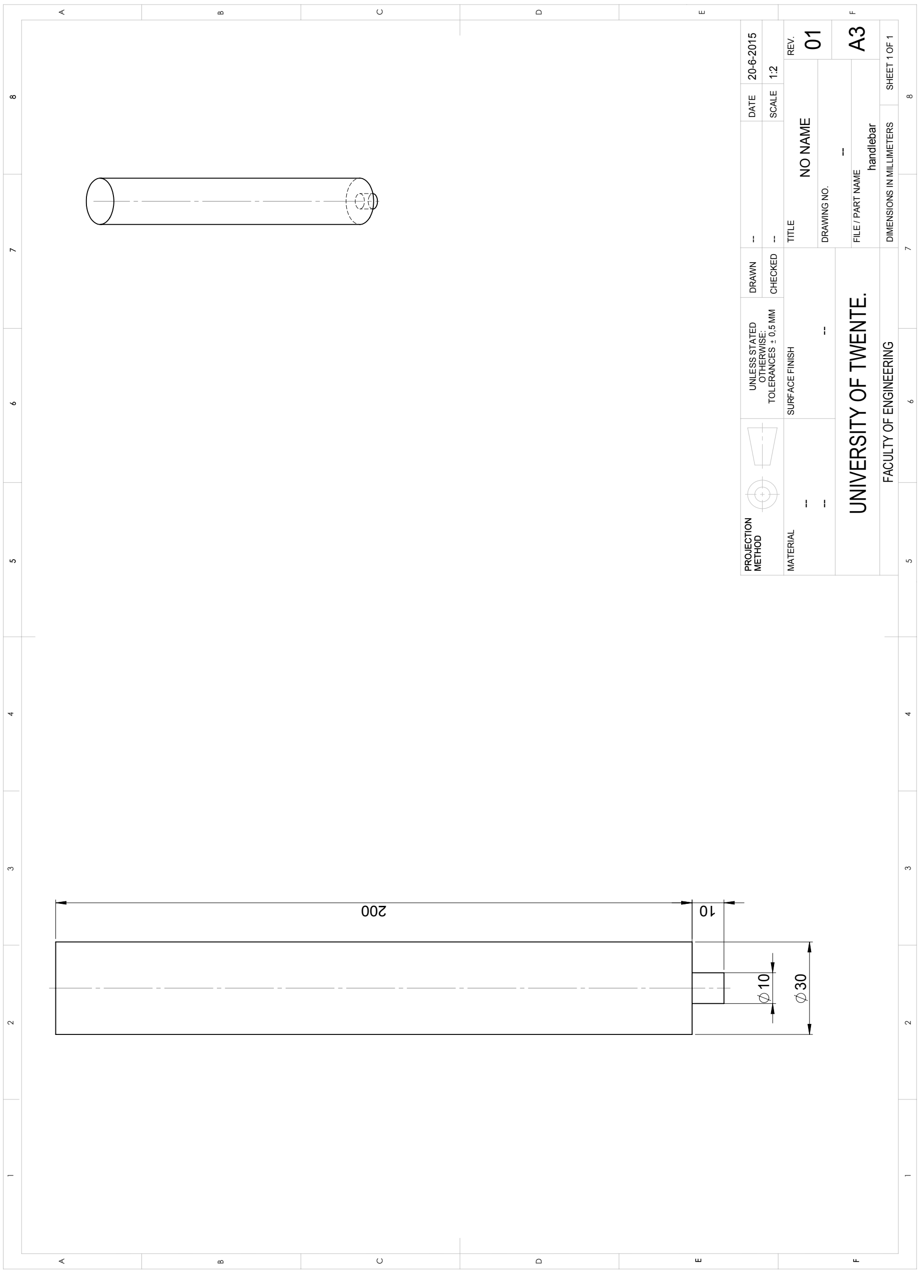

Figure 67: Technical drawing of the handlebar

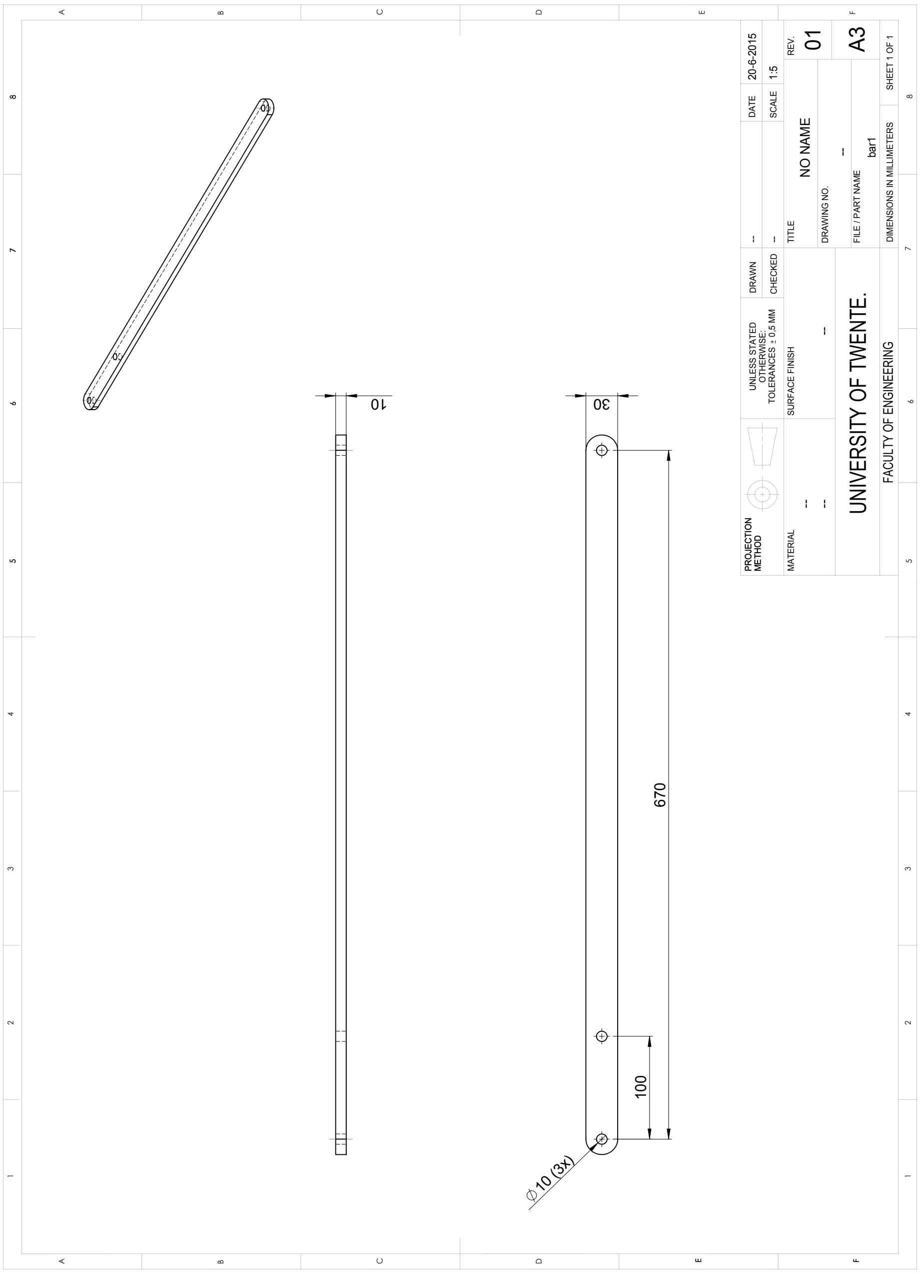

Figure 68: Technical drawing of the horizontal bar

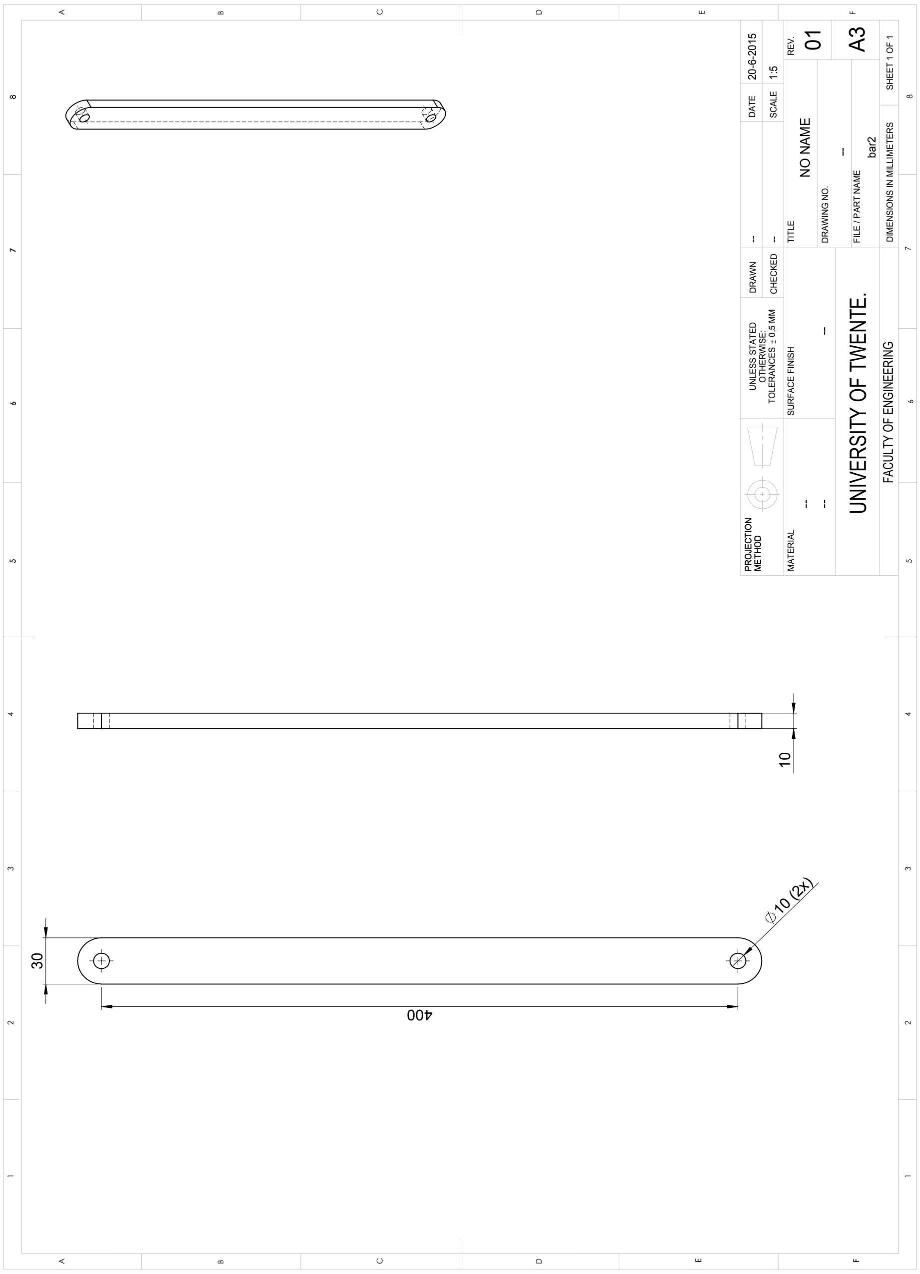

Figure 69: Technical drawing of the vertical flat bar

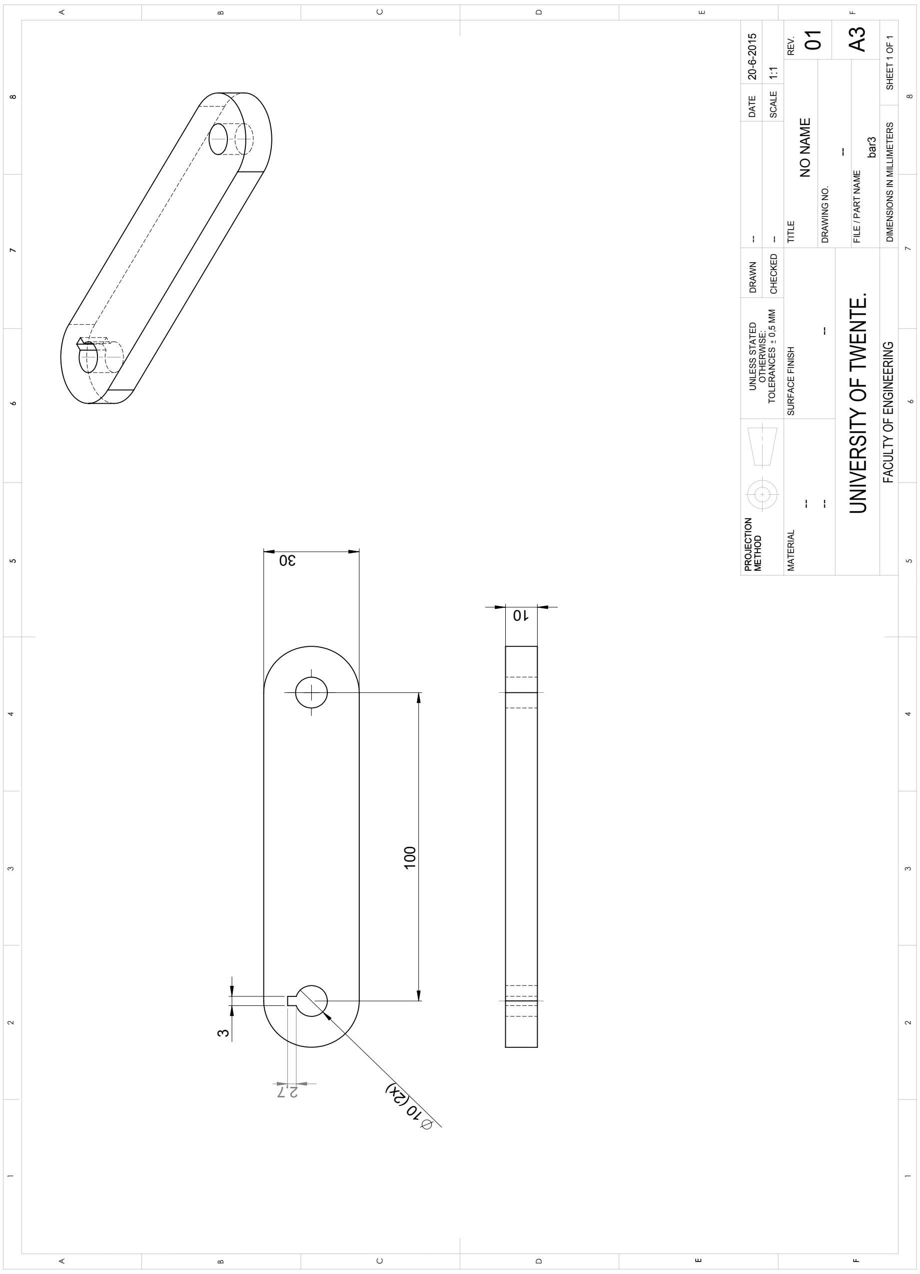

Figure 70: Technical drawing of the small bar

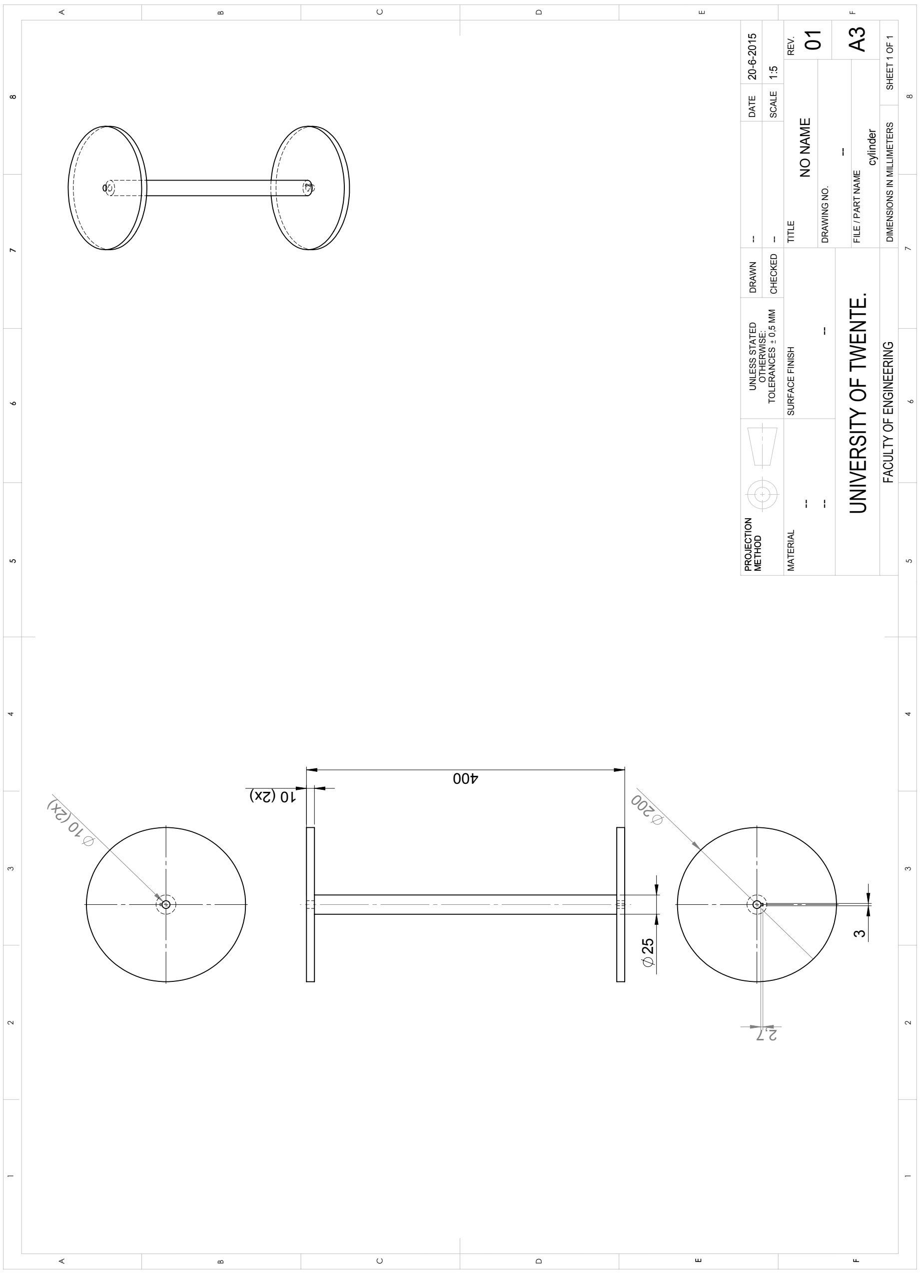

Figure 71: Technical drawing of the cylinder and axis of rotation

D Technical Drawing Flipper

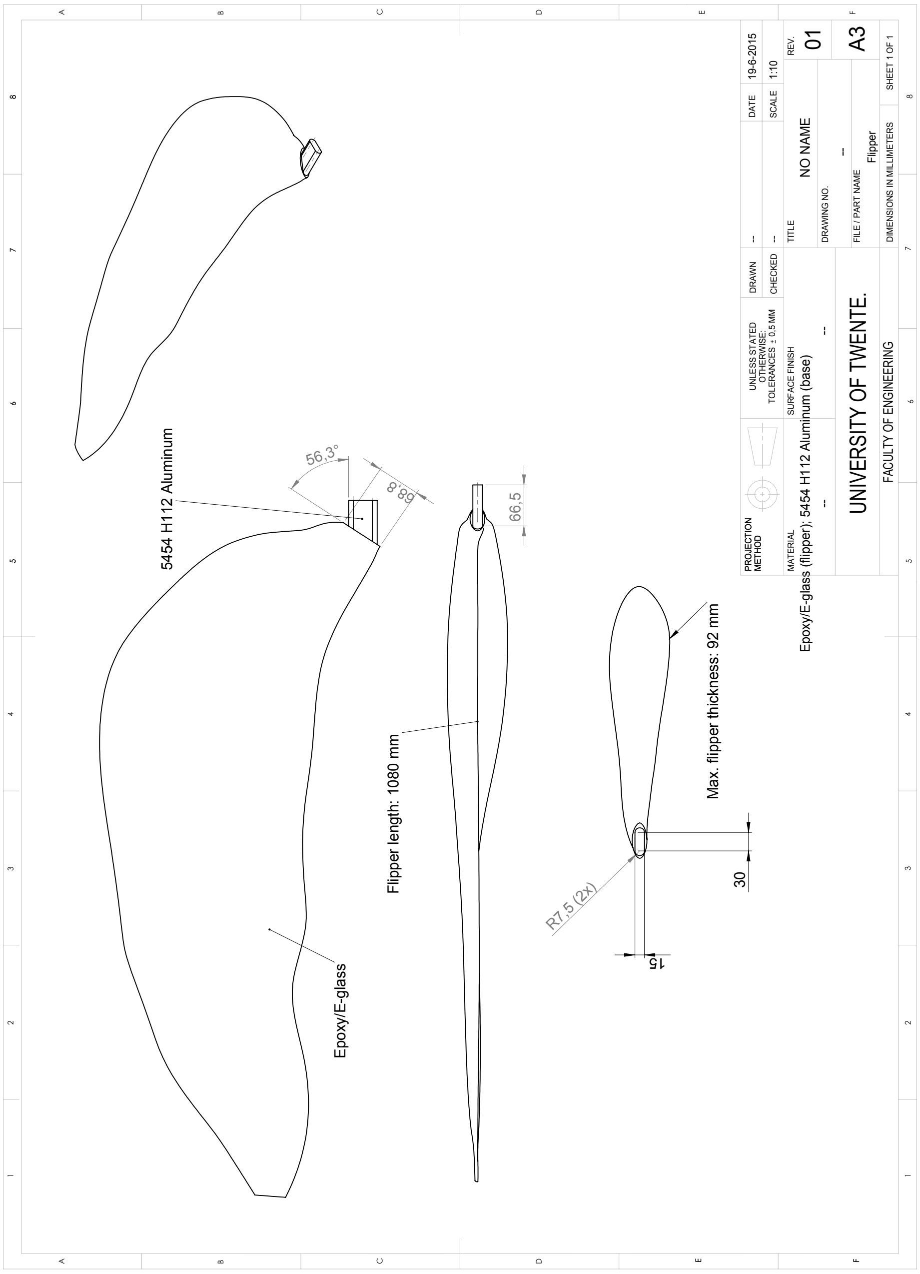

Figure 72: Technical drawing of the flipper. Note that due to limitations in SolidWorks the program is unable to show all dimensions.

E Technical Drawing Final Concept

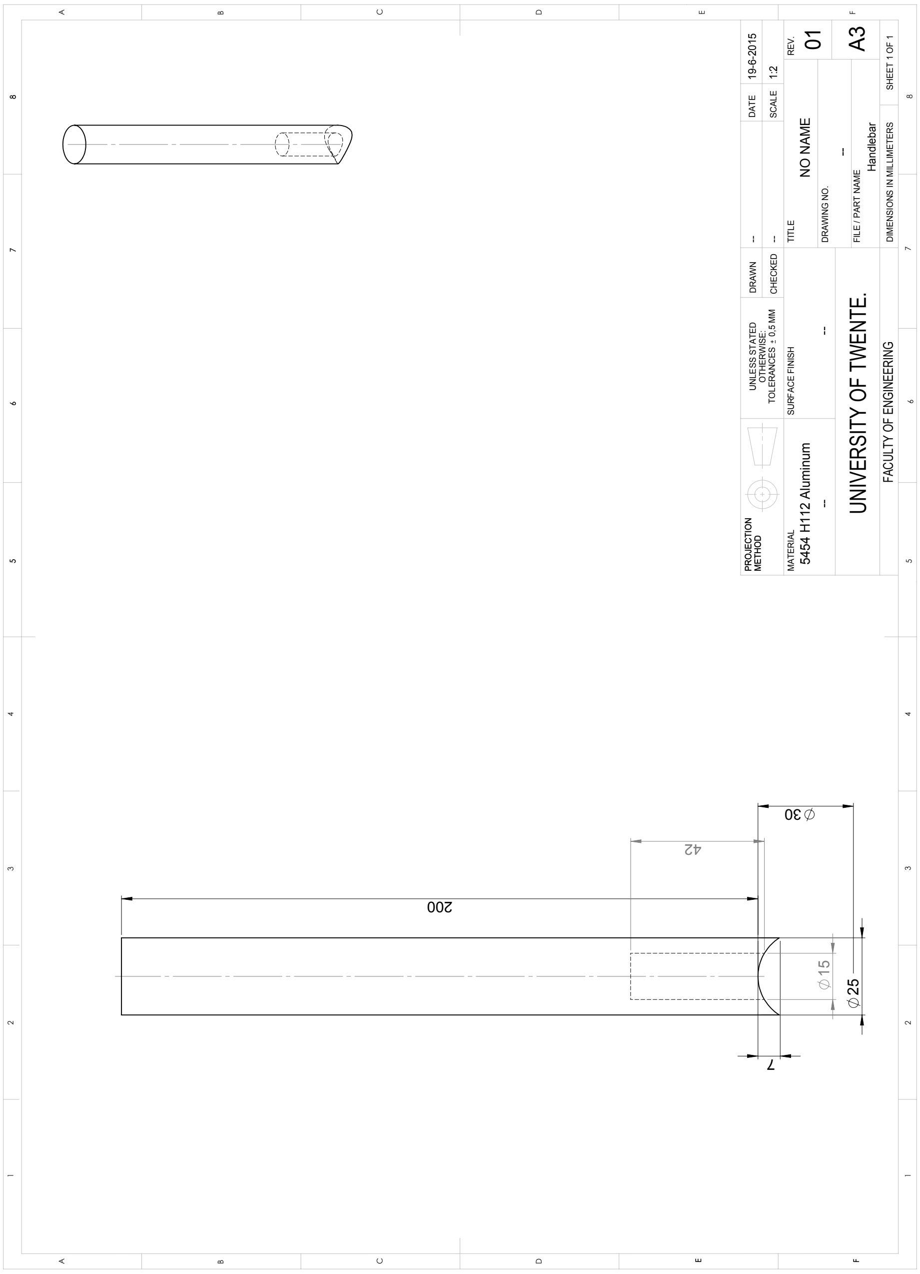

Figure 73: Technical drawing of the handlebar

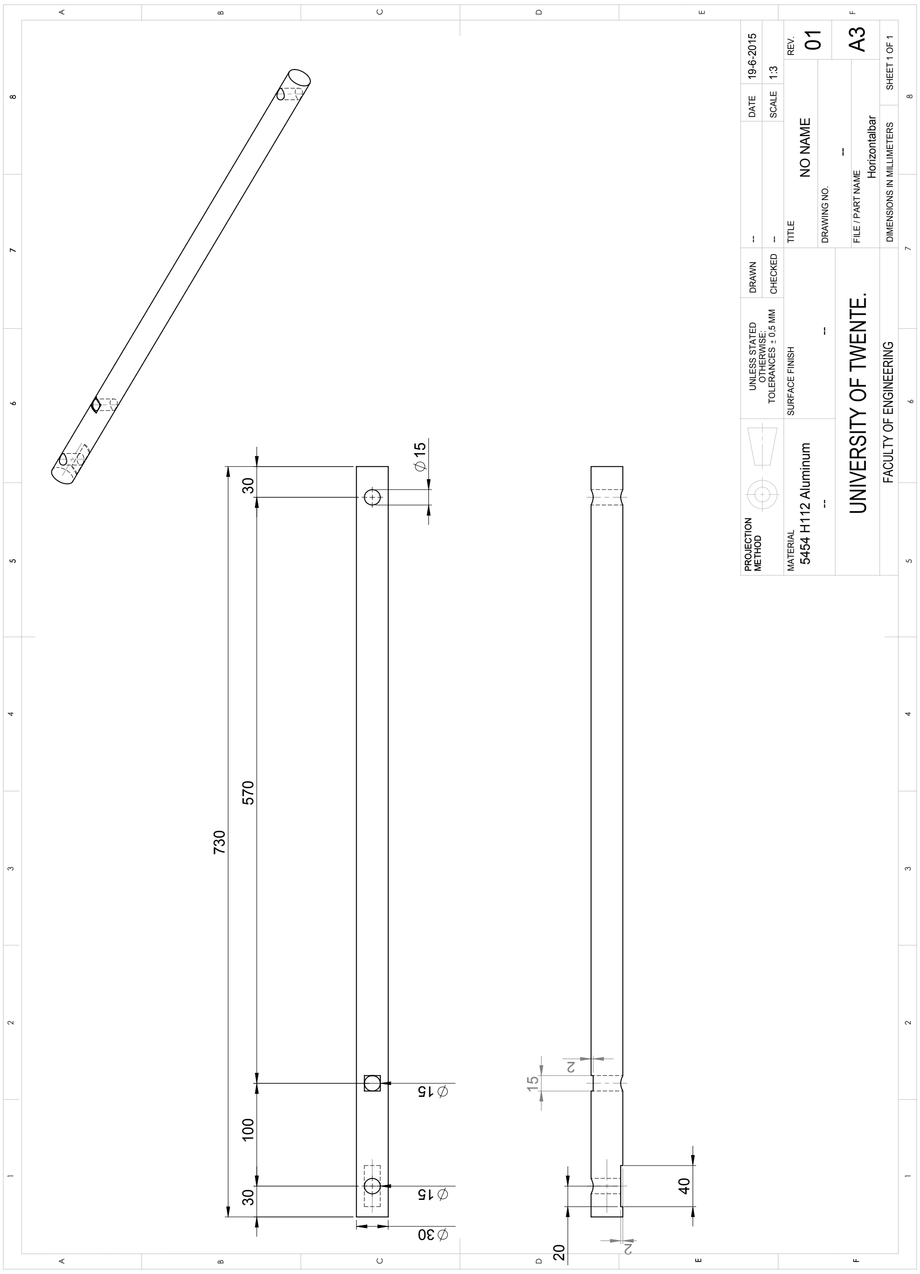

Figure 74: Technical drawing of the horizontal lever

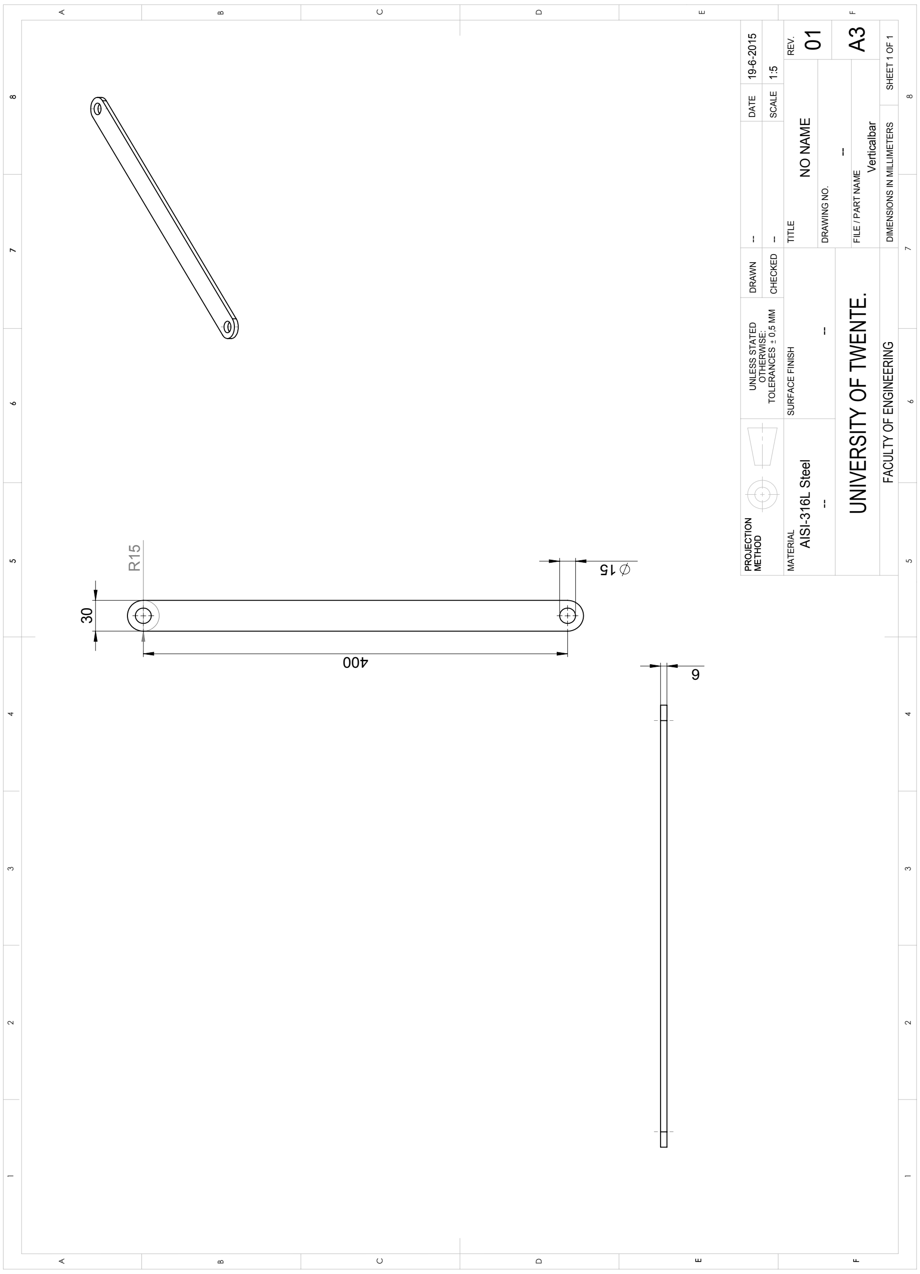

Figure 75: Technical drawing of the flat bar

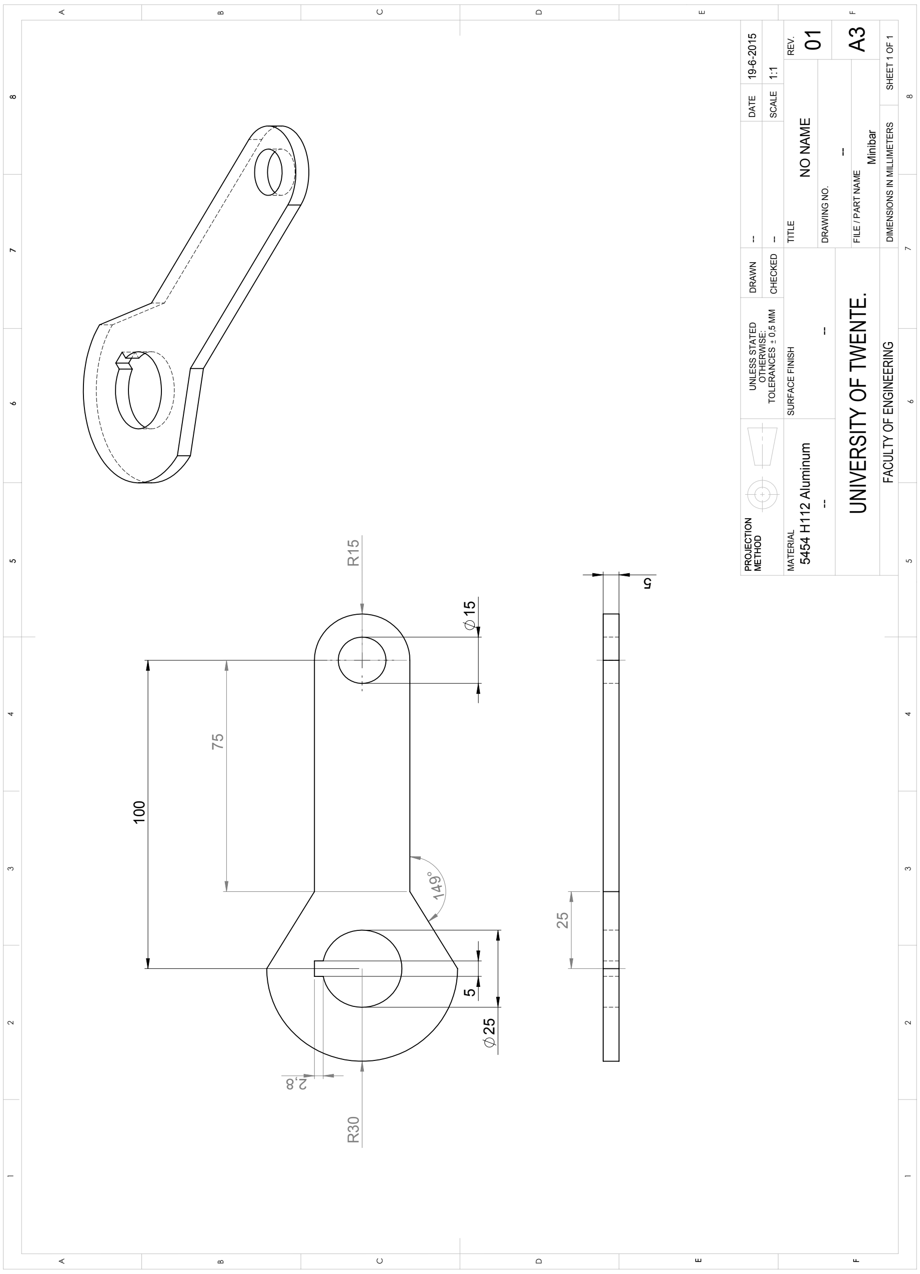

Figure 76: Technical drawing of the small lever

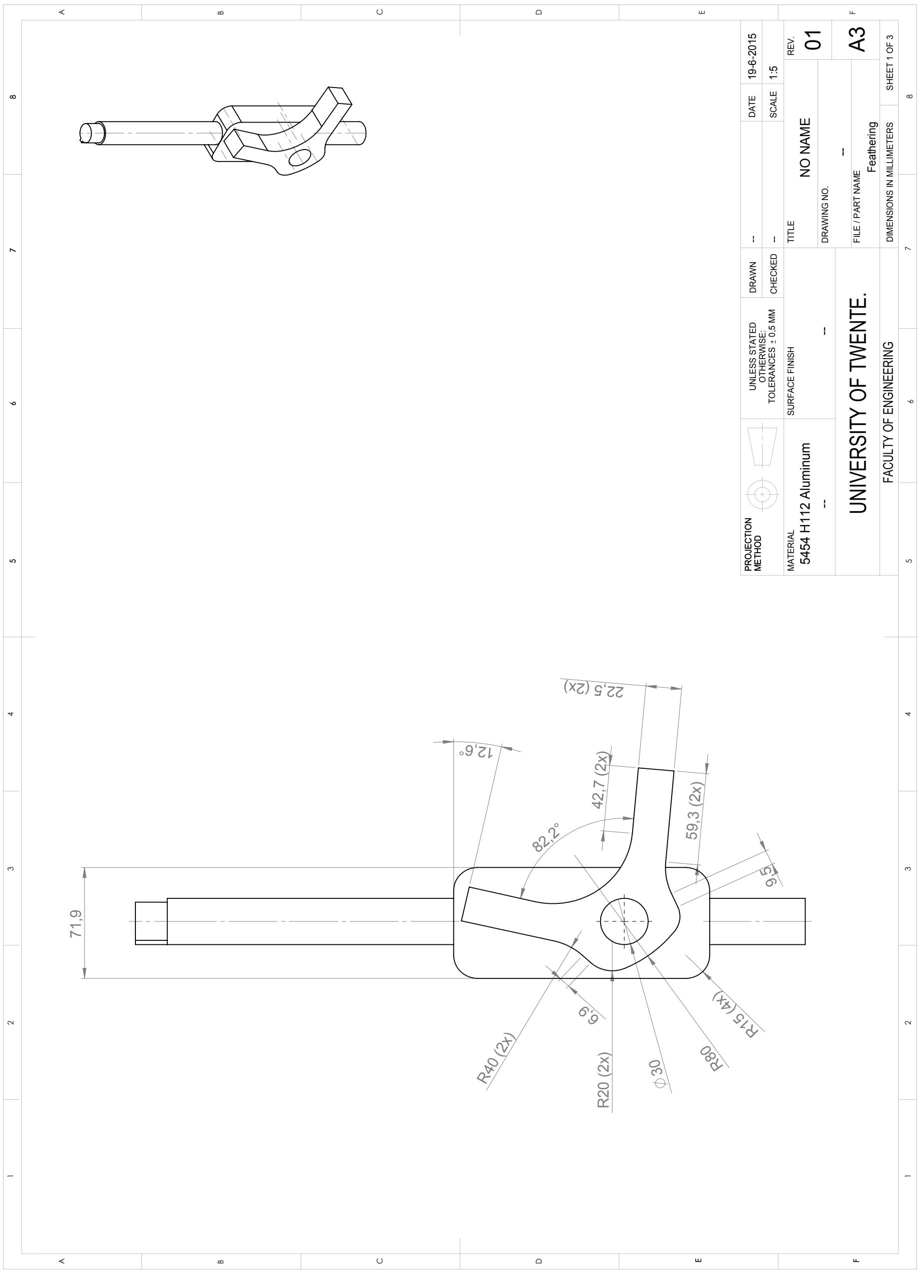

Figure 77: Technical drawing of the feathering mechanism

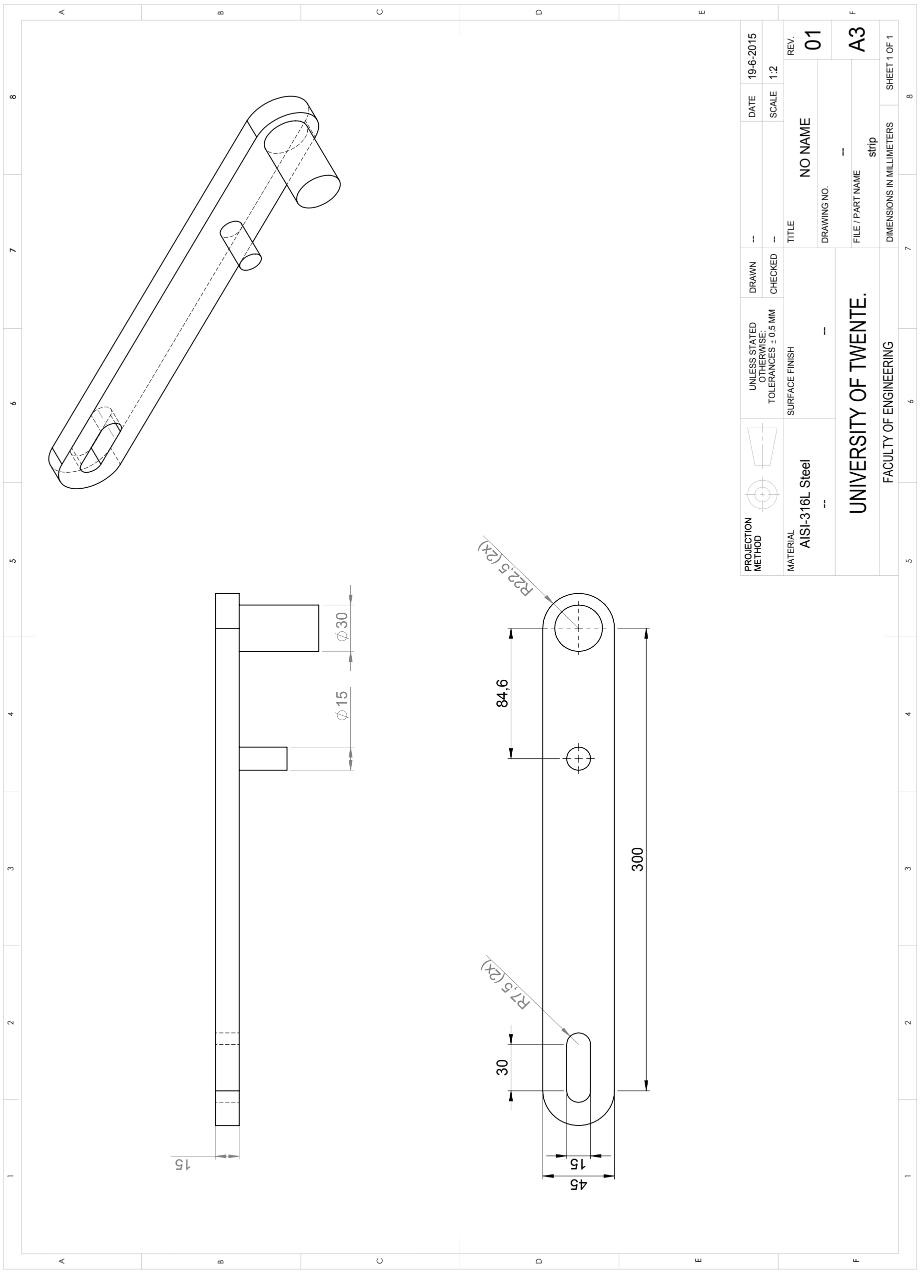

Figure 78: Technical drawing of the strip connecting the flipper to the feathering mechanism

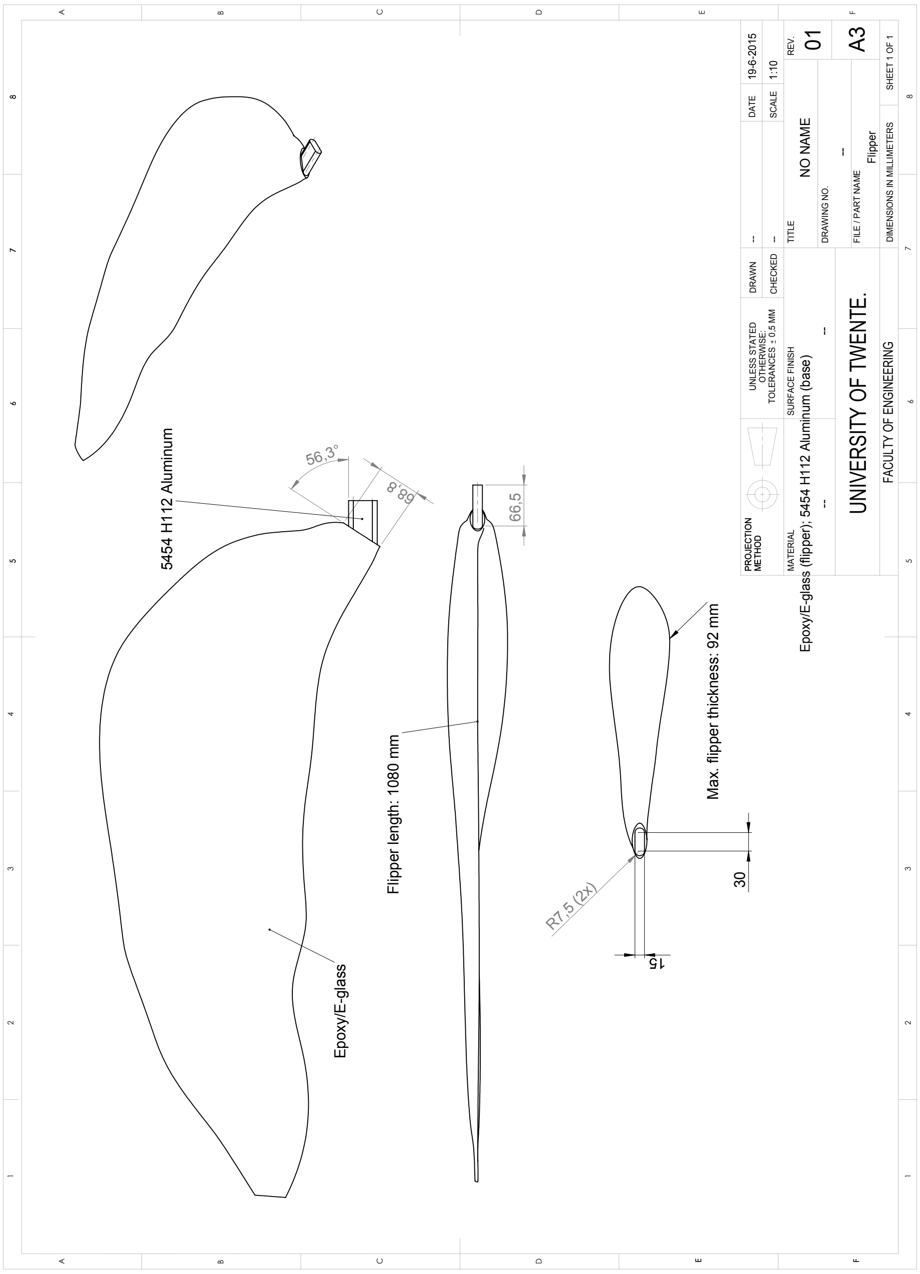

Figure 79: Technical drawing of the flipper. Note that due to limitations in SolidWorks the program is unable to show all dimensions.